Universität für Bodenkultur Wien
University of Natural Resources and Life Sciences, Vienna
Department Bautechnik und Naturgefahren
Institut für Ingenieurbiologie und Landschaftsbau

Dissertation zur Erlangung des Doktorgrades
an der Universität für Bodenkultur Wien

Charakterisierung der Ufervegetation mit Hilfe physikalisch basierter Pflanzenparameter

Betreuer:
Priv. Doz. DI Dr. Hans Peter Rauch

Beraterteam:
em. O. Univ. Prof. Dr. Florin Florineth
Prof. Dr. João Paulo Fernandes
Prof. Dr. Eva Hacker

eingereicht von
DI Clemens Weissteiner

Wien, Dezember 2018

Inhalt

Zusammenfassung

Die Herausforderung bei der Umsetzung von ingenieurbiologischen Bauweisen an Fließgewässern besteht darin, die hydromechanischen Effekte von Pflanzen in einen zeitlichen und räumlichen Kontext zu stellen. Die notwendige Dimensionierung der Wirkungen von ingenieurbiologischen Systemen ist dabei eine Voraussetzung für die Entwicklung von Standards auf dem Gebiet der Ingenieurbiologie.

Die vorliegende Arbeit befasst sich mit der biologisch-technischen Charakterisierung der Ufervegetation mit Hilfe von physikalisch basierten Pflanzenparametern. Die Architektur, Materialeigenschaften und das Verhalten unter statischer und dynamischer Belastung von Gehölzexemplaren unterschiedlichster autypischer Arten wurden dafür untersucht.

Die Ergebnisse zeigen, dass die Gehölzarchitektur einen maßgebenden Einfluss auf das Strömungsverhalten der Pflanzen hat. Es konnten große Unterschiede der Pflanzarchitektur zwischen unterschiedlichen Gehölzarten festgestellt werden. Innerartlich spiegeln sich unterschiedliche Wuchsstadien in charakteristischen vertikalen Verteilungen der anströmbaren Fläche wider. Ein starker Einfluss des jeweiligen Wuchsstandortes bzw. der Umweltsituation ist jedoch zu berücksichtigen.

Die Pflanzenarchitektur, in Kombination mit dem Blattwerk, beeinflusst das Kontraktionsverhalten von Gehölzen stark. Es hat sich gezeigt, dass Arten, welche den Schwerpunkt der projizierten Astflächen im unteren Drittel der relativen Pflanzhöhe haben, einen anderes Kontraktionsverhalten aufweisen als Arten, bei welchen der Flächenschwerpunkt höher liegt. In Bezug auf die dynamische Interaktion wurde festgestellt, dass die Blätter des Baumes einen signifikanten Einfluss auf den Dämpfungsgrad haben, jedoch wird dies stark vom Längen-Durchmesser-Verhältnis der zugrundeliegenden Achsenordnungen beeinflusst. Die Ergebnisse liefern wichtige Erkenntnisse für die quantitative Erfassung vom Verhalten der Pflanzen, welche hydro- und aerodynamischen Belastungen ausgesetzt sind. In Zukunft wird es mit der Entwicklung und Anwendung neuer Technologien möglich sein, die Gehölzarchitektur großräumig und periodisch im Detail zu erfassen. Damit kann der Parameter Gehölzarchitektur im Interaktionsprozess Pflanze und Strömung berücksichtigt werden und findet damit Eingang in die numerische Modellierung.

[10]

Abstract

While in civil engineering, the verification of stability and load-bearing capacity is state of the art, soil and water bioengineers using plants for erosion control are faced with the problem of dimensioning the mechanical effects of this complex system in a temporal and spatial context. The dimensioning of complex plants to protect slopes from erosion is a central issue and a prerequisite for the development of standards in the field of soil and water bioengineering.

The present work deals with the characterization of riparian vegetation by means of physically based plant parameters. Woody specimens of various typical riparian species were examined for material properties, architecture and their behaviour under static and dynamic load.

The results have confirmed that the tree architecture has a significant influence on the flow-plant interaction process. Differences in plant architecture were found between different types of woodland species. Between the species themselves, differences between growth phases are reflected in a characteristic vertical distribution of morphological parameters of the specimens. However, a strong influence of the respective growth location or the environmental situation must be considered.

The plant architecture, in combination with the foliage, strongly influences the contraction behaviour of woody plants. It has been shown that species which have the centre of gravity of the projected branch area in the lower third of the relative plant height have a different contraction behaviour than species that have its centroid higher. In terms of dynamic interaction, it has been found that the leaves of trees have a significant effect on the degree of damping, but this behaviour depends greatly on the length-to-diameter ratio (slenderness ratio) of the underlying axis orders.

In the future, new developments and applications will be available for assessing the plant architecture on a large scale level. This is a precondition to get more detailed information about the plant architecture and the capacity to link it with current hydrodynamic models. Therefore, with ongoing research the complex issue of tree architecture can be applied in a practical modelling approach.

[12]

1 Einleitung

Die Ingenieurbiologie ist ein bautechnisches Fachgebiet, welches sich historisch betrachtet aus den Bedürfnissen der Menschen entwickelte mit vorhandenen, natürlichen Baustoffen Bodenerosion und Bodenbewegungen zu vermeiden und dadurch Land nutzbar zu machen (Bischetti et al. 2012, Evette et al. 2009, Fernandes und Guiomar 2016, Schiechtl 1988). In der neuzeitlichen Geschichte der Ingenieurbiologie hat sich diese zu einer Disziplin entwickelt, mit welcher bautechnische Problemstellungen auf eine naturnahe Art und Weise gelöst werden.

Heute ist die Ingenieurbiologie ein Teilgebiet des Bauwesens, das technische, ökologische, gestalterische und ökonomische Ziele verfolgt und zwar vorwiegend durch den Einsatz lebender Baustoffe, also Saatgut, Pflanzenteile und Pflanzengesellschaften (Zeh, 2007). Für die Anwendung von ingenieurbiologischen Bauweisen dient eine europäische Richtlinie für Ingenieurbiologie (Hacker, 2015). Diese Richtlinie definiert die Ingenieurbiologie als technisch-biologische Disziplin, welche durch den richtigen Einsatz von Pflanzen und Pflanzenteilen als lebende Baustoffe im Laufe ihrer Entwicklung im Zusammenhang mit Boden und Gestein einen wesentlichen Beitrag zu einem nachhaltigen Erosionsschutz leisten. Dies bedeutet, dass der Erfolg eines ingenieurbiologischen Bauwerkes sehr stark von den Eigenschaften und der Entwicklung der eingesetzten Pflanzen abhängig ist (v. d. Thannen et al., 2017). Zur Steigerung des Wirkungsgrades am Anfang des Lebenszyklus werden lebende Materialien häufig in Kombination mit unbelebten Materialien wie z.B. Stein und Holz und diversen Hilfsmaterialien (Geotextilien) verwendet, welche abhängig von der speziellen Umgebungssituation des Bauwerkes Sicherungseffekte übernehmen (Gray und Sotir, 1996, Evette et al. 2009, Florineth, 2012, Gerstgraser 2000, Li und Edelmann, 2002, Zeh 2007). Die häufigsten Einsatzgebiete der Ingenieurbiologie sind der Erd- und Wasserbau.

Die Ingenieurbiologie kann als Schnittmaterie verschiedenster technischer, ökologischer, soziologischer Disziplinen betrachtet werden und bietet ein weites Feld an Grundlagen- und angewandter Forschung. Kenntnisse über die technischen und biologischen Eigenschaften von Pflanzen bilden eine wesentliche Grundlage für eine erfolgreiche Anwendung und Verbreitung von ingenieurbiologischen Bautechniken. Diese Kenntnisse

sind für ein fundiertes Prozessverständnis und für die Festlegung „ingenieurbiologischer Grenzen“ von besonderer Bedeutung. Damit ergeben sich für die angewandte Ingenieurpraxis bei der Umsetzung von ingenieurbiologischen Bauweisen zwei wesentliche Herausforderungen: Einerseits muss eine auf die lokalen Standortbedingungen abgestimmte Pflanzenauswahl getroffen werden und andererseits müssen die biomechanischen Eigenschaften der Pflanzen für eine Dimensionierung berücksichtigt werden (Fernandes und Guiomar 2016). Im Erdbau müssen Standsicherheits- und Tragfähigkeitsnachweise erbracht werden. Beim Einsatz von Pflanzen zur Erhöhung der Böschungsstabilität müssen für eine Dimensionierung die mechanischen und hydrologischen Effekte dieses komplexen Mehrebenensystems in einem zeitlichen und räumlichen Kontext verstanden werden.

1.1 **Problemstellung und Zielsetzung**

Die technischen Eigenschaften von Pflanzen wurden in ihren verschiedensten Anwendungsfeldern intensiv untersucht. Im Forschungsbereich wird generell zwischen bodenstabilisierender Wirkung von Pflanzen an Hängen und Böschungen und der Interaktion von Pflanzen mit Fluiden (Wasser, Wind) unterschieden. Diese Aufteilung in Teilbereiche ist jedoch rein auf einen methodischen Ansatz zurückzuführen, da die Interaktion der Pflanze mit oberirdisch wirkenden Prozessen über Kraftübertragungen stark mit den in der Boden-Wurzelmatrix ablaufenden Interaktionen in Verbindung steht.

Im Vergleich zu konventionellen Baumaterialien (Holz, Stahl, Stein, Beton) ist beim Einsatz von Pflanzen eine technische Charakterisierung aufgrund mehrerer Faktoren schwieriger. Pflanzen sind individuelle Organismen, wobei die Morphologie und Anatomie der Pflanzen einem artspezifischen Bauplan folgt, welcher schwach bis starke individuelle Prägungen aufweisen kann. Zudem entwickeln sich Pflanzenindividuen in unterschiedlichen Umgebungen abhängig von den gegebenen Umwelteinflüssen. Aufbauend auf dem individuellen Bauplan und den Umwelteinflüssen können Pflanzenindividuen ein und derselben Art unterschiedliche technische Eigenschaften aufweisen. Der Standort stellt somit neben dem individuellen Bauplan der Pflanzen die Grundlage für die ingenieurbiologische Wirkung des Systems. Unabhängig vom Standort

ändern sich mit dem Wachstum der Pflanzen ihre technischen Eigenschaften und damit ihre Wirkungsweise. Dies spiegelt sich in ihrer Morphologie sowie in der Veränderung der biomechanischen Materialeigenschaften wider. Ein Beispiel dafür ist ein artspezifisch unterschiedlich schnelles Wachstum der unter- bzw.- oberirdischen Pflanzenteile, welches sich auf ihre Materialeigenschaften sowie auf die Architektur der Pflanze (Wurzel und Sprosse) auswirkt.

Da Pflanzen aus verschiedenen Gewebeschichten mit unterschiedlichen biomechanischen Eigenschaften bestehen, die sich während der Ontogenese verändern, ist die Reaktion von Pflanzen unter Belastungen schwierig zu prognostizieren. Darüber hinaus erhöht die geometrische Struktur die Interaktion von Ästen untereinander, die biologische Regenerationsfähigkeit bedingt zudem die Komplexität des biomechanischen Systems.

Die Dimensionierung komplex wirkender Pflanzen ist ein zentrales Thema und Voraussetzung für die Entwicklung von Standards auf dem Gebiet der Ingenieurbiologie. Die geometrische Erfassung von Pflanzen einerseits und die Interaktion von Pflanzen unter Belastungen (statisch sowie dynamisch) und die daraus resultierenden Kräfte andererseits sind von entscheidender Bedeutung für eine Dimensionierung ingenieurbiologischer Systeme.

Die vorliegende Arbeit befasst sich anhand von 6 Publikationen mit der Charakterisierung der Ufervegetation unter Strömungsbelastung. Die Charakterisierung erfolgt durch physikalisch basierte Pflanzenparameter. Dabei liegt der Schwerpunkt einerseits auf der architektonisch präzisen Erfassung von Gehölzen und andererseits, wie sich die Pflanzenarchitektur auf statische und dynamische Belastungen auswirkt. Mit den Interaktionsprozessen müssen die Medien „Wasser und Luft“ berücksichtigt werden, da Gehölze an Uferbereichen sowohl Wind als auch Hochwässern ausgesetzt sind und sich diese Belastungsprozesse teilweise überlagern.

Das Ziel der vorliegenden Dissertation ist es, den Einfluss der Gehölzarchitektur auf die Reaktion der Pflanze durch die Strömungsbelastung zu erfassen. Damit wird ein Beitrag zur Erfassung der Ufervegetation als strömungsbedingter Widerstand geleistet und eine wichtige Grundlage für die numerische Modellierung von ingenieurbiologischen

Systemen. Die Forschungsfragen wurden aus dem übergeordneten Ziel folgendermaßen abgeleitet und in den Publikationen 1 -6 behandelt.

- Wie verhalten sich Ufergehölze unter Strömungsbelastung? [Publikation 3,4]
- Welche topologischen und/oder geometrischen Parameter der Gehölzarchitektur haben einen Einfluss auf die Reaktion der Pflanze durch die Strömungsbelastung? [Publikation 1,2,5]
- Wie unterscheiden sich unterschiedliche Gehölzarten in ihrer Architektur? [Publikation 5]
- Wie wirkt sich die Gehölzarchitektur auf den Dämpfungsgrad und die natürliche Frequenz der Pflanzen aus? [Publikation 6]

Das Hauptaugenmerk bei den Untersuchungen wurde auf verholzende Einzelpflanzen gelegt unter der Belastung durch hydrodynamische und aerodynamische Prozesse. Im folgenden Kapitel 2 wird der für die Forschungsfragen relevante Stand des Wissens dargelegt. Im Kapitel 3 wird ein Überblick über die Publikationen gegeben, welche die einzelnen Forschungsfragen beantworten. Im Kapitel 4 wird mit der Synthese und den Schlussfolgerungerungen ein Bogen zur Ingenieurpraxis gespannt. Den Abschluss bildet ein Ausblick mit weiterführenden Forschungsfragen.

2 Stand des Wissens

Die Wechselwirkungen von Vegetation und Strömung sind bedeutsam für viele Fragestellungen in der Hydrodynamik, im Wasserbau, in der Geotechnik sowie für das Forstwesen und die Städteplanung. In den genannten Disziplinen werden sie zum Beispiel für Hochwasserrisikobewertungen, für Sedimenttransportstudien, für ökologisch-hydraulische Studien, für Waldbewirtschaftungen sowie für Standsicherheitsnachweise von Stadtbäumen eingesetzt. Darüber hinaus sind Klimawandel und Überschwemmungen zu wichtigen gesellschaftlichen Themen geworden, die zusammen mit den EU-Richtlinien (Habitat-Richtlinie 92/43 / EWG; Wasserrahmenrichtlinie 2000/60 / EG) diesen Studien zusätzliche Bedeutung verleihen. Das bestehende Kapitel soll einen Überblick über den Stand des Wissens im Bereich der Wechselwirkung von Vegetation und Strömung geben. Dabei werden im Folgenden die mechanischen Eigenschaften von Ufergehölzen, die Interaktion mit Fluiddynamischen Prozessen sowie die Gehölzarchitektur getrennt voneinander behandelt.

2.1 Biomechanische Eigenschaften der Ufervegetation

Abhängig von pflanzenspezifischen Materialeigenschaften und dem lokalen Strömungsangriff kann das Widerstandsverhalten von Vegetation unabhängig von der Vegetationsart starr oder flexibel sein (DWA, 2018). Die Durchbiegung von Pflanzenästen und das dadurch entstehende seitliche und vertikale Kontraktionsverhalten von flexiblen Ufergehölzen trägt weitgehend zum Oberflächen- Schutz der Uferböschungen sowie der Verringerung des Widerstandsverhaltens bei.

Das Materialverhalten wird abhängig von der Belastung in linear-elastisches Verhalten und elastisch-plastisches Verhalten unterschieden. Bei Einwirkungen, deren Größe weit unter der Bruchspannung liegen, weist ein Prüfkörper in sehr guter Näherung linear-elastisches Materialverhalten auf. Deformationen werden dabei als reversibel angenommen, auftretende Spannungen und Dehnungen als direkt proportional zueinander. Das Hooksche Gesetz beschreibt diesen Zusammenhang:

$$\sigma = E * \varepsilon$$

Das Elastizitätsmodul E ist dabei der Proportionalitätsfaktor zwischen Dehnung E und Spannung σ.

Unterhalb der Proportionalitätsgrenze ist die Annahme einer linearen Spannungsverteilung ausreichend. Bei höheren Belastungen kommt es zu einer ungleichförmigen Verteilung der Spannung über den Probenquerschnitt, die durch Unterschiede im Spannungs-Dehnungsverhalten sowie durch Festigkeitsunterschiede bei Zug – bzw. Druckbelastung verursacht wird (Niemz, 1993)

Die Biegesteifigkeit dient als Maß für die Verformbarkeit von Materialien. Diese wird durch den E-Modul (E) sowie dem Flächenträgheitsmoment beeinflusst und wie folgt berechnet:

$$Biegesteifigkeit = E * I$$

$$I_{Kreis} = \pi * \frac{d^4}{64}$$

Untersuchungen von Vollsinger et al. (2000) haben gezeigt, dass typische Arten, welche die Fließgewässer begleiten (Schwarzerle, Silberweide), leichter verformt und umgelegt werden können als Eschen oder Bergahorne. Der E-Modul stellt jedoch als Parameter zur Quantifizierung der Biegesteifigkeit eines Baumes keine universale artspezifische Materialkonstante dar, da E im hohen Maße vom Alter der Pflanzen und äußeren Einflüssen bestimmt wird (DWA, 2018). Holz ist ein heterogenes Material: Beim Biegen hängt der Elastizitätsmodul, d. h. das Steifigkeitsmaß, nicht nur von der Menge der verschiedenen Gewebe ab, sondern auch von deren Verteilung in Bezug auf die neutrale Achse (Spatz und Brüchert, 2000). Niklas und Spatz (2012) halten fest, dass die Fähigkeit von biologischen Materialien, ihre Materialeigenschaften durch Wachstum und Entwicklung zu verändern, dem mechanischen Verhalten des Pflanzenkörpers und seiner Bestandteile eine räumliche und zeitliche Heterogenität verleiht. Pflanzen unterscheiden sich in diesem Verhalten gänzlich von allen anderen technischen Konstruktionen. Herkömmliche technische Konstruktionen müssen meist steif sein, während die Natur auf mechanische Belastungen mit Flexibilität reagiert (Spatz und Brüchert, 2000). Dies ist der erschwerende Punkt in der Standardisierung von Pflanzenmaterialeigenschaften. Man

muss sich stets darüber bewusst sein, dass ein einmal bestimmter Parameter lediglich eine Momentaufnahme darstellt und dies ist in Berechnungsansätzen zu berücksichtigen (DWA, 2018).

2.2 Pflanzenarchitektur – Definition, Aufnahme und Analyse

Neben den Materialeigenschaften einer Pflanze ist ihre räumliche Struktur ausschlaggebend für die Interaktion Strömung und Pflanze. Deshalb ist die Parametrisierung der räumlichen Pflanzenstruktur (der Pflanzenarchitektur) ihre Aufnahme und Modellierung ein essentieller Punkt, welcher zu einem besseren Verständnis der Interaktion Strömung-Pflanze führt.

Das Wachstum von Pflanzen findet nicht willkürlich über das ganze Individuum verteilt statt. Vielmehr werden neue Teile der Pflanze durch das Wachstum der Apikalmeristeme auf bestehende Pflanzenteile „aufgesetzt“. Dies hat auch die Verbindung sämtlicher Komponenten mit dem Stamm zur Folge und wird im Allgemeinen als Baumstruktur wahrgenommen (Godin und Caraglio, 1997). Analog zu Barthèlèmy und Caraglio (2007) werden, in dieser Arbeit, die Ordnungen der Pflanzenachsen folgendermaßen bezeichnet (siehe **Fehler! Verweisquelle konnte nicht gefunden werden.**):

- Als Achse 1. Ordnung wird der Stamm bezeichnet. Er ist direkt mit dem Untergrund verbunden und bildet entlang seiner Achse die Ausgangspunkte für Äste 2. Ordnung.
- Achsen oder Äste 2. Ordnung entspringen der Achse 1. Ordnung. Sie verbinden Achsen 3. Ordnung mit dem Stamm.
- Theoretisch können auch Achsen höherer Ordnungen entlang einer Pflanze in Erscheinung treten. Ihre Bezeichnung entwickelt sich analog zu den bestehenden Strukturen (Äste 4.Ordnung, 5.Ordnung usw.).

Das Konzept der topologischen Strukturen basiert darauf, eine Pflanze in einzelne Bestandteile zu zerlegen und die Verbindungen dieser Teile zu beschreiben. Durch wiederholte Beobachtungen und topologische Aufnahmen einer Pflanze, zum Beispiel vor und nach einer Vegetationsperiode, wird die Entwicklung dieser durch die Erweiterung von neuen topologischen Strukturen festgehalten.

Aufgrund neuer technologischer Entwicklung haben sich im Laufe der letzten Jahrzehnte verschiedene Methoden etabliert, um mit verhältnismäßig geringem Aufwand wirklichkeitsnahe Pflanzenmodelle erstellen zu können. Im Allgemeinen wird zwischen drei nichtinvasiven Arten der Pflanzenaufnahme unterschieden:

- Aufnahmen mittels Fotografie-basierten Methoden
- Aufnahmen mittels Laser Scanner
- Aufnahmen mittels elektromagnetischem Digitalisierungsinstrument

Im Folgenden wird jene Methode erläutert, mit welcher in dieser Arbeit gearbeitet wurde. Elektromagnetische Digitalisierungsinstrumente wurden ursprünglich entwickelt, um Bewegungen innerhalb eines künstlich erzeugten elektromagnetischen Feldes (EM) aufzuzeichnen und in virtuelle Räume zu übertragen (Kuipers, 1975, 1977, Raab et al., 1979). Der tatsächliche technische Hintergrund, wie diese elektromagnetischen Felder (EM-Felder) erzeugt und welche Messmethoden verwendet werden, kann von Hersteller zu Hersteller variieren, jedoch gibt es kaum Unterschiede im generellen Aufbau der Systeme (Nixon et al., 1998,). Der Aufbau eines solchen Systems umfasst:

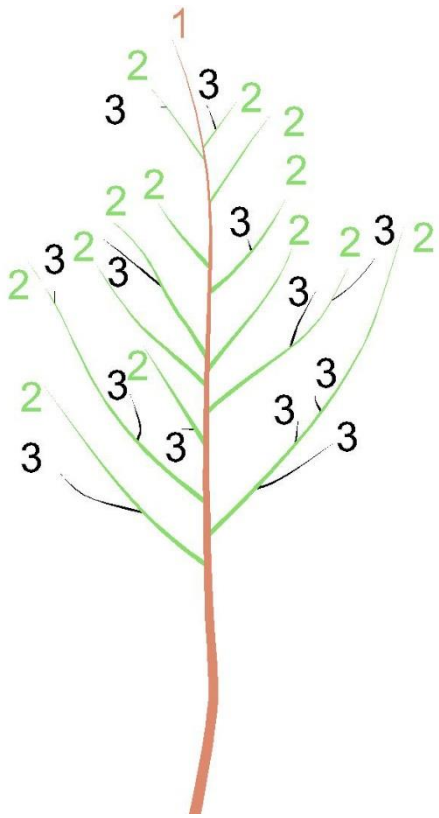

Abbildung 1: **Schematische Darstellung der Astordnungen: braun – Achse 1.Ordnung (Stamm); grün – Achse 2.Ordnung; schwarz – Achse 3. Ordnung**

- Einen EM-Sender (Transmitter): In ihm befinden sich drei orthogonal zueinanderstehende Spulen. Das Aktivieren dieser Spulen erzeugt drei Komponenten (X, Y und Z) eines Magnetfeldes, welches das Referenzkoordinatensystem darstellt. Um Messungen durchführen zu können, muss der Sender während des Messvorganges in einer fixen Position in der Nähe des Aufnahmeobjektes aufgestellt werden. Eine Veränderung der Lage (Umstellen) oder Orientierung (Verdrehen) während des Messvorganges, würde ohne fixe Referenzpunkte zu einem fehlerhaften Ergebnis führen.

- einen EM-Empfänger: In ihm befinden sich drei orthogonal zueinanderstehende Sensoren, welche die Feldstärke des Referenzkoordinatensystems in jedem Punkt innerhalb des vom Transmitter erzeugten EM-Feldes messen.
- eine Steuerungseinheit, die benötigt wird um die beiden oben genannten Komponenten mit entsprechenden Stromspannungen zu versorgen. Sie rechnet die gemessenen Feldstärken in 3D-Koordinaten und Euler-Winkel um und sendet sie an den Computer.

Da das System nicht von abgedeckten Pflanzenteilen beeinträchtigt wird, ist es in der Lage sämtliche Punkte an der Pflanze direkt aufzunehmen. Jedoch reagiert das Instrument sensibel auf die Messumgebung. Deshalb sollte darauf geachtet werden fernab von ferromagnetischen Gegenständen und stromführenden Elektrokabeln die Messungen durchzuführen, da störende Magnetfelder Verfälschungen der Ergebnisse zur Folge haben (Polhemus, 2005, Sinoquet et al., 1997).

Der Vorteil dieser nicht-zerstörenden Methode liegt in der Exaktheit und der Unempfindlichkeit gegenüber Okklusion von Pflanzenteilen während der Aufnahme. Ebenso kann der Zeitaufwand, der für die Modellierung benötigt wird, als gering betrachtet werden. Als negativ anzuführen ist die geringe Reichweite dieser Methode, da nach aktuellem Stand der Technik nur innerhalb eines 4 Meter-Radius gearbeitet werden kann. Zwar kann dieser Radius theoretisch durch Einmessen von Referenzpunkten beliebig erweitert werden, jedoch ist dies mit einem steigenden Zeitaufwand verbunden. Darüber hinaus sollte man beachten, dass zur Abtastung höher gelegener Punkte keine metallischen Gerüste verwendet werden. Ebenso ist die mangelnde Wettertauglichkeit aufgrund der elektronischen Bauteile zu berücksichtigen (Sinoquet und Rivet, 1996).

2.3 Interaktion der Ufervegetation mit Fluiddynamischen Prozessen

Vegetation stellt im Abflussquerschnitt ein Rauigkeitselement dar. Gegenüber einem unbewachsenen Profil kommt es zur Erhöhung der Reibung am Ufer und an der Böschung, zu einer Reduktion der Fließgeschwindigkeit in den bewachsenen Teilen des Durchflussprofils und daher zu einer Verminderung der Abflussleistung. Je nach Dichte und Durchmesserverteilung der Ufervegetation kann sie zu erhöhter Sedimentation von Fest- und Schwebstoffen, durch lokale Turbulenzbildung auch zu Erosion führen. Das

hydraulische Verhalten eines mehr oder weniger starren Uferbewuchses unterscheidet sich grundlegend von dem einer flexiblen Ufervegetation (Vollsinger et al. 2000).

Bei einer Betrachtung des Strömungswiderstandes, der durch Pflanzen induziert wird, muss man die Besonderheiten der Vegetation berücksichtigen, wie ihre durchlässige, heterogene Natur und ihre Fähigkeit, die Form unter Strömungsbelastung zu biegen und zu verändern. Die fluid-dynamische Wechselwirkung von Strömungen mit Pflanzen hängt nicht nur von geometrischen-(z.B. Stamm- und Astdurchmesser, Pflanzhöhe und Blattdichte) und Material- Eigenschaften (z.B. Elastizität, Biegesteifigkeit) der Pflanzen ab, sondern zudem noch vom dynamischen Verhalten der Pflanzen unter Belastung (Stamm / Ast / Blattbiegung sowie horizontale und vertikale Kontraktion) siehe Rauch, 2005, Whittaker et al. 2013, Weissteiner et al. 2015, Järvelä et al. 2016. Nachfolgend werden die wichtigsten Forschungsarbeiten dargelegt, welche das Thema Interaktion zwischen Pflanzen und Strömung aus hydrodynamischer wie aus aerodynamischer Sicht behandeln.

Aus hydrodynamischer Sicht können Gehölze Uferbereiche sichern und für Sedimentanlandungen sorgen, gleichzeitig kann die Ufervegetation aber auch Erosionsprozesse verursachen und den Strömungswiderstand erhöhen. Daher ist ein fundiertes Verständnis der wirkenden Prozesse und maßgebenden Parameter der Vegetation erforderlich (z.B. Aberle und Järvelä 2013, 2015, Jalonen und Järvelä 2014, Luhar und Nepf 2013), um sowohl Hochwassersicherheit zu gewährleisten als auch natürliche Flusslandschaften zu erhalten.

Hydrodynamische Untersuchungen, die das Strömungsfeld der Ufervegetation untersuchen, basieren üblicherweise auf hochauflösenden, räumlichen und zeitlichen Geschwindigkeitsverteilungen. Die strömungsinduzierte Durchbiegung und Kontraktion der Pflanzenstruktur in Fließrichtung werden durch eine Abnahme der projizierten Fläche und der Pflanzenhöhe berücksichtigt (Fathi Moghadam und Kouwen 1997, Jalonen und Järvelä 2014, Oplatka 1998). Umgekehrt werden Vegetationselemente und ihre räumlichen Eigenschaften in der Regel auf der Basis eines ganzheitlichen Ansatzes analysiert. Bei diesem Ansatz wird die komplexe Struktur von Sträuchern und Bäumen, die aus heterogenen Pflanzenteilen bestehen, vereinfacht (Västilä und Järvelä 2014). Versuche, Pflanzenfläche oder -volumen zu charakterisieren, beruhen auf:

- einer Zylinderanalogie mit einer Schätzung des Stammdurchmessers in einer bestimmten Höhe über dem Boden (z. B. DVWK 1991)
- fotografische Bildanalysen (z. B. Järvelä 2002)
- Vermessung der projizierten Fläche des Stammes und Hauptästen (z.B. Armanini et al. 2005, Righetti 2008)
- destruktive Aufnahme ganzer Bäume in kleinen Ast- und Stammteilen (Wilson et al. 2006)
- dem Produkt aus effektiver Pflanzenhöhe und effektiver Pflanzenbreite (Freeman et al. 2000)
- dem Blattflächenindex (Järvelä 2004, Jalonen et al., 2013) und
- dem Verhältnis zwischen Blatt- und Stammfläche (Västilä et al. 2013).

Im Gegensatz zu hydrodynamischen Studien konzentrierte sich die Forschung im Bereich aerodynamischer Studien auf die Reaktion der Pflanzen auf dynamische Belastungen (z. B. Milne 1991, Gardiner 1995, Moore und Maguire 2008, Sellier und Fourcaud 2009). In diesem Zusammenhang wurde die Reaktion der Pflanzen auf Wind zusammen mit biomechanischen und dynamischen Eigenschaften verschiedener Pflanzenarten untersucht (z. B. Spatz et al. 1999, Sellier und Fourcaud 2005, 2009, Kane und James 2011). Die Quantifizierung der maximalen statisch erträglichen Lasten liefert wertvolle Informationen über die biomechanischen Eigenschaften von Bäumen. Sie spiegelt jedoch nicht den Grad der Wechselwirkung bei dynamischen Belastungen, wie sie in der Realität auftreten, wider. Tatsächlich können viel niedrigere dynamische Belastungen als die durch statische Tests ermittelten zu einem Versagen führen (Peltola 2006). Um die Reaktion von Pflanzen auf turbulente Fluidbelastung (Luft und Wasser) zu charakterisieren, müssen daher die dynamischen Eigenschaften der Pflanzen (Eigenfrequenz (f_n) und Dämpfungsgrad (ζ)) bestimmt werden (Moore und Maguire 2005).

Die Beschreibung der wichtigsten hydraulischen Eigenschaften von Pflanzen, nämlich der Geometrie und der Flexibilität, mit artspezifischen Parametern ist komplizierter als die in der Wasserbaupraxis gebräuchliche Starrzylinder-Analogie (Aberle und Järvelä 2013). Darüber hinaus unterstreichen Aberle und Järvelä (2013) die Notwendigkeit, objektive und genaue Methoden zur Charakterisierung der natürlichen Vegetation zu erarbeiten.

Die Struktur einer Pflanze (einschließlich geometrischer und topologischer Informationen) hängt von ihren Eigenschaften und der relativen Anordnung jedes ihrer Teile ab. Eine Untersuchung architektonischer Eigenschaften von Gehölzen mit dem gleichen Detaillierungsgrad wie die Untersuchung hydraulischer Strömungsprozesse bietet daher eine neue Perspektive auf die Wechselwirkung beider Elemente (Whittaker et al. 2013, Weissteiner et al. 2015). Ein genaues geometrisches 3D-Pflanzenmodell ermöglicht die Extraktion räumlich-struktureller und topologischer Pflanzenparameter, welche die Pflanzenexemplare in unterschiedlichen Detaillierungsgraden charakterisieren (Barthelemy und Caraglio 2007). Dadurch werden das erzeugte Pflanzenmodell und das hydraulische Modell miteinander verknüpft, sie bilden somit die Grundlage für einen ganzheitlichen Ansatz zur Berücksichtigung von Wechselwirkungen zwischen Pflanzen und Strömungsinteraktionen.

Aktuell werden Pflanzen vereinfacht hinsichtlich Geometrie und Materialeigenschaften in Berechnungen berücksichtigt. Dies führt zu Unsicherheiten in Berechnungsansätzen, da die Pflanze in ihrer Geometrie und ihrem Widerstandsverhalten nicht der Realität entsprechend berücksichtigt wird.

3 Überblick über die Publikationen

Aus hydraulischer Sicht sind die räumliche Verteilung, die Form und die Materialeigenschaften wesentliche Parameter zur Charakterisierung der Flussvegetation. In diesem Kontext sind die Publikationen [1] bis [6] zu sehen.

Die Publikationen [1] und [2] basieren auf Arbeiten, die im Rahmen des internationalen Forschungsprojekts „Hydrodynamic Drag Measurements of Riparian Woodland Trees and Shrubs“ durchgeführt wurden. Gemeinsam mit ExpertInnen vom Hydro-Environmental Research Centre, Forest Research Centre (England) und vom Leichtweiß Institut für Wasserbau (Deutschland) wurden in einem Schleppkanal in Madrid (CEHIPAR) Versuche an lebensgroßen Ufergehölzen durchgeführt. In Summe wurde an 22 Bäumen (*Salix* ssp., *Alnus glutinosa* L. und *Populus alba* L.) bei unterschiedlichen Geschwindigkeiten die Widerstandskraft und das Strömungsverhalten (streamlining) der Pflanzen gemessen. Eines der Hauptziele dieser Studie bestand darin, die Schleppspannung-Fließgeschwindigkeits-beziehungen in hoher Auflösung zu untersuchen und somit das Verhalten von flexibler, verholzter Vegetation unter Strömungsbelastung mit (i) ihren physikalischen Eigenschaften und (ii) den verschiedenen Zuständen der Flächenkontraktion in Beziehung zu setzen. Um die induzierten Widerstandskräfte von Pflanzen unter hydraulischer Belastung zu bestimmen, wurden die Weiden kopfüber auf einem Wagen in einem Schleppkanal montiert. Die Vegetation wurde am beweglichen Wagen befestigt und in den Kanal eingetaucht. Der Wagen wurde in Längsrichtung entlang des Kanals bewegt, die Vegetation durch das Wasser gezogen und die Widerstandskraft gemessen. Vor dem Eintauchen in den Kanal wurden die Proben von vorne und von der Seite fotografiert, um eine gemittelte projizierte Fläche zu erhalten. Die Pflanzenfotos wurden verwendet, um die frontale Projektionsfläche sowie die Kronenfläche zu bestimmen, indem eine umgebende Formlinie gezeichnet und die umschlossene Fläche bestimmt wurde. Zusätzlich wurden nach den Versuchen die Trockenbiomasse und die Blattflächen aufgeteilt und in 4 Höhenstufen der Gesamthöhe der Pflanzen gemessen. Über die Unterwasserkameras wurden die Pflanzhöhenreduktion sowie die Reduktion der Pflanzenbreite unter Belastung bestimmt.

Publikation [3] beschäftigt sich mit dem Biegeverhalten von potentiellen Gehölzarten für ingenieurbiologische Zwecke in Südbrasilien. Es wurden die Biegeeigenschaften ausgewählter Pflanzen untersucht, um neben den biologischen auch die technischen Eigenschaften bei der Auswahl von Pflanzen für ingenieurbiologische Projekte in Südbrasilien zu berücksichtigen. Das Biegeverhalten einer ingenieurbiologisch eingesetzten Pflanze ist verantwortlich dafür, ob die Pflanze im flexiblen Zustand zum Schutz der Böschung beitragen kann, oder im starren Zustand für das Auslösen von Erosionsprozessen verantwortlich ist. Dabei sind sowohl eine genetische Veranlagung der Art, die lokalen Umwelteinflüsse sowie eine zeitliche Wachstumsentwicklung zu berücksichtigen. An 50 Exemplaren der Arten *Phyllanthus sellowianus* M. A., *Sebastiania schottiana* M. A., *Salix humboldtiana* W. und *Salix × rubens* S. wurden statische Biegebelastungstest durchgeführt. Die Biegeversuche basieren auf der DIN Norm 52186 (1978) für 3-Punkt Biegeprüfungen am Holz. Ziel war es, für die ausgewählten Arten durchmesserspezifische Spannungs-Dehnungs-Diagramme zu erstellen, die als Grundlagen für die Ermittlung des elastischen und plastischen Biegeverhaltens dienen. Die Proben wurden mit Rinde und unmittelbar nach der Ernte in frischem Zustand getestet. Die eingeleitete Kraft, die Durchbiegung im Zentrum des Probestücks und die Zeit wurden automatisch aufgezeichnet. Mit diesen Daten konnten der Elastizitätsmodul, die elastische und plastische Dehnung, die maximale Biegesteifigkeit und das Trägheitsmoment bestimmt bzw. berechnet werden. Nach jedem Versuch wurden der Feuchtegehalt, die Dichte, der prozentuelle Anteil der Rinde und das Alter des Versuchsstücks gemessen. Diese Parameter haben einen Einfluss auf die Biegeeigenschaften der Probestücke.

Publikation [4] gibt dazu einen Literaturüberblick über Forschungsarbeiten, welche sich mit dem überspannenden Thema der Publikation befassen. Dabei wurden die wichtigsten Arbeiten miteinander in Zusammenhang gebracht und Wissenslücken aufgezeigt. Die Publikation diente als Konzept und Leitfaden für weiterführende Arbeiten.

Ziel der Publikation [5] war es, die räumliche Verteilung sowie topologische Informationen der Äste und Astordnungen verschiedener Au-typischer Gehölze zu erfassen und diese in Relation mit dem Kontraktionsverhalten unter Strömungsbelastung zu untersuchen. Die Untersuchungen wurden in Zusammenarbeit mit dem Department of

Civil and Environmental Engineering der Aalto University in Helsinki im Rahmen eines gemeinsamen Forschungsprojektes durchgeführt. Die autypischen Arten Schwarzerle (*Alnus glutinosa* L.), Weissbirke (*Betula pendula* Roth), Moorbirke (*Betula pubescens* Ehrh.) und Sal-Weide (*Salix caprea* L.) wurden untersucht. Dabei sind insgesamt 20 Exemplare mit unterschiedlicher Morphologie und Pflanzenhöhen von 0,9 bis 3,3 m vermessen und anschließend analysiert worden. Die Pflanzenarchitektur wird in Form von Achsen und Segmenten unterschiedlicher Ordnungen beschrieben und basiert auf den Multi-Scale-Tree-Graph- (MTG) Formalismen (Godin & Caraglio, 1998). Die Pflanzenvermessung erfolgte mittels des Instruments Polhemus Fastrak. Das Prinzip der Vermessung basiert auf einem Bewegungs-Verfolgungs-System, welches sich mittels Induktion von 2 dreidimensionalen elektromagnetischen Feldern (EMF) untereinander räumlich orientieren kann. Dabei wird ein größeres EMF-Feld (Radius ca. 4.5 m) mittels drei Spulen generiert, in welchem man sich durch ein zweites generiertes EMF-Feld wieder basierend auf 3 Spulen die Orientierung und räumliche Position des kleinen EMF-Senders errechnen kann. Zu Vermessung wird die Pflanze beginnend mit dem Hauptstamm entlang aller Ast-Verzweigungen unterschiedlichster Ordnung punktweise mit dem Instrument digitalisiert. Der Durchmesser wird bei jedem aufgenommen 3D-Punkt manuell dazu gemessen. Aus diesen Daten wird mittels der Aufnahmesoftware Piafdigit und XPLO ein 3D-Modell der Pflanze erstellt. Dieses reale geometrische Pflanzenmodell bildet die Grundlage für die weiteren Analysen. Die projizierte Fläche ergibt sich aus Multiplikation der Länge mit dem Durchmesser eines Segments. Jedes Segment ist räumlich zuordenbar, somit ist eine vertikale Verteilung aller angeströmten Pflanzflächen im Gegensatz zu photographischen Aufnahmen (Überlagerung mehrerer Astteile) möglich. Für die Berechnung der Porosität einer Pflanze wurde eine Referenzfläche aus maximaler Gehölzbreite und Gehölzhöhe herangezogen. Für alle Individuen zeigte sich hinsichtlich des basalen Durchmessers und der gesamten projizierten Fläche ein linearer Zusammenhang.

Nach der Erfassung der Pflanzenstruktur wurden die Baumproben im Aalto University Schleppkanal hydrodynamischen Belastungen ausgesetzt. Zugkräfte wurden direkt mit Kraftmessdosen gemessen. Die Bäume wurden in belaubten und unbelaubten Zustand in einem Geschwindigkeitsbereich von 0,1 bis 1,5 m/s in verschiedenen Geschwindigkeitsschritten durchgezogen. Das Videomaterial wurde von zwei Kameras

aufgenommen, die an der Seite und hinter der Schlepprichtung in einem Abstand von 3 m bzw. 5,5 m angebracht waren. Die Kameraaufnahmen wurden dazu verwendet, die reduzierten Höhen und die kontrahierte Breite der Gehölze zu messen.

Das Ziel von Publikation [6] war es, den Einfluss der architektonischen Eigenschaften junger Ufergehölze (*Salix purpurea* L.) auf deren dynamisches Verhalten zu bestimmen und damit die physikalische Charakterisierung von Ufergehölzen in ingenieurbiologischen Systemen zu verbessern. Die Experimente wurden im Labor des Instituts für Ingenieurbiologie und Landschaftsbau durchgeführt. Die zu untersuchenden Gehölzexemplare wurden von einer Weidenkultur im Versuchsgarten des Instituts geerntet. Alle Exemplare (Hauptstamm mit mehreren Seitenästen) wurden aus mehrstämmigen Purpurweidenexemplaren (*Salix purpurea* L.) entnommen, welche fast 4 Jahre alt waren. Die drei Exemplare wurden so ausgewählt, dass ein breites Spektrum architektonischer Variabilität (Morphologie und Höhe) abgedeckt wird. Zur Bestimmung des Schwingungsverhaltens und der Berechnung der natürlichen Frequenz sowie des Dämpfungsgrades wurden die Weiden am Fuß in eine feste Vorrichtung eingespannt und durch ein Seil in eine Richtung gezogen. Durch das Abschneiden des gespannten Seiles wurden die Gehölze in Schwingung versetzt. Die Schwingungsbewegung wurde durch ein Bewegungsverfolgungssystem, welches auf Elektromagnetische Felder aufbaut (Polhemus Fastrak), mit 30 Hz gemessen. Nach wiederholten Messungen wurden die Äste der 5. Ordnung entfernt und die Versuche wiederholt. Dies wurde solange fortgeführt, bis nur noch die Hauptachse der Pflanze übrigblieb. Die Architektur der Gehölze wurde ebenso wie bei der Publikation [5] digitalisiert.

4 Ergebnisse der Forschungsarbeiten

Die Ergebnisse der Schleppversuche in Publikation [1] bestätigen die Erkenntnisse von Oplatka (1998), dass bei flexiblen Gehölzen die Kraft linear mit der Geschwindigkeit zunimmt. Newtons Gesetz des Widerstands impliziert, dass die Kraft mit der Geschwindigkeit im Quadrat zunimmt. Bei hydraulisch belasteten Pflanzen gilt diese Beziehung aufgrund der Flächenänderung und der sich verändernden Materialeigenschaften nicht. Die Versuche zeigen, dass Pflanzen ab einer gewissen Belastung nicht mehr flexibel reagieren und sich aus hydraulischer Sicht als starre Elemente verhalten. Folglich weicht die Beziehung von Kraft und steigender Pflanzhöhenreduktion von einer linearen Verteilung ab.

Bei weiterführenden Analysen in Publikation [2] zeigt sich, dass auch bei geringer Geschwindigkeit die Pflanze sich wie ein starrer Körper verhält, während sich bei größeren Geschwindigkeiten die Widerstandskraft auf Grund der Höhen- und Seitenkontraktion linear verhält (Wilson, et al., 2008). Ein ähnliches Verhalten von Pflanzen unter hydrodynamischer Belastung zeigen die Arbeiten von Schoneboom & Aberle (2009). Bei höheren Geschwindigkeiten spielt die Belaubung für das Widerstandsverhalten mit 24,4% bis 54,8 % eine große Rolle. Im Bereich des linearen Zusammenhangs von Widerstandskraft und Geschwindigkeit wurden der Widerstandskoeffizient und die angeströmte Fläche bestimmt.

Bei den Forschungsarbeiten zu Publikation 1 und 2 wurden die angeströmten Flächen der Proben von vorne und von der Seite fotografiert, um eine gemittelte projizierte Fläche zu erhalten. Die Pflanzenfotos wurden verwendet, um die frontale Projektionsfläche sowie die Kronenfläche zu berechnen, indem eine umgebende Formlinie gezeichnet und die umschlossene Fläche bestimmt wurde. Zusätzlich wurden Biomassedaten für 4 verschiedene Höhenstufen erhoben. Die Aufnahmemethodik der angeströmten Flächen der Pflanze in der integralen Form erwies sich dabei als mäßig zufriedenstellend, da der Detailierungsgrad der erhaltenen geometrischen und topologischen Information sehr gering war. In den Forschungsarbeiten zur Publikation [5] und [6] wurde auf Basis dieser Erkenntnis eine andere Methode gewählt.

Im Zuge der Forschungsarbeiten zu Publikation 3 wurde ein 3-Punkt Biegeprüfverfahren verwendet, um die technischen Eigenschaften von 4 potentiellen ingenieurbiologischen Gehölzen für die Region Südbrasiliens zu bestimmen. *Phyllanthus sellowianus* M.A. zeigte dabei die höchste Biegesteifigkeit bei gleichen Durchmessern, *Salix humboldtiana* W. hingegen war jene Art mit der höchsten Flexibilität. Bei größeren Durchmessern bzw. mit höherem Alter kam es zu einer leichten Abnahme des Elastizitätsmoduls, ein ähnliches Verhalten wird bei Niklas (1992) und Brüchert, et al. (2003) beschrieben. Die ermittelten Elastizitätsmodule waren im Vergleich zu den bestehenden Forschungsergebnissen am Institut für Ingenieurbiologie und Landschaftsbau für die Gehölzarten *Alnus glutinosa* L., *Fraxinus excelsior* L., *Salix alba* L., *Salix caprea* L. und *Acer pseudoplatanus* L. geringer (Vollsinger, et al., 2000). Die Bruchfestigkeit ist neben dem Elastizitätsmodul, welcher das elastische Verhalten des Materials beschreibt, für ingenieurbiologische Fragestellungen von besonderer Bedeutung, da eine Pflanze auch nach Überschreiten der elastischen Grenze seine Eigenschaften regenerieren und erst ab dem Bruch ihre Funktion nicht mehr erfüllen kann. Die Unterschiede zwischen den Arten sind im plastischen Dehnungsbereich wesentlich größer als im elastischen Bereich. *Phyllanthus sellowianus* M.A. erreicht die höchsten Bruchspannungen. Zusätzlich wurde für die einzelnen Arten der Biegewinkel im elastischen Bereich und bei maximaler Belastung berechnet. Bei einem Durchmesser von 20 mm zeigt *Phyllanthus sellowianus* M.A. maximale Biegewinkel von 45°, während ein Probestück von *Salix x rubens* S. einen maximalen Winkel von 25° erreicht. Bei größeren Durchmessern nimmt der maximale Bruchwinkel ab. Die artspezifische Beziehung von Durchmesser und Alter wurde abschließend mit dem maximalen Bruchwinkel gekoppelt. Die Entwicklung des Durchmessers ist sehr stark von lokalen standörtlichen und klimatischen Bedingungen abhängig. Die Ergebnisse dieser Forschungsarbeit zeigen die charakteristischen technischen Eigenschaften von Arten, die bei ingenieurbiologischen Arbeiten in Südbrasilien eingesetzt werden. *Phyllanthus sellowianus* M.A. und *Salix humboldtiana* W. weisen günstigere Eigenschaften hinsichtlich Erosionsschutz von Uferböschungen, Biegewinkel und Bruchfestigkeit und Pflanzenwachstum auf. Die Arten *Sebastiania schottiana* M.A. und *Salix x rubens* S. benötigen für ähnliche Erosionsschutzeigenschaften Pflegeschnitte, um das erforderliche Maß an Flexibilität zu erhalten.

Aufbauend auf die Forschungsarbeiten zu Publikation [1] und Publikation [2] wurde bei den Forschungsuntersuchungen zu Publikation [5] und [6] eine neue Methodik angewandt, welche die Pflanzenarchitektur mit topologischen und geometrischen Eigenschaften sehr detailliert beschreibt und aus dem erstellten digitalen Pflanzenmodell verschiedenste Informationen extrahiert. Dabei wurden 4 unterschiedliche Auenspezifische Gehölze in ihrer Architektur und in ihrem Strömungsverhalten untersucht. Die Ergebnisse zeigen, dass der basale Durchmesser und die projizierte Fläche der Exemplare eine lineare Korrelation hatten. *Salix caprea*-L. Exemplare zeigten im Vergleich zu *Alnus glutinosa*-Exemplaren im Vergleich zum Basaldurchmesser eine höhere projizierte Gesamtfläche. Die Korrelation der gesamten Projektionsfläche und der Gesamthöhe der Bäume zeigt eine logarithmische Beziehung. Dies kann durch den Pioniercharakter der Pflanzen erklärt werden. Der Anteil des Hauptstammes an der gesamten Projektionsfläche liegt unter 50%. Im Mittel haben die Seitenäste einen Anteil von 55-60% an der gesamten projizierten Fläche. Der Anteil der Seitenäste an der gesamten Projektionsfläche ist bei größeren Individuen (Höhe > 2 m) um bis zu 4-mal höher im Vergleich zum Anteil des Hauptstammes. Daraus folgt, dass die Seitenäste einen hohen Beitrag zum Gesamtwiderstandsverhalten einer Pflanze leisten.

Die untersuchten Gehölzexemplare zeigen ein breites Spektrum in der kumulativen projizierten Astfläche und im Volumen über die Höhe. Kleinere Exemplare (bis zu ~ 2 m) weisen eine fast lineare Korrelation der kumulativen projizierten Astfläche über die Höhe auf. Im Gegensatz dazu zeigen größere Exemplare eine stärkere Zunahme der projizierten Astfläche über die Höhe. Die ermittelten Projektionsflächen variieren im Speziellen bei größeren Individuen signifikant. Dies ist möglicherweise auf den für „ingenieurbiologische Baumarten“ charakteristischen Pioniercharakter zurückzuführen. Je nach Standort, Alter und lokaler klimatischer Bedingungen zeigt die Pflanze ein individuelles Höhen- und Breitenwachstum.

Beim artenspezifischen Vergleich der projizierten Astflächen über die Höhe zeigt sich, dass sich die Schwarzerle von der Sal-Weide deutlich unterscheidet. Schwarzerlenexemplare zeigen bei einer relativen Höhe zwischen 0,125 und 0,625 ihren größten Anteil der projizierten Astflächen. Salweiden Exemplare hingegen zeigen den größten Anteil der projizierten Astflächen von 0,375 bis 0,875 der relativen Gesamthöhe.

Nimmt man für beide Arten ähnliche Materialeigenschaften an, so ist der hydraulische Widerstand im unteren Teil der Pflanzen für Schwarzerlen im Vergleich zu Salweiden aufgrund des höheren Anteils der projizierten Astfläche höher. Deshalb kann auch ein unterschiedliches Kontraktionsverhalten zwischen den Arten bei Überschwemmungen angenommen werden, da der Wasserstand von der Gehölzbasis zur Spitze der Gehölze steigt. Die Unterschiede in der Verteilung der einseitigen Stammfläche über die Höhe können durch den Pioniercharakter der Arten erklärt werden. Beide Arten sind bekannte Pioniergehölze, welche vegetationsfreie Flächen besiedeln. Es zeigt sich jedoch, dass die Salweide ein schnelleres Höhen-Wachstum hat und dort eine größere Verzweigungsrate aufweist.

Mit der Interaktion von Pflanze und Strömung ändern sich durch die Höhen- und Breitenkontraktion der Pflanzen wichtige Vegetationsparameter wie der Widerstandskoeffizient mit der angeströmten Fläche und die Porosität. Eine wichtige Eigenschaft der ufernahen Vegetation ist das Biegeverhalten von Vegetationselementen unter Belastung. Die Neuheit der Untersuchungen ergab sich aus der Charakterisierung der Rekonfiguration der Gehölze, die durch die Kombination aus den Parametern der kontrahierten Breite, der reduzierten Höhe und der projizierten Unterwasserfläche der Gehölze erreicht wurde, um die Porosität bei verschiedenen Geschwindigkeiten zu bestimmen. Die durch die Strömung induzierte Breitenkontraktion trug signifikant zur Verringerung der von der Pflanze eingenommenen rechteckigen Querschnittsfläche bei. Die Porosität der blättrigen Bäume nahm bei den niedrigeren Geschwindigkeiten zu und dann bei höheren Geschwindigkeiten ab. Der anfängliche Anstieg der Porosität kann durch die Reduktion der angeströmten Fläche durch das Anlegen der Blätter an die Äste erklärt werden, wobei sich die Gehölzstruktur selbst noch wenig kontrahiert. Anschließend erfolgt die ansteigende Seiten- und Höhenkontraktion der Gehölzstruktur, womit die Porosität verringert wird.

Die Forschungsarbeit zu Publikation [6] wurde durchgeführt, um die architektonischen Eigenschaften junger *Salix purpurea*-Gehölze mit ihren dynamischen Eigenschaften (Eigenfrequenzen und Dämpfungsgrad) in Beziehung zu setzen. Die drei ausgewählten Exemplare spiegeln die breite Variabilität des Wachstums dieser Pionierart wieder. Aus Gehölzarchitektonischer Sicht wurde ein großer Unterschied der Gehölzexemplare

hinsichtlich der Verteilung der projizierten Fläche entlang der Baumhöhen und für das Längen-Durchmesser-Verhältnis über die Achsenordnungen gefunden. Die Baumproben oszillierten visuell erkennbar bis zu 7-8 Sekunden. Insbesondere bei vollblättrigen Bedingungen wurde jedoch eine schnelle Rückkehr in die Ruheposition beobachtet. Die Eigenfrequenz (f_n) variierte nicht wesentlich zwischen den Schwingungszyklen oder an verschiedenen Positionen auf dem Hauptstamm. Unsere Ergebnisse zeigten, dass die natürliche Frequenz der Achse zweiter Ordnung jener des Hauptstamms sehr ähnlich war.

Alle Achsenordnungen haben Einfluss auf die natürliche Frequenz der Ufergehölze. Die Reduktion der Biomasse führt zu einer Zunahme der natürlichen Frequenz ab der ersten Entfernung der höchsten Achsenebene und erhöht sich zunehmend während weiterer Achsenentnahmen. Die normalisierte natürliche Frequenz (f_n/f_{n_tot}) zeigt während aller Schnittphasen eine lineare Korrelation mit der Biomasse.

Der Einfluss der Blätter der Gehölze ist hinsichtlich Dämpfungsgrad (ζ) signifikant, jedoch hängt dies stark vom Längen-Durchmesser-Verhältnis der zugrunde liegenden Achsenordnungen ab. Ein hohes Längen-Durchmesser-Verhältnis der Gehölzachsen erhöhte die Flexibilität des Astsystems und reduzierte die Auswirkungen der Blätter auf den Dämpfungsgrad. Im Vergleich dazu führt ein niedriges Längen-Durchmesser-Verhältnis zu einer steiferen Gehölzstruktur, daher hatte der Dämpfungsgrad aufgrund des aerodynamischen Widerstands der Blätter einen höheren Anteil am Gesamtdämpfungsgrad. Gehölze mit flexiblen Achsen können aufgrund ihrer Rekonfiguration und einer damit einhergehenden Reduzierung der projizierten Fläche und einer Verringerung des Luftwiderstands die Energie besser ableiten. Das bedeutet, dass schlanke Achsen einer hohen potentiellen Anströmfläche der Blätter entgegenwirken können. Die technische Charakterisierung junger flexibler Pflanzen, die auf den Blattflächenindex oder anderen Indizes in Bezug auf die Blattfläche basieren, könnte daher zu falschen Annahmen führen. Aus fluid-dynamischer Sicht ist es daher wichtig, die projizierte Fläche, das Längen-Durchmesser-Verhältnis und das Blattwerk zu berücksichtigen.

5 Synthese und Schlussfolgerungen

Die Quantifizierung der ingenieurbiologischen Anwendungen ist aus technischer, ökologischer, sozial-ökonomischer sowie ästhetischer Sicht sinnvoll, da nur ein integraler Bewertungsansatz, der auch die zeitliche Entwicklung der Systeme berücksichtigt, zeitgemäß ist und die geforderten Ansprüche erfüllt.

Im Falle von ingenieurbiologischen Systemen interagieren Gehölze mit fluiddynamischen Belastungen während verschiedener Wachstumsphasen. Die Untersuchung von Materialeigenschaften einerseits, sowie deren Verteilung entlang der einzelnen Pflanzenachsen ist ein wichtiges Grundlagenwissen. Die Architektur von Gehölzen spiegelt, aufbauend auf ein 3-dimensionales Pflanzenmodell, die Verteilung von anströmbaren Flächen und die topologische Beziehung einzelner Achsen untereinander wider. Ein besseres Verständnis vom statischen sowie dynamischen Verhalten von Pflanzen unter Berücksichtigung ihres Alters, ihres Standortes und ihrer entsprechenden Architektur führt zu einer verbesserten Quantifizierung der Leistung von ingenieurbiologischen Systemen.

Eine Quantifizierung von der technischen Leistung der Ufervegetation ist eine Voraussetzung zu einem optimierten Einsatz und Pflege derselben. Der Einsatz von Pflanzen zur Sicherung von Flussufern erhöht die hydraulische Rauigkeit des Abflussprofils. Uferbewuchs und Auwaldsituationen können die Hochwasserganglinie abschwächen und den Ablauf von Hochwasserwellen in flussabwärts gelegene Städte verzögern. Die gezielte Wiederherstellung oder Schaffung von bewaldeten Überflutungsflächen kann einen wichtigen Beitrag zum Schutz der ländlichen und städtischen Gemeinden vor künftigen Überschwemmungen leisten und eine breite Palette weiterer Vorteile wie Kohlenstoffbindung, biologische Vielfalt, Erholung und verbesserte Wasserqualität bringen.

Die Modellierung von Abflüssen durch Auwälder bzw. Vegetationsgesäumte Flussufer wird jedoch durch fehlende Informationen zu Vegetation-Abfluss-Interaktionen eingeschränkt. In einer Zeit, in der die weitreichenden Vorteile der Revitalisierung und Wiederbepflanzung von Flussufern zunehmend im Hinblick auf ökologische und klimatische Vorteile anerkannt werden, ist es von entscheidender Bedeutung, dass das

Verständnis des Einflusses der Vegetation auf den hydraulischen Zustand des Gewässers mit den kontinuierlichen Verbesserungen der numerischen Verfahren zur hydrodynamischen Modellierung Schritt hält.

Die vorliegende Dissertation hat sich auf die technische Quantifizierung eines ingenieurbiologischen Systems konzentriert. Die Untersuchungen in dieser Arbeit haben gezeigt, dass eine Charakterisierung des Strömungswiderstandes von Gehölzen sehr komplex ist und von vielen Faktoren abhängen kann. Die Ergebnisse weisen darauf hin, dass die Architektur der Pflanze, und damit die vertikale und horizontale Verteilung der Astflächen, die Interaktion mit einem belastenden Prozess maßgeblich beeinflussen kann. Die Ergebnisse zeigen, dass eine Berücksichtigung der Pflanzenarchitektur das Verständnis der Interaktion Pflanze-Strömung wesentlich verbessert. Neben der horizontalen und vertikalen Verteilung der Astfläche ist auch deren topologischer Aufbau maßgebend. Die Verteilung der projizierten Ebenen pro Astordnung kann das Schwingungsverhalten, bzw. das Kontraktionsverhalten stark beeinflussen. Die Form der Äste sind mit den Materialeigenschaften und der Porosität der Struktur weitere wichtige Parameter, welche bei der Pflanzen-Strömungsinteraktion zu berücksichtigen sind. Es ist daher notwendig, ein Verständnis dafür zu entwickeln, dass es einerseits architektonische Unterschiede zwischen unterschiedlichen Arten gibt und dass andererseits diese architektonischen Unterschiede sehr stark von den lokalen Umgebungsbedingungen geprägt werden. Des Weiteren ist zu berücksichtigen, dass bei einem ingenieurbiologischen System die zeitliche Komponente eine Rolle spielt, da eine dynamische Pflanzenentwicklung gegeben ist.

Für zukünftige Forschungsarbeiten ist es wichtig, die Architektur von unterschiedlichen Gehölzen abhängig von Ihrem Lebensraum, ihrer zeitlichen Entwicklung und den auf ihnen wirkenden Prozessen zu untersuchen. Ein noch wenig untersuchter Zusammenhang ist das Zusammenspiel von oberirdisch und unterirdisch wirkenden Prozessen und ihre Interaktion mit der Pflanze. Die Übertragung der Kräfte, aus dynamischen Belastungen auf oberirdische Pflanzteile, auf unterirdische Pflanzteile ist noch weitgehend unbekannt.

Mit der vorliegenden Dissertation konnten erste Gehölzarten hinsichtlich ihrer Architektur und ihrem Biegeverhalten untersucht werden. Die angewandten Methoden sind für die Erfassung von Einzelpflanzen geeignet. Zukünftig ist es wichtig, die Pflanzenarchitektur von den am Fließgewässer vorkommenden Arten zu erfassen, um die Rauheit der Pflanzen in einem hydrodynamischen Modell berücksichtigen zu können.

Aus praktischer Sicht ist eine Aufnahme der Gehölzarchitektur auf jenem Detailierungsgrad, wie er in den Publikationen beschrieben wurde, jedoch kein praktikabler Zugang für einen Flussbauingenieur, der das Abflussverhalten von bewachsenen Uferböschungen modellieren muss. Ein nächster Schritt ist die Einbindung und Validierung von 3D-Gehölzmodellen in Simulationsmodelle, mit welchen eine Abstrahierung der gewonnenen Ergebnisse möglich ist. Die Weiterentwicklung bei automatisierten Aufnahmeverfahren wie LIDAR lässt bereits jetzt eine hohe Extrahierung von morphologischen Vegetationsparametern zu. Eine Kombination von automatisiert erfassbaren Daten sowie einer verbesserten Vegetations-Strömungsmodellierung eröffnet Möglichkeiten, mit welcher in Zukunft natürliche Gewässerabschnitte realitätsnah hydrodynamisch modelliert werden können. Für Erreichung dieser Ziele bedarf es intensiver interdisziplinärer Forschungsarbeiten.

Die Koppelung des „lebenden“ Baustoffs Pflanze in ihrer zeitlichen und räumlichen Entwicklung mit bautechnischen Belastungsansätzen und ökologischen Wirkungen ist eine Herausforderung, um Lösungsansätze für das Spannungsfeld Technik-Ökologie und Ästhetik über die gesamte Lebensphase zu entwickeln. Dadurch werden Voraussetzungen geschaffen, damit sich die Ingenieurbiologie als Disziplin in der Ingenieurpraxis nachhaltig etabliert.

6 Literatur

Aberle, J., Järvelä, J. (2013): Flow resistance of emergent rigid and flexible vegetation. Journal of Hydraulic Research 51(1): 33-45. doi: 10.1080/00221686.2012.754795.

Aberle, J., and Järvelä, J. (2015): Hydrodynamics of vegetated channels, In: Rowinski, P. and Radecki-Pawlik, A. (eds) "Rivers – physical, fluvial and environmental processes." GeoPlanet: Earth and Planetary Sciences, Springer, Berlin, 519-541. DOI: 10.1007/978-3-319-17719-9_21.

Armanini, A., Righetti, M. and Grisenti, P. (2005): Direct measurement of vegetation resistance in prototype scale, J HYDRAUL RES, 43(5), 481–487.

Barthèlèmy D., Caraglio Y. (2007): Plant architecture: a dynamic, multilevel and comprehensive approach to plant form, structure and ontogeny. Ann. Bot. Lond. 99(3), 375–407, http://dx.doi.org/10.1093/aob/mcl260.

Bischetti, G.B., di fi Dio, M., Florineth, F. (2012): On the origin of soil bioengineering. Landsc. Res. 39, 583–595, http://dx.doi.org/10.1080/01426397.2012.730139 .

Burylo, M., Rey, F., Delcros, P. (2007): Abiotic and biotic factors influencing the early stages of vegetation colonization in restored marly gullies (Southern Alps, France). Ecol. Eng. 30, 231–239.

Brüchert, F., Gallenmüller, F., Bogenrieder, A., Speck, T. (2003): Stem Mechanics, Functional Anatomy and Ecology of Alnus viridis and Alnus glutinosa. Journal of Botanical Taxonomy and Geobotany; Feddes Repertorium; Berlin, pp. 181-197.

DVWK (1991): Hydraulische Berechnung von Fließgewässern. Merkblätter zur Wasserwirtschaft, 220, Verlag Paul Parey, Hamburg/Berlin, in German.

DWA (2018): Hydraulische Berechnung von Fließgewässern mit Vegetation, in Druck

Evette, A., Labonne, S., Rey, F., Liebault, F., Jancke, O., Girel, J. (2009): History of bio-engineering techniques for erosion control in rivers in western Europe. Environ.Manag. 43, 972–984, http://dx.doi.org/10.1007/s00267-009-9275-y .

Fathi-Maghadam, M. und Kouwen, N. (1997): Nonrigid, Nonsubmerged, Vegetative Roughness on Floodplains, J HYDRAUL ENG-ASCE, January 1997, 123 (1), 51-57, (doi: 10.1061/(ASCE)0733-9429(1997)123:1(51)).

Fernandes, J.P., Guiomar, N. (2016): Simulating the stabilization effect of soil bioengineering interventions in mediterranean environments using limit equilibrium stability models and combinations of plant species. Ecol. Eng. 88, 122–142. https://doi.org/10.1016/j.ecoleng.2015.12.035.

Florineth, F. (2012). Pflanzen statt Beton. Sichern und Gestalten mit Pflanzen. 2. Auflage. Patzer Verlag Berlin-Hannover.

Freeman, G., Rahmeyer, W. and Copeland, R.R. (2000): Determination of resistance due to shrubs and woody vegetation, US Army Corps of Engineers Engineer Research and Development Centre Report No. ERDC/CHL TR-00-25.

Gardiner, B.A. (1995): The interactions of wind and tree movement in forest canopies. Wind and Trees, pp. 41-59.

Gerstgraser, C. (2000): Ingenieurbiologische Bauweisen an Fließgewässern. Grundlagen zu Bau, Belastbarkeiten und Wirkungsweisen. Wien: Österr. Kunst- u. Kulturverlag.

Godin, C., Caraglio, Y. (1997): A Multiscale Model of Plant Topological Structures. In: Journal of Theoretical Biology 191 (1998), Elsevier, S.1-46.

Gray, D.H., Sotir, R.B. (1996): Biotechnical and Soil Bioengineering Slope Stabilization, A Practical Guide for Erosion Control. J. Wiley & Sons Inc., New York.

Hacker, E. (Ed.), 2015. European Guidelines for Soil and Water Bioengineering. European Federation for Soil Bioengineering, Aachen.

Hacker, E., Johannsen, R. (2012): Ingenieurbiologie. s.l.: Ulmer Verlag Stuttgart.

Jalonen, J., Järvelä, J. and Aberle, J. (2013): Leaf area index as vegetation density measure in hydraulic analyses, J HYDRAUL ENG, 139(5): 461-469. DOI: 10.1061/(ASCE)HY.1943-7900.0000700.

Jalonen, J., Järvelä, J. (2014): Estimation of drag forces caused by natural woody vegetation of different scales. Journal of Hydrodynamics 26(4):608-623. doi: 10.1016/S1001-6058(14)60068-8

Järvelä, J. (2002): Determination of flow resistance of vegetated channel banks and flood plains. Proc. Int. Conf. River Flow 2002, Louvain-La-Neuve, 311–318, D. Bousmar, Y. Zech, eds. A.A. Balkema, Rotterdam, NL, 311-318, ISBN 9058095096.

Järvelä, J. (2004): Determination of flow resistance caused by non-submerged woody vegetation, JRBM, 2(1): 61-70, DOI: 10.1080/15715124.2004.9635222.

Järvelä, J., Aberle, J., Jalonen, J. (2016): Dynamic reconfiguration of riparian trees in towing tank experiments. River Flow 2016 – Constantinescu, Garcia & Hanes (Eds) ISBN 978-1-138-02913-2.

Kane, B., James, K.R. (2011): Dynamic properties of open-grown deciduous trees. Canadian Journal of Forest Research, 41 (2), 321-330. doi: 10.1139/X10-211.

Kuipers, J. (1975): United States Patent 3,868,565: Object tracking and Orientation determination means, system and process.

Kuipers, J. (1977): United States Patent 4,017,858: Apparatus for generating a nutating electromagnetic Field.

Li, M.H., Eddleman, K.E., (2002): Biotechnical engineering as an alternative to traditional engineering methods. A biotechnical streambank stabilization design approach. Landsc. Urban Plan. 60, 225–242, http://dx.doi.org/10.1016/S0169-2046(02)00057 .

Luhar, M., Nepf H.M. (2013): From the blade scale to the reach scale: A characterization of aquatic vegetative drag, Adv. Water Resour. 2013, 51:305-316.

Milne, R. (1991): Dynamics of swaying of Picea sitchensis. Tree- Physiology, 9 (3), 383-399.

Moore, J.R., Maguire, D.A. (2005): Natural sway frequencies and damping ratios of trees: influence of crown structure. Trees (Berl.), 19(4): 363–373. doi:10.1007/s00468-004-0387-y.

Moore, J.R., Maguire, D.A. (2008): Simulating the dynamic behavior of Douglas-fir trees under applied loads by the finite element method. Tree Physiology, 28 (1), 75-83.

Niemtz, P. (1993): Holz, in 3 Bänden. Physik des Holzes und der Holzwerktstoffe. 1. Auflage. Braun, Karlsruhe. ISBN 3871813249

Niklas, K. (1992): Plant Biomechanics - an Engineering Approach to Plant Form and Function. Press Chicago & London, pp 607 Hrsg. Chicago: University of Chicago.

Niklas, K., Spatz H.C. (2012): Plant Physics. The University of Chicago press, Ltd., London pp. 426, Chicago and London.

Nixon, M.A. et al. (1998): The Effects of Metals and Interfering Fields on Electromagnetic Trackers. In: Presence, Vol. 7, No.2, April 1998, Massachusetts Institute of Technology.

Oplatka, M. (1998): Stabilität von Weidenverbauungen an Flussufern, Diss. Techn. Wiss. ETH Zürich, Nr. 12575, DOI: 10.3929/ethz-a-001920916.

Peltola, H. (2006): Mechanical stability of trees under static loads. Am. J. Bot. 93(10), 1501–1511. doi:10.3732/ajb.93.10.1501.

Polhemus (2005): 3Space™ Fastrak® User´s Manual, Revision E. Polhemus, Colchester, VT.

Raab, F.H. et al. (1979): Magnetic Position and Orientation Tracking System. In: IEEE Transactions on Aerospace and Electronic Systems Vol. AES-15, No.5. 1979.

Rauch, H.P. (2005): Hydraulischer Einfluss von Gehölzstrukturen am Beispiel der ingenieurbiologischen Versuchsstrecke am Wienfluss. Dissertation an der Universität für Bodenkultur Wien, 222 pages.

Righetti, M. (2008): Flow analysis in a channel with flexible vegetation using double-averaging method, ACTA GEOPHYS, 56 (3), 801–823, DOI: 10.2478/s11600-008-0032-z.

Schoneboom, T., Aberle, J. (2009): Influence of foliage on drag force of flexible vegetation. 33rd IAHR Congress, Vancouver, Canada, Papers on CD-Rom.

Sellier, D., Fourcaud, T. (2005): A mechanical analysis of the relationship between free oscillations of Pinus pinaster Ait. saplings and their aerial architecture. J. Exp. Bot. 56(416): 1563–1573. doi:10.1093/jxb/eri151.

Sellier, D., Fourcaud, T. (2009): Crown structure and wood properties: influence on tree sway and response to high winds. Am. J. Bot. 96(5): 885–896. doi:10.3732/ajb.0800226.

Sinoquet, H., Rivet, P. (1996): Measurement and visualization of the architecture of an adult tree based on a three-dimensional digitising device. In: Trees 11 (1997). Springer Verlag 1997.

Sinoquet, H., Rivet, P., Godin, C. (1997): Assessment of the Three-dimensional Architecture of Walnut Trees Using Digitising. In: Silva Fennica 31(3). The Finnish Society of Forest Science and The Finnish Forest Research Institute (Hrsg.).

Spatz, H.C., Köhler, L., Niklas, K.J. (1999): Mechanical behaviour of plant tissues: composite materials or structures? , Journal of Experimental Biology 202, 3269-3272.

Spatz, H.-C., Brüchert, F. (2000): Basic biomechanics of self-supporting plants: Wind loads and gravitational loads on a Norway spruce tree. Forest Ecology and Management. 135. 33-44. 10.1016/S0378-1127(00)00296-6.

Schiechtl, H.M. (1988): Hangsicherungen mit ingenieurbiologischen Methoden im Alpenraum: Erosionsbekämpfung im Hochgebirge. Jahrb. Ges. Ingenieurbiol. 3,50–77.

Västilä, K., Järvelä, J., Aberle, J. (2013): Characteristic reference areas for estimating flow resistance of natural foliated vegetation, J HYDROL, 492, 49-60, DOI: 10.1016/j.jhydrol.2013.04.015.

Västilä, K., and Järvelä, J. (2014): Modelling the flow resistance of woody vegetation using physically based properties of the foliage and stem, WATER RESOUR RES, 50 (1), 229-245, DOI: 10.1002/2013WR013819.

Vollsinger, S. (2000): Biegsamkeit von Ufergehölzen als Grundlage für Pflegemaßnahmen. Zeitschrift für Ingenieurbiologie, Band Nr. 2, pp. 19-21.

Vollsinger, S., Doppler, F., Florineth, F. (2000): Ermittlung des Stabilitätsverhaltens von Ufergehölzen im Zusammenhang mit Erosionsprozessen an Wildbächen. Hrsg.: Institut für Landschaftsplanung und Ingenieurbiologie, Universität für Bodenkultur, Wien.

von der Thannen, M., Hörbinger, S., Paratscha, R., Smutny, R., Lampalzer, T., Strauss, A. und Rauch, H.P. (2017): Development of an environmental life cycle assessment model for soil bioengineering constructions, European Journal of Environmental and Civil Engineering, DOI: 10.1080/19648189.2017.1369460.

Weissteiner, C., Jalonen, J., Järvelä, J., Rauch, H.P. (2015): Spatial-structural properties of woody riparian vegetation with a view to reconfiguration under hydrodynamic loading. Ecological Engineering, 85,85-94. DOI: 10.1016/j.ecoleng.2015.09.053.

Whittaker, P., Wilson, C., Aberle, J., Rauch, H.P., Xavier, P. (2013): A drag force model to incorporate the reconfiguration of full-scale riparian trees under hydrodynamic loading. Journal of Hydraulic Research, 51 (5), 569-580. DOI: 10.1080/00221686.2013.822936.

Wilson, C.A.M.E., Yagci, O., Rauch, H.P., Stoesser, T. (2006): Application of the drag force approach to model the flow-interaction of natural vegetation, JRBM, 4 (2), 137-146; DOI: 10.1080/15715124.2006.9635283.

Wilson, C.A.M.E., Hoyt, J., Schnauder, I. (2008): Impact of foliage on the drag force of vegetation in aquatic flows. J. Hydraul. Eng., 134(7), 885-891.

Zeh, H. (2007): Ingenieurbiologie. Handbuch Bautypen. Vdf Hochschulverlag, Zürich.

7 Anhang

7.1 Publikation 1

Biomechanical behaviour of plants under hydraulic load

Report for the research service of the
University of Natural Resources and Applied Life Sciences, Vienna

March, 2009

Funded by the 6th European Framework Program
Hydralab III

and the
Post-graduation grant
of the University of Natural Resources and Applied Life Sciences, Vienna

Author:	Supervision:
	Univ. Ass. Dr. Hans Peter Rauch
DI Clemens Weissteiner	DI Walter Lammeranner
Institute of Soil Bioengineering and Landscape Construction Department of Civil Engineering and Natural Hazards	

1. Introduction

Vegetation-flow interactions are central to many problems of hydrologists and hydraulic engineers including flood risk assessment, sediment transport studies and eco-hydraulic studies. Furthermore climate change and floods have both become major issues for society and this, together with recent EU directives (Habitat Directive92/43/EEC; Water Framework Directive2000/60/EC) give these types of studies added significance.
The hydraulic interaction of flow with plants depends not only on geometrical properties (e.g. stem and branch diameter, length and leaf density), but also on the dynamic response of plants under flood conditions (stem/branch/leaf bending and reduction of plant height; e.g. FATHI-MOGHADAM & KOUWEN, 1997; OPLATKA, 1998; GERSTGRASER, 2000; MEIXNER, 2004; RAUCH, 2005. The mechanical properties like flexural stiffness, modulus of elasticity and plastic deformation are indicators to assess the impact of plants on hydraulic conditions.
Currently, flow resistance is assigned to vegetated channels and floodplains on an ad hoc basis (CHOW, 1959). The aim of this work was to develop physically-based understanding to quantify hydraulic resistance of plants as a function of their characteristics. This provides a basic knowledge to improve numerical modelling tools for integrated environmental and hydraulic management.
In determining separately the hydraulic resistance or drag induced by plant obstructions, we need to account for the peculiarities associated with vegetation such as its permeable, heterogeneous nature and its ability to bend and change the shape under flow action. In previous studies the drag force was measured directly (OPLATKA, 1998, FREEMAN et al., 2000, JAMES et al., 2004, ARMANINI et al., 2005 and WILSON et al 2008). These studies have measured the drag for a single plant using a load cell whereby its change in resistance due to a displacement (compression or extension) is related to a force.
This report represents the determination of the different tested plant samples as well as their performance under hydraulic load. Furthermore the correlations between geometrical plant parameters and the measured drag forces are analysed.

2. Methodology

The focus of the experimental program was to examine the relationship between the behaviour of the riparian vegetation specimens under varying velocity conditions and the drag force exerted.

In order to determine the induced drag forces by plants under hydraulic load, willows were mounted upside down on a carriage in a ship testing basin. The specimens have been attached to the moving carriage via an adjustable stem supporting frame and immersed in the tank (Figure 2). Moving the carriage longitudinally along the flume, the specimen was pulled through the water until it reached a constant velocity. Once at constant velocity, the force transmitted to the strain gauge transducer was recorded.

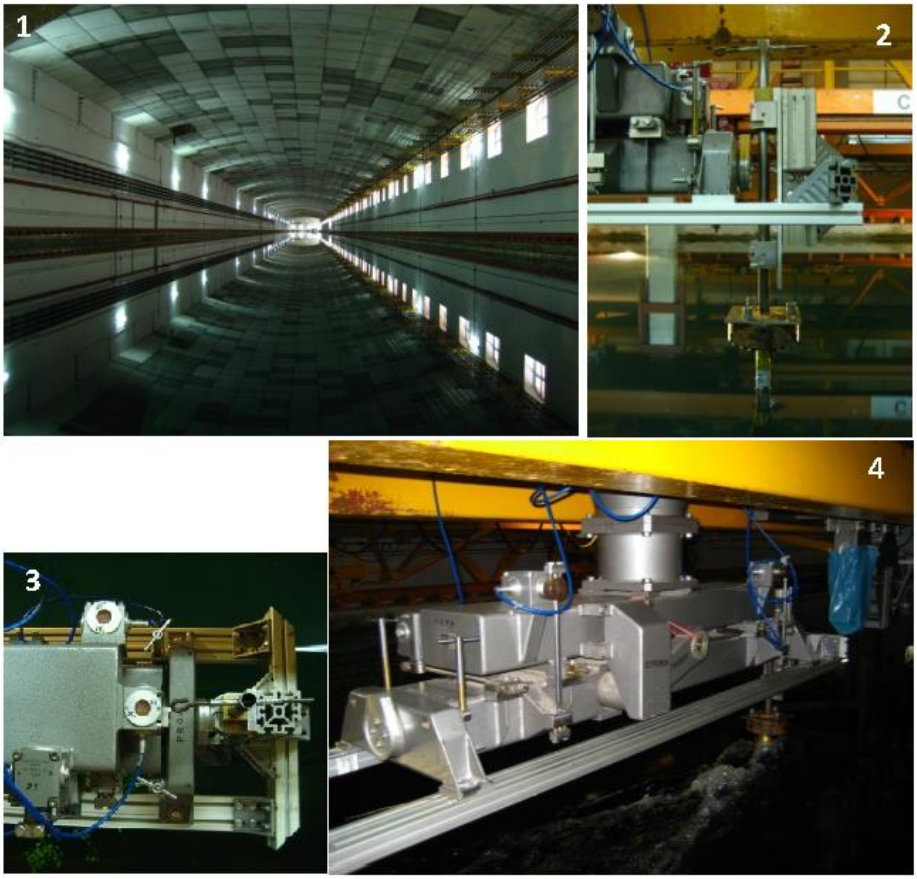

Fig. 1: Testing basin at El Pardo (1), side (2) and plane (3) view of the mounting device and carriage pulling plant through the channel (4)

The laboratory tests started in the end of March 2008 and ended on 24th of April 2008 and were carried out at the Hydralab facility in the ship testing basin of the Institute of Water Engineering, El Pardo, near Madrid.

The basin dimensions were 12,5 m wide, 6,5 m deep and 320 m long. The large width ensured that side wall effects didn't influence the measurements. The carriage could move up to 10 m/s, with an accuracy of approximately 1 mm/s. Tests were carried out in both directions. In order to save time several velocities were tested during one run. At least 2 measurements of each velocity were taken (forward and backward) to ensure consistency. More measurements were conducted when the measurements of the forward and backward runs showed inconsistencies.

Underwater cameras were mounted to film each plant at each run from the side and the front to capture its deflection. Potential interaction effects from the underwater cameras were tested by repeating runs with and without the submerged cameras.

In order to calibrate the measurement devices the first runs were carried out with a rigid steel cylinder. The regular shape of the cylinder allowed to test and to calibrate the

measurement devices and to detect potential sources of error that could occur. Potential errors that may influence the drag force measurements were:

a) Inherent random fluctuations

b) Influence from the wake of the submerged cameras

The recorded forces for the forward and backward runs were different at higher velocities. Potential reasons for this could be:

c) Inconsistencies in the fastening of the cylinder

d) Dimensional inconsistencies of the cylinder

The procedures of the calculations of the forces and lever arms have been established by a project partner from the Technical University in Braunschweig and are not analyzed in detail.

2.1 Plant parameters

The plant material was collected at a river near Madrid. Due to cold weather conditions not all plant samples were completely foliated. Samples of willows, different in size and species were selected to cover a broad range of growth habits (8 specimens of *Salix atrocinerea* Brot. and 5 specimens of *Salix alba* L.). Before immersing in the tank, the specimens have been photographed from the front and the side view to obtain an averaged projected frontal area. The plant photos were used to determine the frontal projected area as well as the crown area, by drawing a surrounding shape line and determining the enclosed area. The area was calculated by using Adobe Photoshop CS4 ver. 11 (Adobe Systems Incorporated) calculating the plant area as well as the area of a photographed ball (as reference area). A second method was used only for 3 willows to determine more precisely the photographed plant area. In this procedure every single part of the plant was selected manually. Beside plant height diameters were measured at different heights (25, 50 and 75 %).

After concluding the tests the plants were cut into 4 proportional height sections. The wood and leaf volume likewise their moist and dry mass were measured separately for the different height sections. For some plants even the leave area has been determined by scanning a sample of 100 hundred leaves of each plant. Due to the intensive time consuming measurements and the limited time range it wasn't possible to gather all geometrical parameters for every plant sample.

Snapshots from the video data were used to determine the reduced plant height. The frontal plant area reduction couldn't be calculated because of the image distortion caused by the change of the camera plant distance while carrying the plant through the channel. Due to the large height of different plant samples and a low distance between plant and side camera only on a few runs the whole plant could be videotaped. Mainly runs with high velocities were useable to determine the plant height reduction.

Snapshots were analyzed when the whole plants were visible on the image. The image distortion from the pictures of the side camera has been considered negligible. The following figure shows one snapshot series.

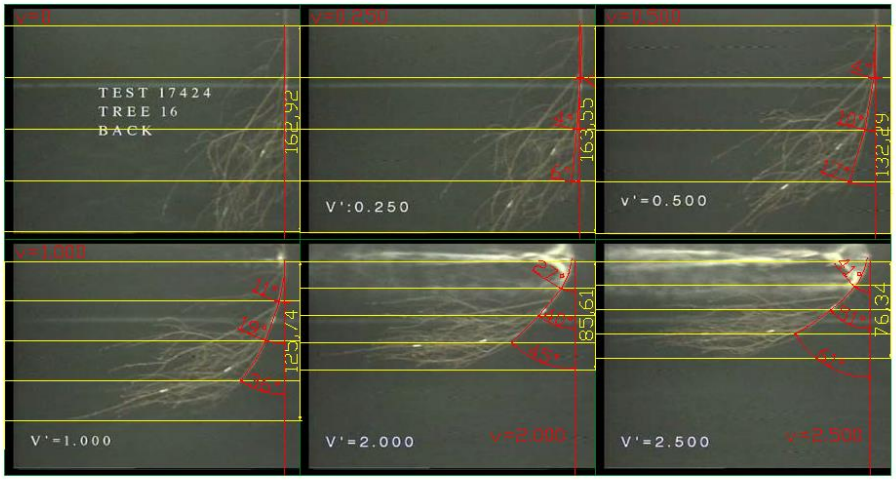

Fig. 2: Screen shot series of Salix 4 while carrying through the channel

Finally geo-statistical analyses were done to find correlations between plant parameters and the induced drag forces of the test runs.

3. Results

3.1 Plant parameters

One of the most important parameters while selecting the different plant samples was the growth habit of the willows. In order to gather a broad range of drag forces, single and multi stemmed as well as different shaped plant samples have been carried through the channel. The plant heights started at a minimum of l_0= 210 cm and reached a maximum of l_0= 410 cm, the basal diameters were in the range between db_0=20 mm and db_0=47 mm. Fig. 3 shows that the relation between plant height and diameter builds a relative homogeneous point cloud, only Salix 3 and Salix 5 have a larger basal diameter at the same height (2 parallel linear relations). Fig. 4 states a strong correlation between wood volume and height diameter quotient, the higher the height-diameter ratio the lower the wood volume. This relation is helpful to determine an approximate value for the wood volume by measuring the height and the basal diameter of a plant. A large height-diameter ratio means a slim tree shape and consequently a reduced wood volume

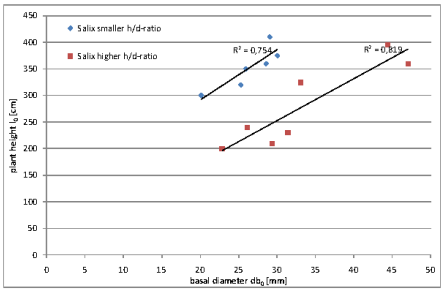

Fig. 3: Relation between plant height and basal diameter of the tested willows

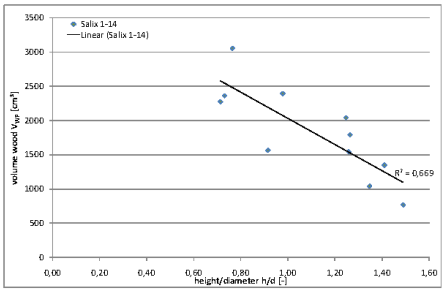

Fig. 4: Relation between displacement volume wood and height to diameter

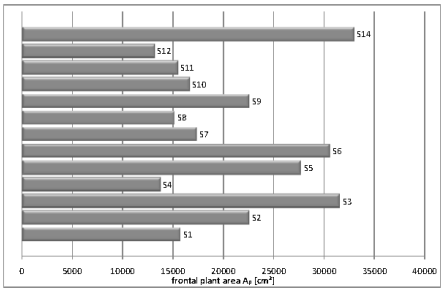

Fig. 5: Frontal projected plant area

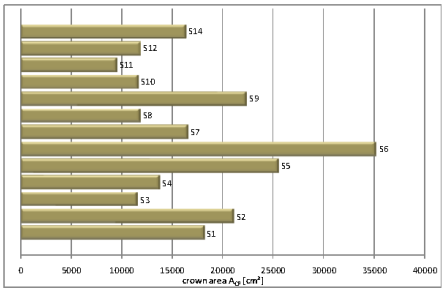

Fig. 6: Projected crown area

The willow samples showed a wide range of frontal plant area A_P (Fig. 5) as well as crown area A_{CP} (Fig. 6). The ratio between A_P and A_{CP} lies between 0,49 and 1,15, Salix 1 and Salix 6 have a larger A_{CP} then A_P. The comparison of the dry mass data of the plant samples (Fig. 7) among themselves as well as the displacement volume (Fig. 9) shows the variety of habit growth of the selected plants. The percentage of leaves compared to the total plant biomass and volume is almost negligible.

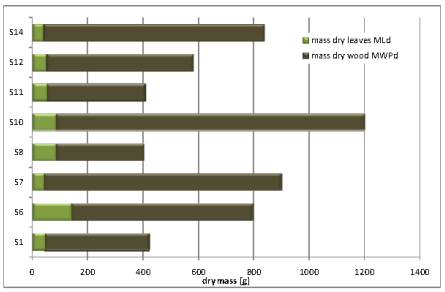

Fig. 7: Dry mass of leaves and wood of willows

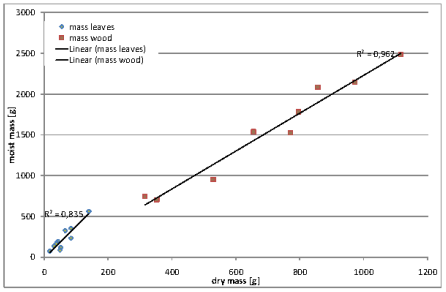

Fig. 8: Correlation between moist and dry biomass

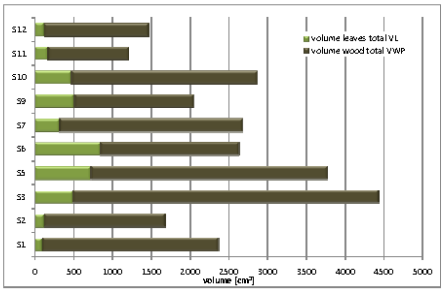

Fig. 9: Displacement volume wood and leaves of willows

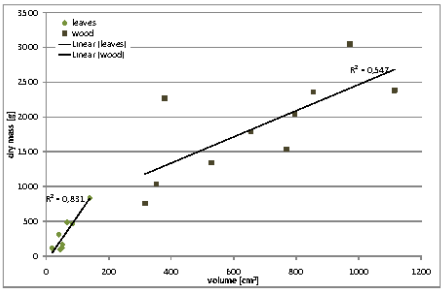

Fig. 10: Correlation between dry mass and volume of wood and leaves

The correlation between dry mass and volume of the wood is not as high (Fig. 10), due to the different growth rate of pioneer plant species induced by specific local environmental conditions of the plants. However the leaf dry mass – volume correlation is strong.

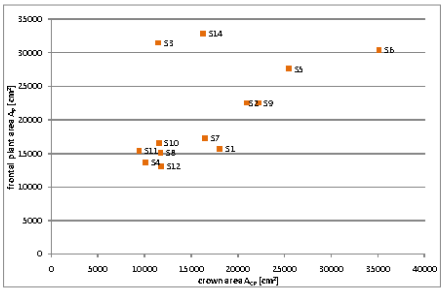

Fig. 11: Correlation between frontal projected area A_P and projected crown area A_{CP}

The correlation between A_P and A_{CP} shows a linear trend (Fig. 11). Salix 3 and Salix 14 are out of the linear trend; their frontal area is much higher in comparison to their crown area.

More Information about geometrical plant characteristics are listed in the plant data sheets added in the appendix.

3.2 Velocity versus force and plant height reduction

The following diagrams display the correlation between velocity u and force Fx as well as velocity and plant height reduction H_{PR}. The induced drag force rises linear with the increase of velocity. The increase in plant height reduction decreases at higher velocities. The difference of induced forces by foliated and defoliated willows increases with velocity.

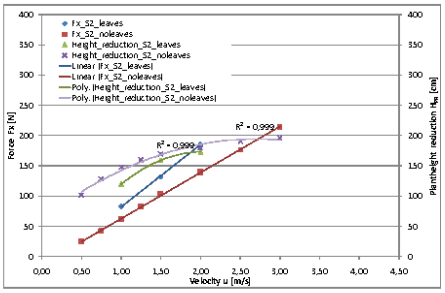

Fig. 12: Correlation between u, Fx and H_{PR} for Salix 2 in leafy and defoliated condition

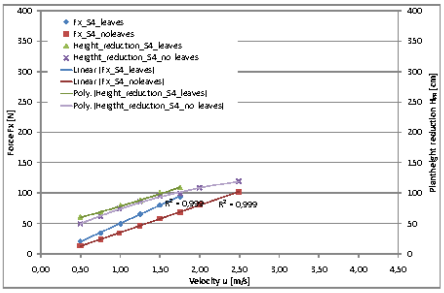

Fig. 13: Correlation between u, Fx and H_{PR} for Salix 4 in leafy and defoliated condition

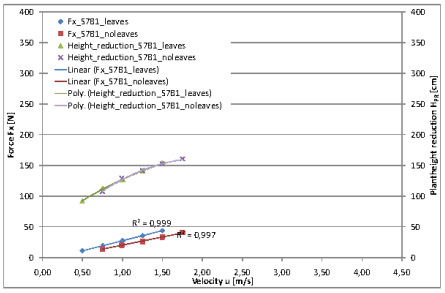

Fig. 14: Correlation between u, Fx and H_{PR} for Salix 7 branch 1 in leafy and defoliated condition

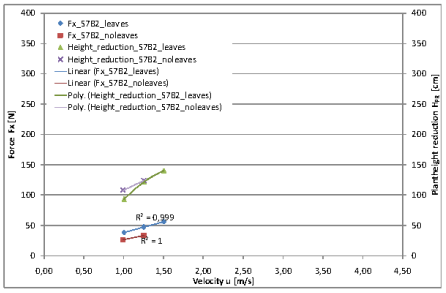

Fig. 15: Correlation between u, Fx and H_{PR} for Salix 7 branch 2 in leafy and defoliated condition

Fig. 14 , Fig. 15 and Fig. 16 show partial results of Salix 7. This specimen was divided into 3 different parts. After carrying the whole plant through the channel the 3 parts have been pulled through the channel to determine the single and the connective impact of the different plant parts.

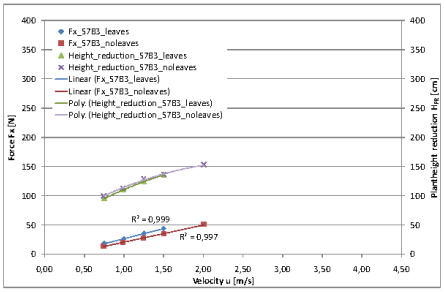

Fig. 16: Correlation between u, Fx and H_{PR} for Salix 7 branch 3 in leafy and defoliated condition

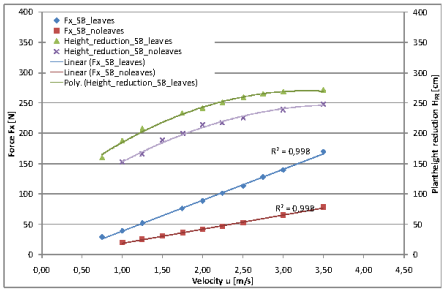

Fig. 17: Correlation between u, Fx and H_{PR} for Salix 8 in leafy and defoliated condition

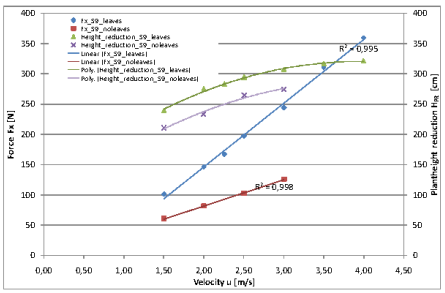

Fig. 18: Correlation between u, Fx and H_{PR} for Salix 9 in leafy and defoliated condition

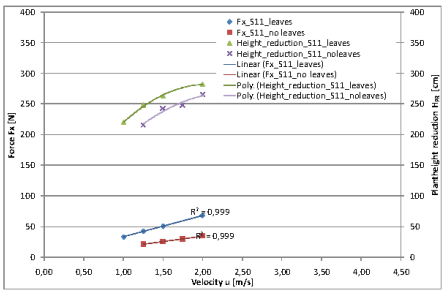

Fig. 19: Correlation between u, Fx and H_{PR} for Salix 11 in leafy and defoliated condition

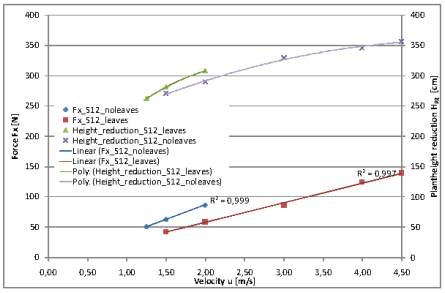

Fig. 20: Correlation between u, Fx and H_{PR} for Salix 12 in leafy and defoliated condition

Fig. 21 and Fig. 22 reproduce a summary of the gathered plant height reduction data. Several plants reach a maximum of height reduction H_{PR} of up to 90%. Both correlations show a linear distribution in the first part up to 70-80% of the H_{PR}. At higher velocities of 2-2,5 m/s the plant height reduction curve is flattening, reaching maximum values of 90 percent.

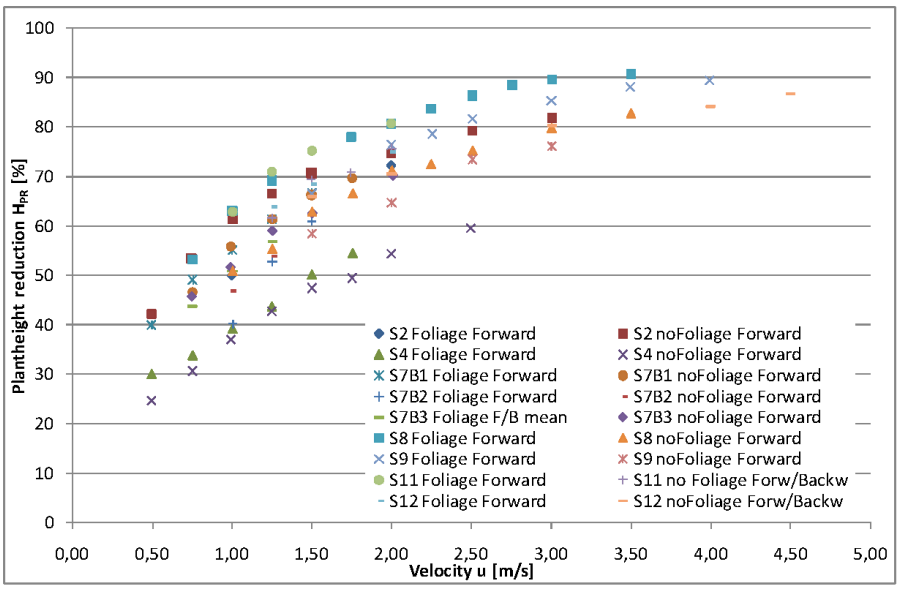

Fig. 21: Velocity u versus percental height reduction H_{PR} of the tested willows

The force curve shows a similar characteristic, a linear trend up to 50% plant height reduction and a non linear trend at higher H_{PR} values.

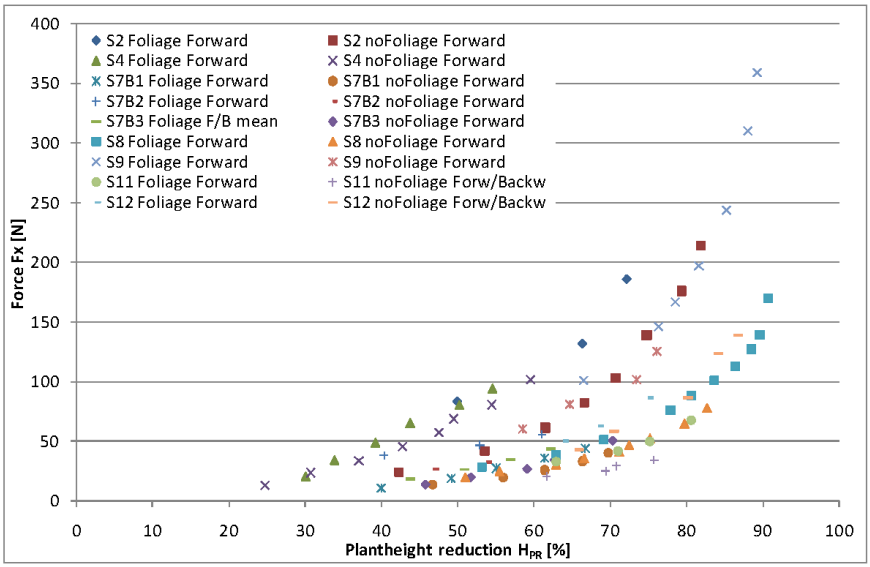

Fig. 22: Percental height reduction H_{PR} versus Force Fx of the tested willows

3.3 Plant parameter versus Force Fx

Different plant parameters have been correlated with the measured force Fx in order to find a geometric plant parameter to describe the induced drag force by the plants.

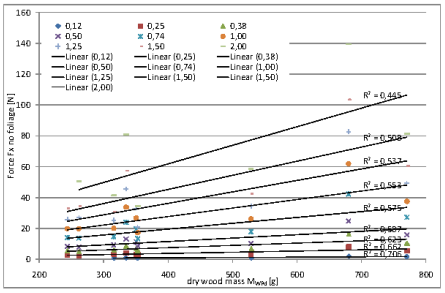

Fig. 23: Correlation between Force Fx and dry plant mass M_{Pd} at different velocities

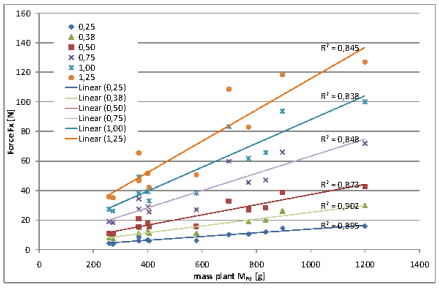

Fig. 24: Correlation between Force Fx no foliage and dry wood mass M_{WPd} at different velocities

Fig. 23 states a strong correlation between dry plant mass and force Fx at different velocities. Whereas the correlation are not as high between the forces of the runs without leaves and the dry wood mass (Fig. 24), due to the change of the material properties of the wood evoked during the prior runs.

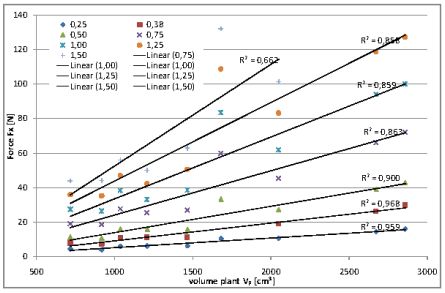

Fig. 25: Correlation between Force Fx and plant volume V_P at different velocities

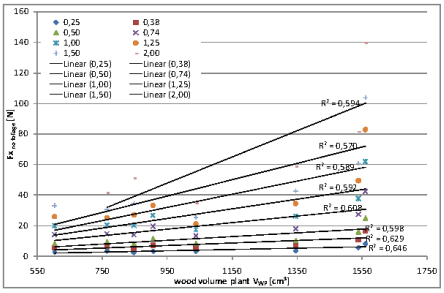

Fig. 26: Correlation between Force Fx and wood volume V_{WP} at different velocities

Fig. 25 and Fig. 26 state similar correlations as found in Fig. 23 and Fig. 24. The whole plant volume shows a high correlation with the force at different velocities. The correlations decrease with increasing velocities. The correlation between wood volume and forces of runs without leaves show a smaller correlation, likewise decreasing with increasing velocity.

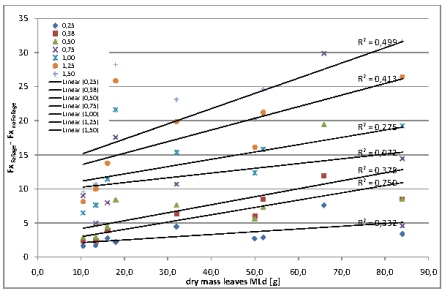

Fig. 27: Correlation between the differences of the forces between the runs with and without leaves and the dry leaf mass

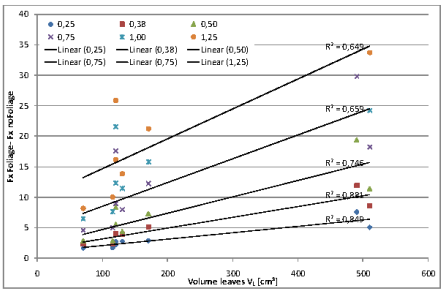

Fig. 28: Correlation between the differences of the forces between the runs with and without leaves and the leaf volume

The differences of the forces between the runs with and without leaves (F_{dif}) state a slight linear correlation to the measured leave parameters as dry mass or volume. The correlation between F_{dif} and the dry leave mass is unstable and rather low at different velocities. The linear correlation between F_{dif} and the leave volume is higher, however decreases with increasing velocity.

4. Discussion

The interaction between hydraulic load and plants under real conditions is influenced by several parameters. Investigating the problem under laboratory conditions allows more precise statements under a circumscribed frame. As the plants were pulled upside down through the channel they are exposed to the buoyancy-effect of the water which influences its habit. Applying the hydraulic load from the beginning on over the whole plant area does not reflect the conditions in reality where the water level increases step by step and the lower part of the plants are exposed earlier to the load. Furthermore the hydraulic conditions in a near nature riverbed are much more complex as in the testing basin. It is crucial to investigate properly the bending properties of riparian vegetation under load.

The results confirm the findings of OPLATKA, 1998, who stated that the force is increasing linearly with the velocity. Newton's law of resistance implies that the force is increasing with the velocity squared. In the case of plants under hydraulic load this proportion is not valid because of the change in area and material properties. So therefore one of the key parameters is the longitudinal and lateral plant contraction. The vertical contraction was measured by video analyses of the plant height reduction. It can be stated that the point of maximal height reduction depends on the material and geometrical properties. The experiments showed that from a certain level of load on the plants are not any more flexible but behave as rigid elements from a hydraulic point of view. Consequently the relationship of force and increasing H_{PR} deviates from a linear distribution.

The linear relation between the displaced volumes of the plants and the induced forces are strong and diminishes with increasing velocity. Likewise dry plant mass and force Fx show a strong linear relation. However, both parameters, especially the volume do not implicate the material parameters and has therefore to be considered with caution.

The differences between foliated and defoliated runs have to be considered with care because in the defoliated runs the willows have already been exposed to a hydraulic load and therefore material fatigue could have influenced the measurements.

Further test runs have to be analysed to gain more results and more data in order to describe the plant bending behaviour properly. Video analysing techniques have to be improved (e.g. calibration of camera) to gain more precise results. Other parameters of importance are the material properties which have to be analysed in order to sustain physical formulae. Including the material properties the material fatigue is a crucial parameter. Carrying the plants often through the channel could affect a change in material properties which again influences the bending behaviour and therefore the measured forces.

5. Literature

ARMANINI A., RIGHETTI M., GRISENTI P. (2005). Direct measurement of vegetation resistance in prototype scale. Journal of Hydraulic Research 43(5): 481-487

CHOW VT. 1959. Open Channel Flow. McGraw-Hill Book Company, Singapore

FATHI-MOGHADAM, M. / KOUWEN, N. (1997): Nonrigid, nonsubmerged, vegetative roughness on floodplains. J. Hydr. Engrg. 123(1): p. 51-57

FREEMAN G. E., RAYMEYER W. J., COPLAND R. R. (2000). Determination of Resistance due to shrubs and woody vegetation. US Army Corps of Engineers. Report ERDC/CHL TR-00-25

GERSTGRASER, C. (2000): Ingenieurbiologische Bauweisen an Fließgewässern. Grundlagen zu Bau, Belastbarkeiten und Wirkungsweisen. Band 52, Dissertation, Universität für Bodenkultur, Wien

JAMES C. S., BIRKHEAD A. L., JORDANOVA A. A., O'SULLIVAN J. J. (2004). Flow resistance of emergent vegetation. IAHR Journal of Hydraulic Research 42(4): 390-398

MEIXNER, H. (2004): Grundsätze zum Management von Ufervegetation. Ingenieurbiologie. Mitteilungsblatt für die Mitglieder des Vereins für Ingenieurbiologie, Nr. 2/2004, 14-18; ISSN 1422-008

OPLATKA, M. (1998): Stabilität von Weidenverbauungen an Flussufern. Mitteilung 156, Versuchsanstalt für Wasserbau, Hydrologie und Glaziologie, ETH-Zürich

RAUCH, H. P. (2005): Hydraulischer Einfluss von Gehölzstrukturen am Beispiel der ingenieurbiologischen Versuchsstrecke am Wienfluss. Dissertation an der Universität für Bodenkultur Wien, 222 pages

Wilson C. A. M. E., Hoyt J., Schnauder I. (2008). The impact of foliage on the drag force of vegetation in aquatic flows. ASCE Journal of Hydraulic Engineering, vol. 134, n°7, pp. 885-891

6. Appendix

Salix 1 - Plant Data Sheet

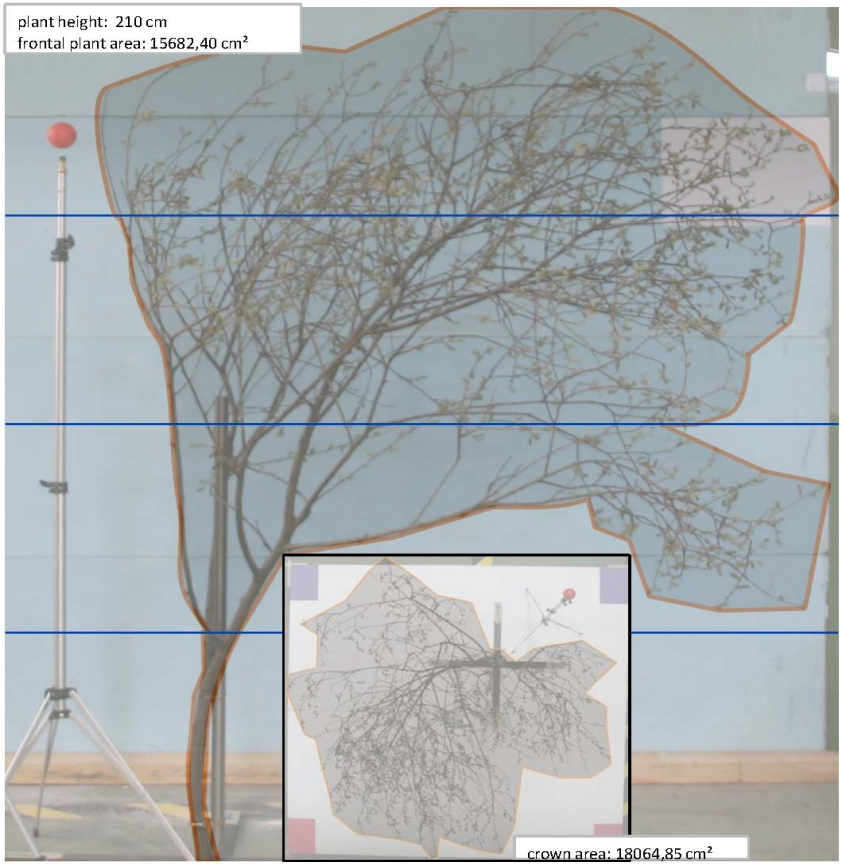

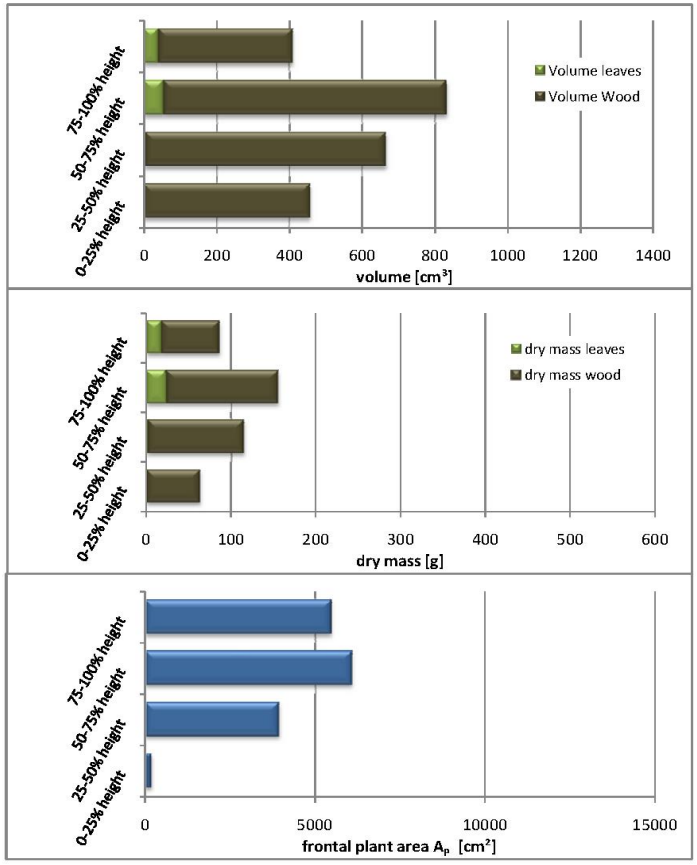

Salix 2 - Plant Data Sheet

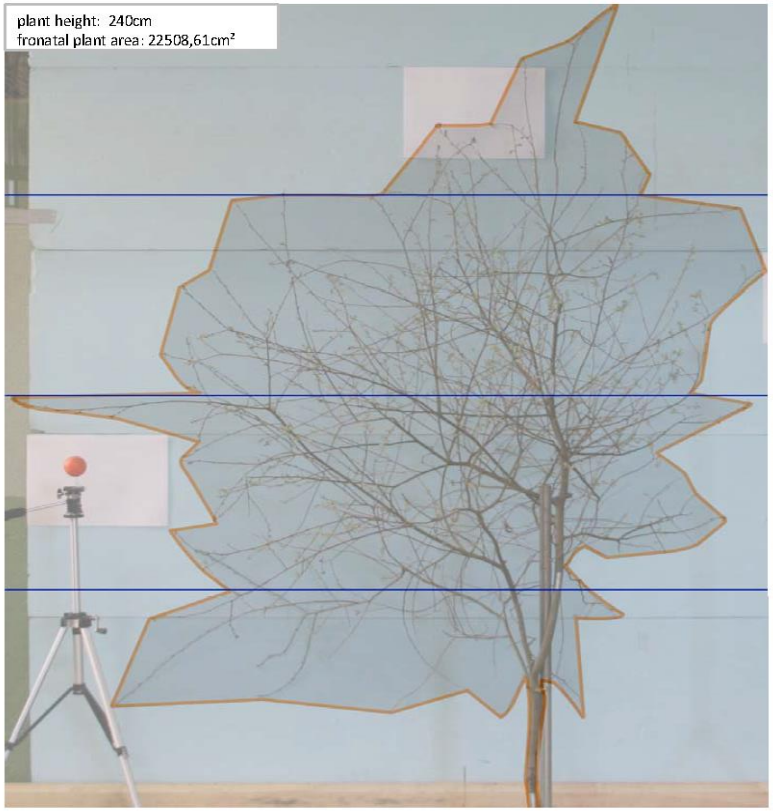

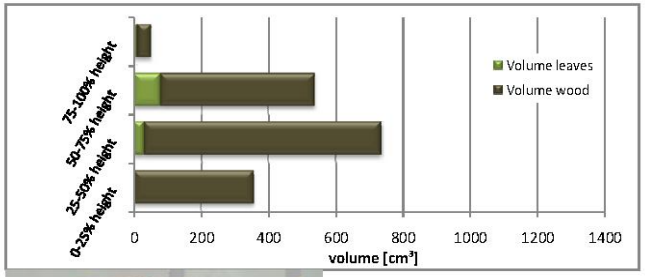

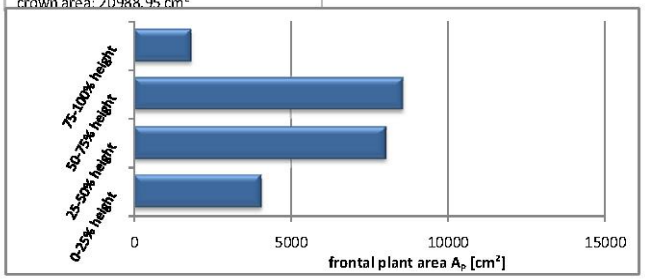

Salix 3 - Plant Data Sheet

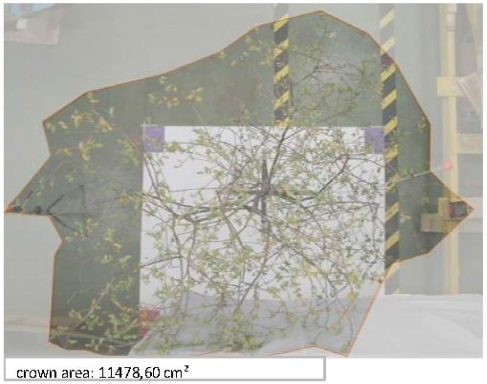

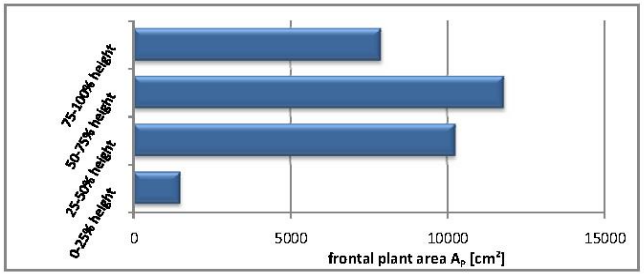

Salix 4 - Plant Data Sheet

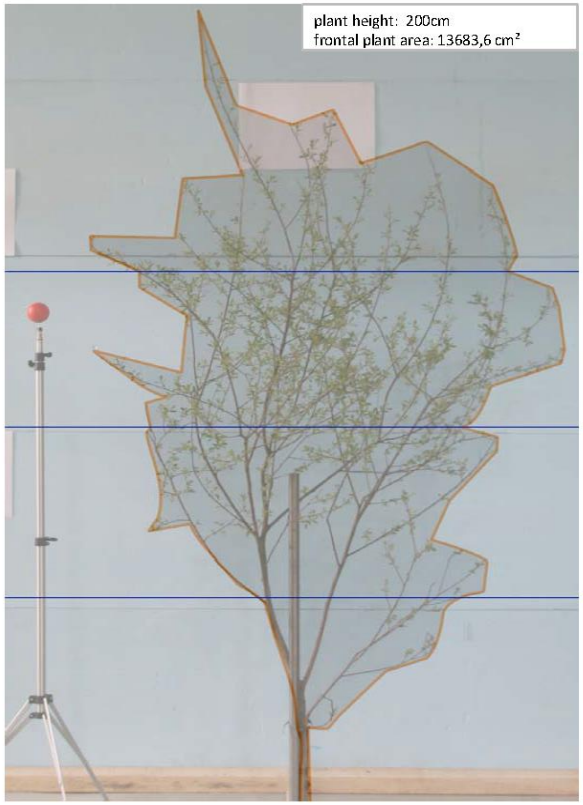

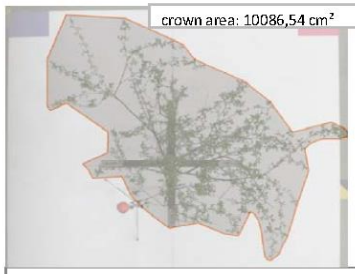

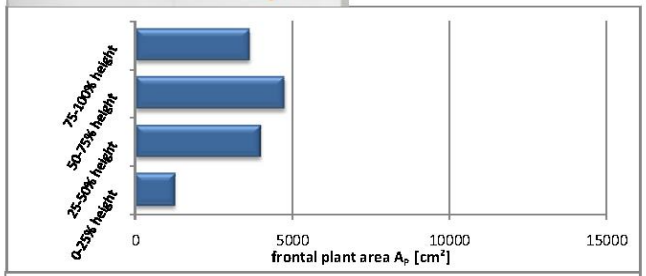

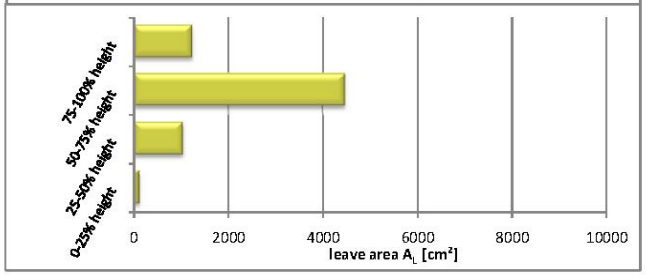

Salix 5 - Plant Data Sheet

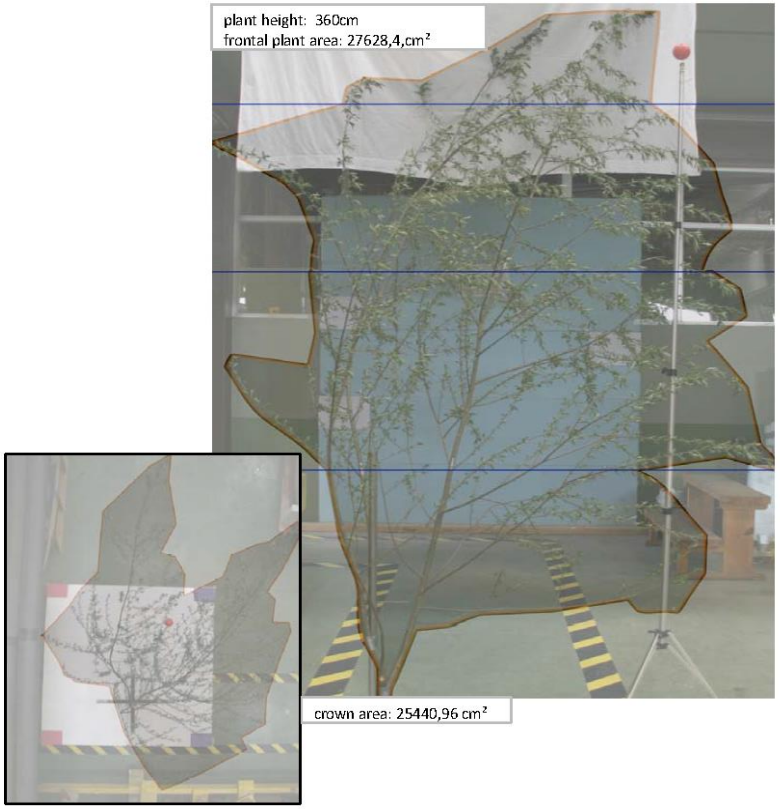

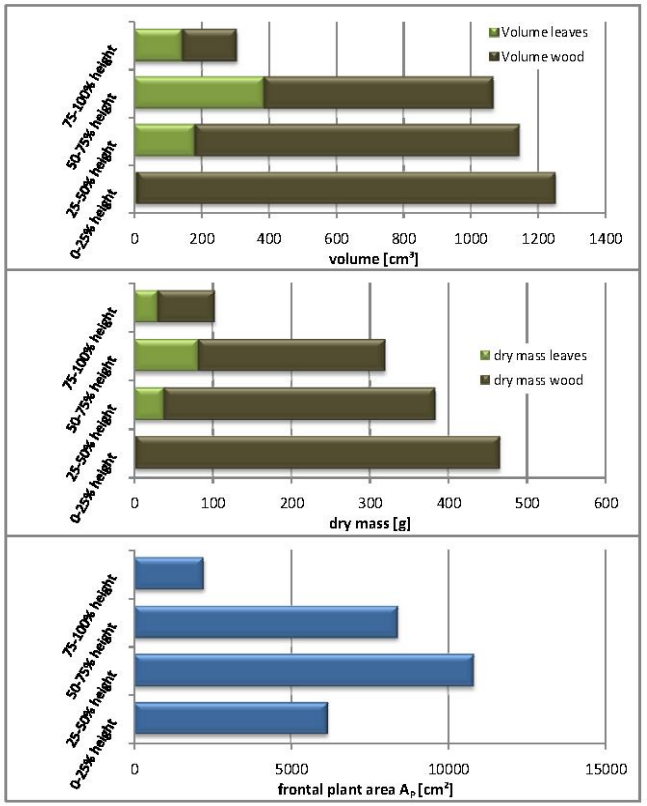

Salix 6 - Plant Data Sheet

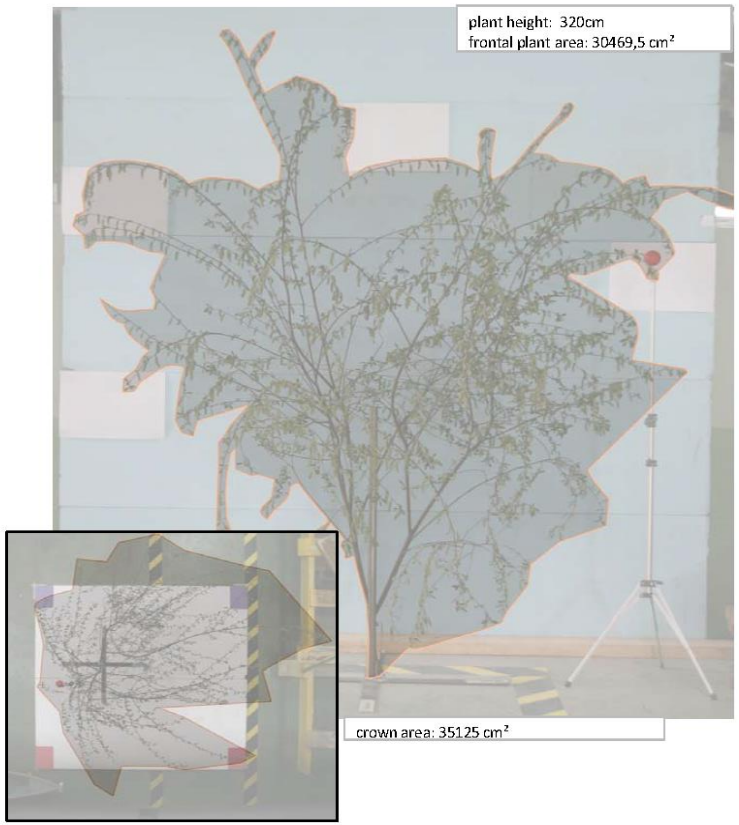

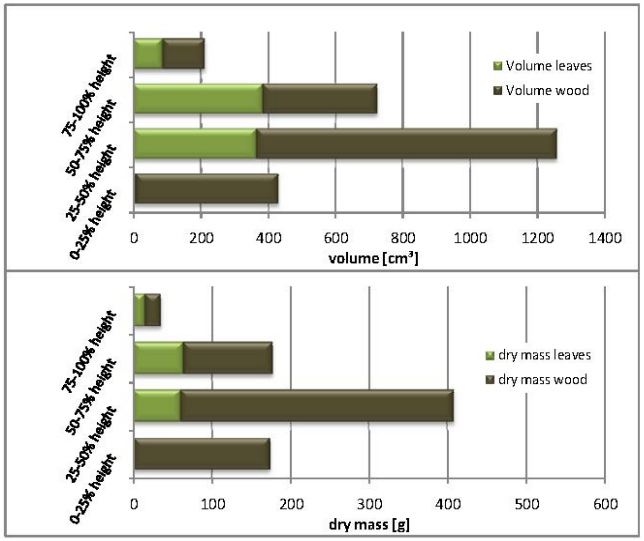

Salix 7 - Plant Data Sheet

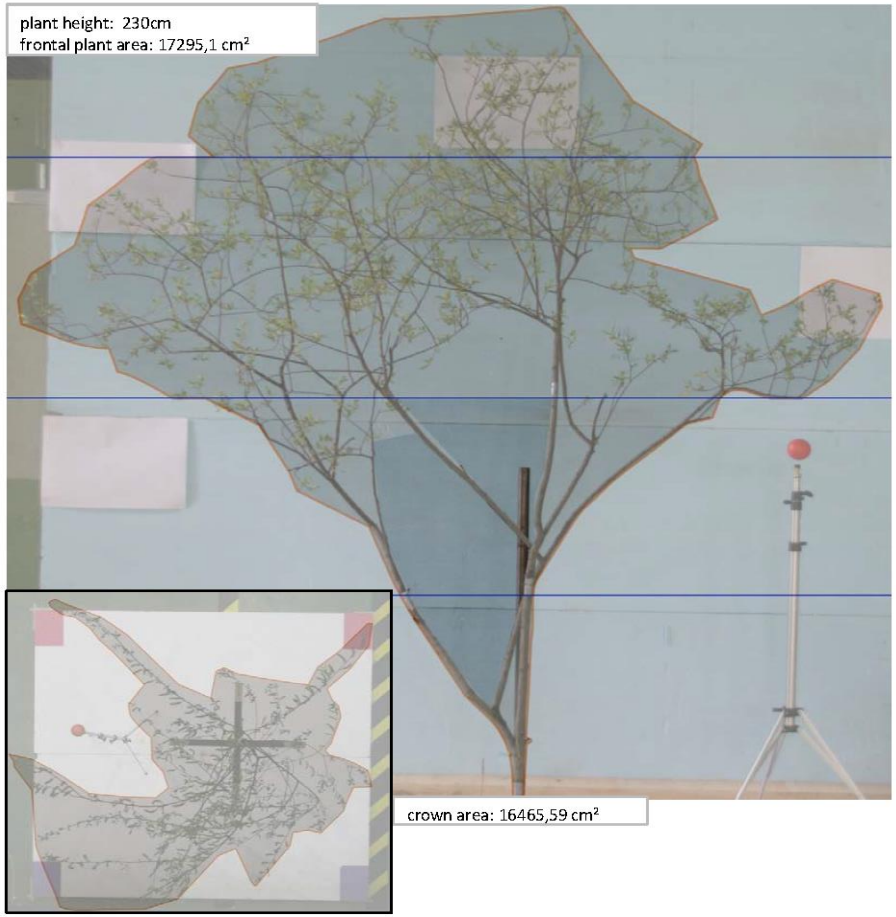

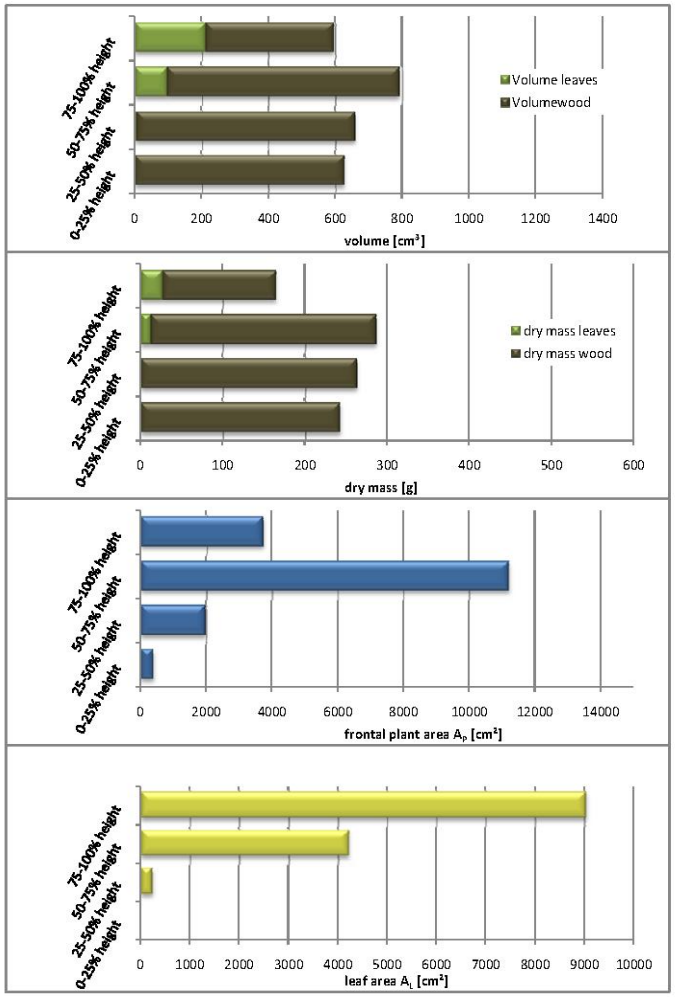

Salix 8 - Plant Data Sheet

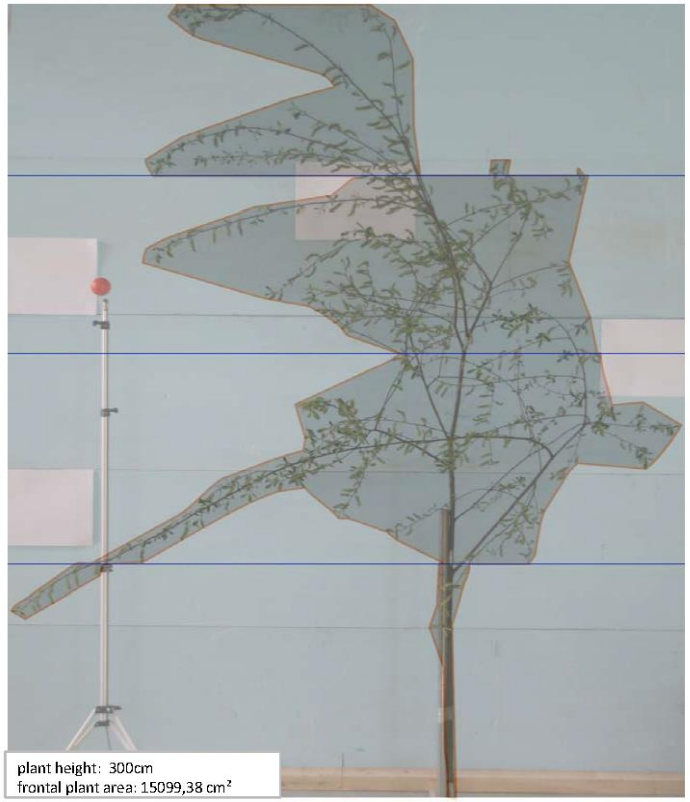

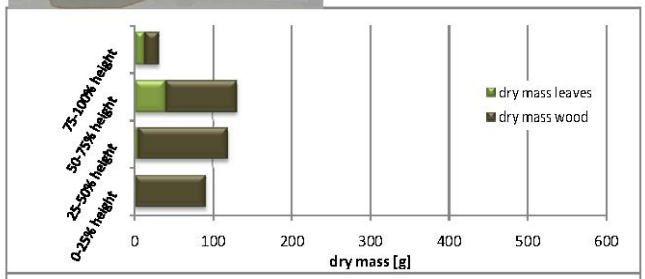

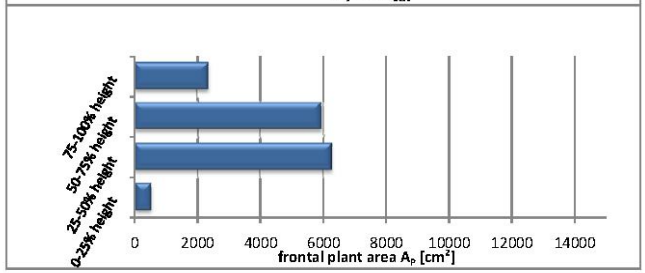

Salix 9 - Plant Data Sheet

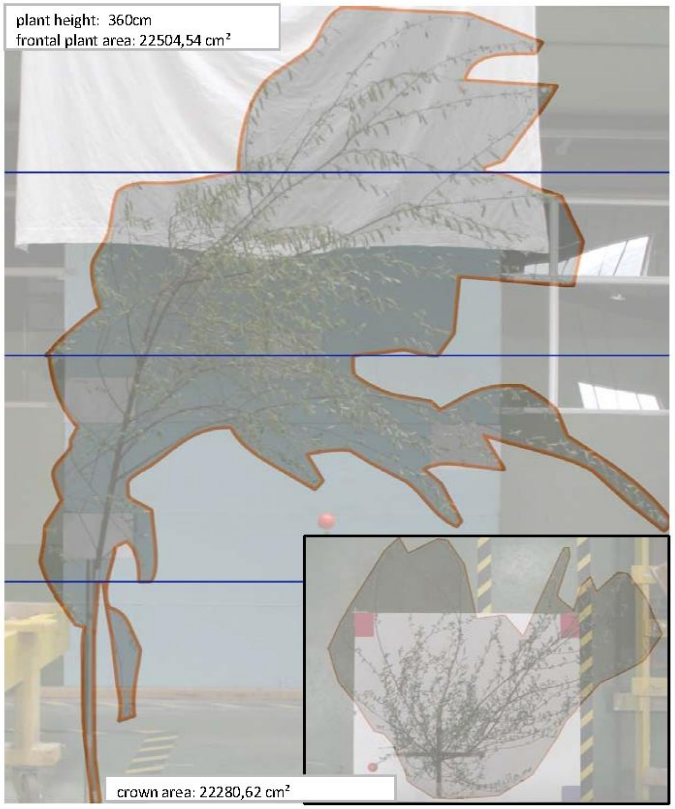

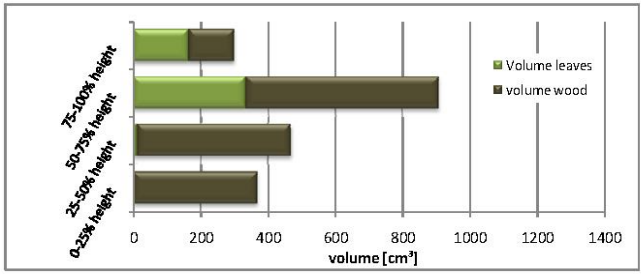

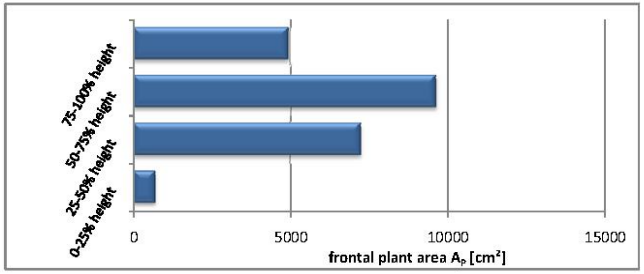

Salix 10 - Plant Data Sheet

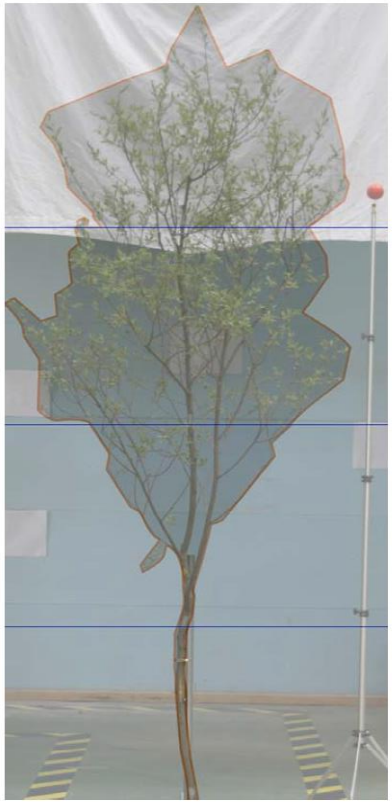

plant height: 324cm
frontal plant area: 16549cm²

crown area: 11569 cm²

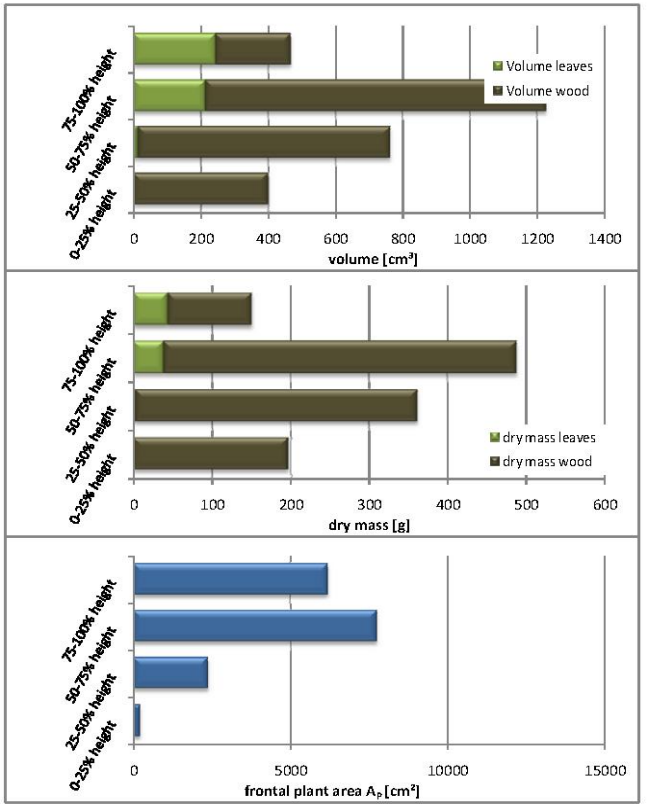

Salix 11 - Plant Data Sheet

plant height: 350cm
frontal plant area: 15376cm²

crown area: 9413 cm²

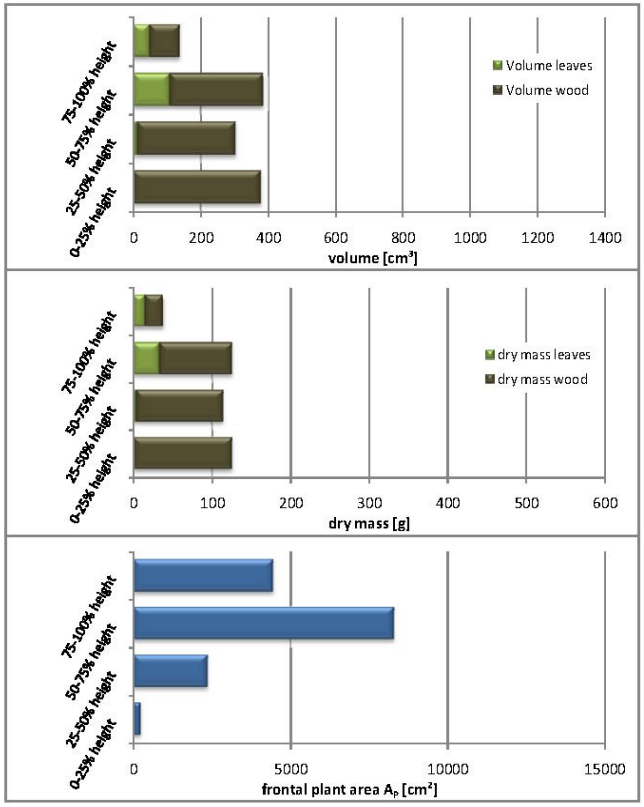

Salix 12 - Plant Data Sheet

plant height: 410cm
frontal plant area: 13067cm²

crown area: 11795cm²

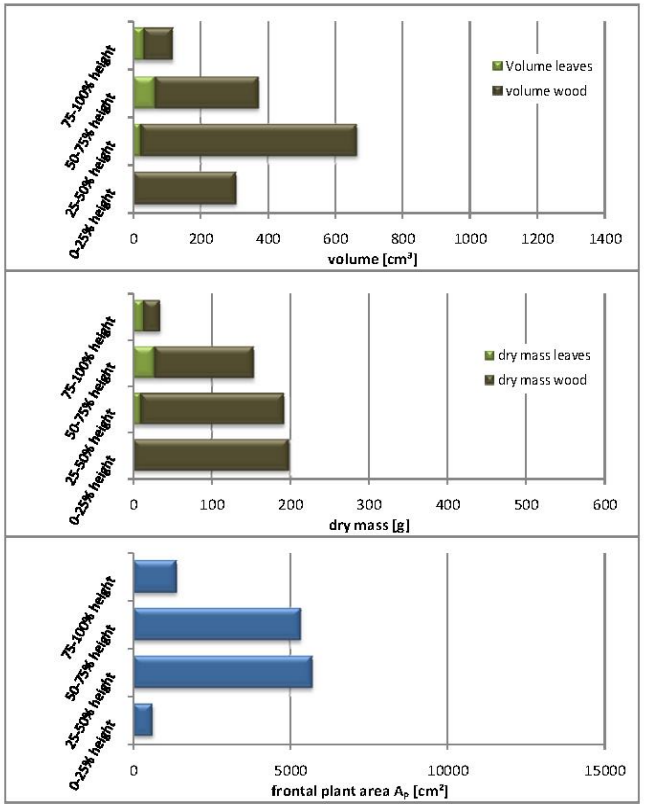

Salix 14 - Plant Data Sheet

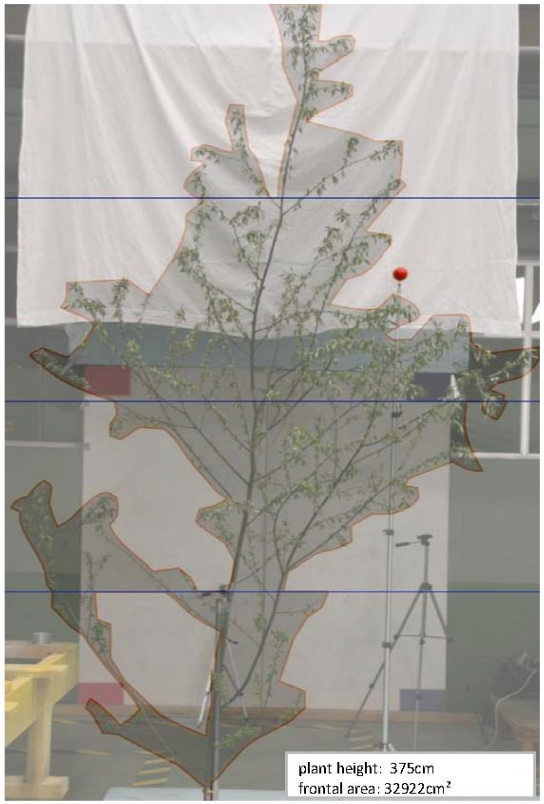

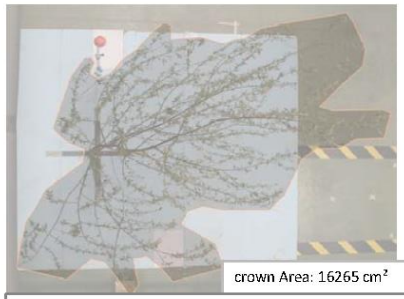

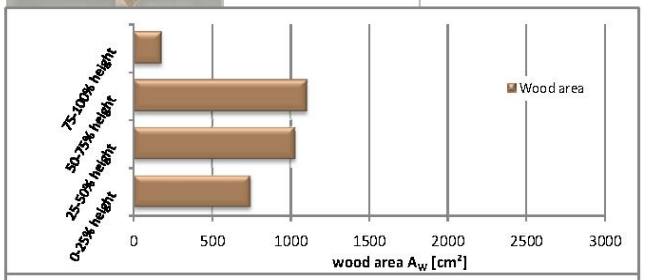

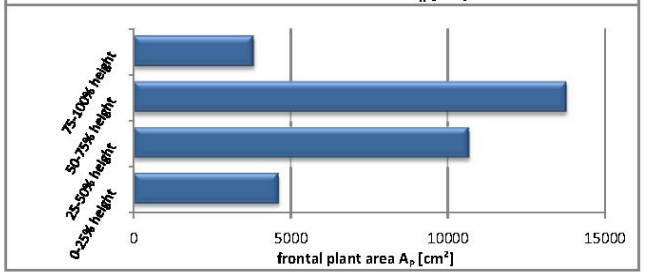

7.2 **Publikation 2**

River Flow 2010 - Dittrich, Koll, Aberle & Geisenhainer (eds) - © 2010 Bundesanstalt für Wasserbau ISBN 978-3-939230-00-7

The Hydrodynamic Drag of Full Scale Trees

C.A.M.E. Wilson & P. Xavier
Hydro-environmental Research Centre, School of Engineering, Cardiff University, UK

T. Schoneboom & J. Aberle
Leichtweiß-Institut für Wasserbau, TU Braunschweig, Braunschweig, Germany

H.-P. Rauch & W. Lammeranner & C. Weissteiner
Institute of Soil Bioengineering and Landscape Construction, University of Natural Resources and Applied Sciences, Vienna, Austria

H. Thomas
Forest Research, Talybont Research Office, Powys, UK

ABSTRACT: This paper presents selected results from a laboratory study which was carried out under the EU Hydralab III programme in a 320 m long towing tank at the CEHIPAR ship canal facility in El Pardo, Madrid. Hydrodynamic drag-velocity relationships were determined for a total of 22 full-scale trees of three different genera (*Salix sp.*, *Alnus glutinosa* and *Populus alba*) of height between 1.4 and 4 metres. In this paper, preliminary results for nine *Salix* specimen are presented. One of the main objectives of this study is to examine these drag-velocity relationships at high resolution and therefore relate the tree's behaviour under flow action to (i) its physical attributes and (ii) different stages of streamlining. It was found that at the lowest velocities (between zero and 0.5 m/s) the drag force-velocity variation approached the squared relationship expected for a bluff body as described by the classical drag force equation. At higher velocities (over approximately 0.5 m/s) the force was found to vary linearly with velocity. For the selection of results presented here, the percentage contribution to drag from spring leaves and flowers was found to vary from 24.4 % to 54.8 % within this linear range. The linear drag-area coefficient (the product of the drag coefficient and the frontal projected area) was determined for all specimen within the zone of linear variation between drag force and velocity. Although the dataset is limited it was found that dry mass and volume of trees were positively correlated to the linear drag-area coefficient.

Keywords: Vegetation, Salix, Leaves, Drag Force

1 INTRODUCTION

It is increasingly recognised that the current reliance on engineered flood protections to defend all areas against future flooding is not sustainable. Instead, attention is shifting towards integrated approaches considering the whole catchment to manage flood risk. Land management and the use of forestation may be seen as having a significant contribution to make, particularly where engineered flood defences cannot be justified on cost-benefit grounds, but also to improve the effectiveness of existing defences against climate change. This is consistent with the delivery of an ecosystem services approach to securing a healthy environment.

By increasing the hydraulic roughness on a wide floodplain, woodland may have the potential to attenuate the flood hydrograph and delay the passage of floodwaters to downstream towns and cities. Woodland can also help to reduce flood flows through increased evapotranspiration and enhanced soil infiltration. The targeted restoration or creation of woodland, including energy plantations, could make a major contribution to protecting rural and urban communities from future flooding, as well as delivering a wide range of other benefits such as carbon sequestration, biodiversity, recreation and improved water quality.

River modelling software and computational fluid dynamics codes are effective and widely used tools in determining river water levels and velocities, particularly in the prediction of high flow events which may endanger life or property (e.g., Pender 2006). However, the modelling of flows through riparian forests is hampered by a lack of data relating to the hydrodynamics of trees and shrubs under fluid action. At a time when the wide-ranging benefits of river restoration and reforestation are increasingly recognized in terms of ecological and climatic benefits (IPCC 2007; UN 2009), it is critical that the understanding of vegetated flows keeps pace with the continuous improvements in the numerical methods used to model free surface flows.

From the earliest approaches and numerical river models, vegetation has been modelled as an extension of boundary skin friction using roughness factors such as Manning's n or the Chezy factor (Chow 1959). However it has been shown that for vegetation that extends throughout the whole water column, bed boundary roughness coefficients such Manning's n vary as a function of flow depth (e.g., Ree 1958). A more appropriate model for representing the hydraulic resistance exerted by a single and/or a group of trees or shrubs is taking into account their hydrodynamic drag (e.g., Li & Shen 1973; Petryk & Bosmajian 1979). In the field of vegetation modelling, this has generally been accomplished on the basis of the classical drag formula (e.g., Hoerner 1965):

$$F_x = \frac{1}{2}\rho C_d A_p U^2 \quad (1)$$

where F_x is the drag force exerted on the vegetation, ρ is the fluid density, C_d is the drag coefficient (in turbulent flows this relates to the shape of the obstacle and is a function of obstacle Reynolds-number), A_p is the projected area of the obstacle and U is the free stream velocity. Applying equation (1) to natural vegetation elements it is often assumed that the plants behave similar as rigid circular cylinders and that the drag coefficient C_d is constant in the order of magnitude around unity.

However, several studies (e.g., Oplatka 1998; Armanini et al. 2005; James et al. 2008; Wilson et al. 2008) showed that the application of equation (1) is hampered when being applied to natural vegetation as it is difficult to account for the tree's flexibility under flow action. In fact, for flexible vegetation elements it has been shown that the trunk and its branches reconfigure and streamline with increasing velocity (e.g., Oplatka 1998). This process causes the projected area and the drag coefficient to vary as a function of the velocity and shows that the simulation of natural vegetation by rigid cylinders is only a crude approximation of the reality and may only be valid for certain vegetation types such as reeds and or rigid tree trunks (e.g., Järvelä 2006).

Several authors have determined the drag coefficient of flexing trees through direct drag force measurements (e.g., Mayhead 1973; Fathi-Maghadam & Kouwen 1997; Oplatka 1998; Freeman et al. 2000; Armanini et al. 2005; Kane & Smiley 2006; Wilson et al. 2008). Oplatka (1998) tested natural trees in a towing tank and reported that, for velocities greater than 1 m/s, the force varies linearly with velocity. This is thought to be due to the significant decrease in projected area of the tree as it flexes longitudinally and laterally under flow action and is in contrast to the quadratic drag force relationship expected for a rigid body (equation 1).

However, the observed linear relationships have, in general, been based on few data points. For example Oplatka (1998) investigated the drag force-velocity relationship at velocities of 1 m/s and above at increments of 0.5 m/s. The flexing behaviour and force-velocity relationship below this value was not reported.

Due to the difficulties involved in measuring the physical parameters of trees and the large population sample needed in order to make definitive conclusions, few researchers have quantified and related physical plant parameters to the drag exerted. Some authors, including Rudnicki et al., (2004) and Vollsinger (2005) studied the relationship between crown mass and drag exerted on trees in wind tunnels, finding that the drag was proportional to the crown mass, wind speed and crown size.

On the other hand, several researchers have characterized the force-velocity behaviour of a flexible plant and the associated influence of the variation in the projected area of the vegetation under flow action, through the drag-area parameter C_dA_P, the product of drag coefficient and projected area (e.g., Armanini et al. 2005; Wilson et al. 2008). In this manner the classical drag formula shown in equation (1) was used to evaluate the product C_dA_P for each velocity examined as the drag coefficient and projected area are both functions of velocity.

The experimental programme on which this study is based is a first step towards further understanding how the physical characteristics of flexing trees relate to the hydrodynamic drag. The results presented in this paper are part of a wider series of experiments undertaken to investigate the hydrodynamic drag imposed by full scale trees with and without foliation. In total, 22 full-scale trees of three different genera (*Salix*, *Alnus* and *Populus*) of height between 1.4 and 4 meters were tested. Here, we concentrate on presenting the results from tests conducted on nine trees of the genus *Salix* where data was recorded at velocity increments of 0.06 m/s to 0.50 m/s, allowing examination of the drag-velocity relationship in greater detail than previously observed. Furthermore, we attempt to understand the linkage between hydrodynamic drag and a tree's physical properties.

2 METHODOLOGY

The experiments were conducted at the 320 m long, 12.5 m wide and 6.5 m deep CEHIPAR ship canal facility in El Pardo, Madrid in March and

April 2008 under the Transnational Access Activities EU Hydralab III scheme. The facility and the carriage which housed an operations room is shown in Figure 1.

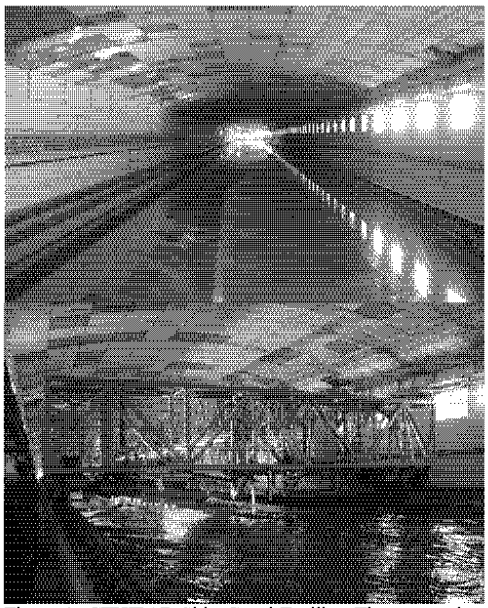

Figure 1: CEHIPAR Ship Canal Facility. The upper photograph shows the canal and the lower photograph the carriage on rails suspended over the canal.

In order to measure drag forces exerted by the trees they were attached upside-down to a dynamometer suspended beneath the carriage spanning the canal width. The tree orientation was selected according to the direction of the tree's tendency to bend while upright. In this way, the bending during testing worked with the natural curvature. The carriage moved along canal-side railings and its velocity was controlled from the operations room to an accuracy of 1 mm/s. The carriage movement was bi-directional and this enabled drag force measurements while the carriage moved along the canal in both directions. During the experiments, this was taken into account by rotating the tree on arrival at the end of the canal through 180°. The direction of the carriage motion will be referred hereafter as a forward run (moving away from the start of the canal to the end of the canal) and a backward run (moving from the canal end to the start of the canal). The carriage rested for a period of a few minutes between the forward and backward runs. This was to ensure that the basin waves generated during each run were sufficiently dissipated and would not affect the data collected. The forces in three directions on the dynamometer were monitored in real time to an accuracy of 0.0098 N.

To verify the accuracy and performance of the drag force measurement system and to provide a baseline with which to compare the tree results, the drag force-velocity relationship was determined for a solid steel cylinder of diameter 30 mm as a first step (not shown here). To ensure repeatability of results, each experiment was carried out twice with both a forward and a backward run.

During a single forward or backward run, force measurements were taken for several velocities in succession. An example of a time-series for velocities in the range of 0.25 to 1.75 m/s is shown in Figure 2. All three force components are shown; F_x, F_y and F_z refer to the force components in the longitudinal, lateral and vertical directions, respectively. Figure 2 shows that the force reached a peak at the transition point between two subsequent velocities where the carriage accelerated. The acceleration and hence the change in velocity was reached in a few seconds. It is clear however that the change in force exerted on the dynamometer continued to change for a much longer period due to plant reconfiguration. This can be seen on the declining force magnitude following the acceleration and it was observed that this effect became more significant at the higher velocities examined.

In order to ensure that representative force measurements are derived from the time-series dataset, a statistical analysis was carried out to find the optimum time segment based on the cumulative average and standard deviation calculations. Considering the acceleration, deceleration and the stabilization of the tree configuration, this analysis was carried out from the end to the beginning of a velocity step (i.e. just before the next velocity increase). This procedure resulted in a maximum time segment of 20 seconds at the end of a velocity step for the time-averaging process.
In order to relate physical characteristics of the trees to the resultant drag, physical properties of the woody parts of the trees were measured and documented in quartile heights, including height, diameter, mass and volume. To determine the contribution to drag from the presence of leaves and flowers (catkins), the mass and volume, and dry mass fraction (the combined leaf and flower mass expressed as a percentage of total tree mass) were also determined. It should be noted that we did not distinguish between leaves and flowers when calculating the dry mass fraction. The experiments were performed during early spring and consequently the leaf size and leaf to wood ratio were relatively low compared to later in the season, although the presence of flowers contributed significantly to the dry mass fraction and the overall increase in drag.

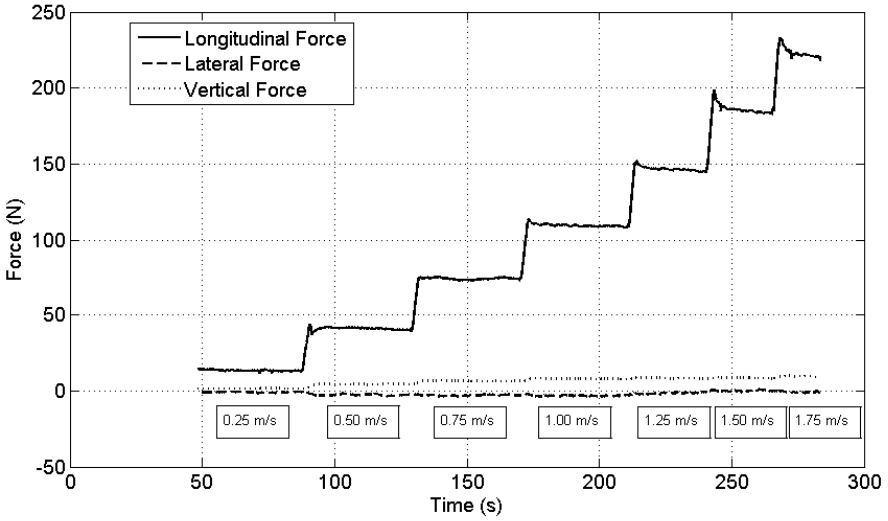

Figure 2 Time-series of force components measured for a succession of velocities.

3 RESULTS

Figure 3 presents the longitudinal drag force variation with velocity for the *Salix* trees both with and without leaves and flowers. The figure indicates that above a threshold velocity (U_T) of approximately 0.5 m/s, the variation of force with velocity is apparently linear for the majority of trees in both conditions. Assuming such a linear behaviour for the high velocity data, the velocity threshold U_T was determined from the intersection point between a linear regression fit applied to the high velocity data and a second-order regression fit applied to the lower velocity data. The subjectively chosen governing condition to identify the linear region was that the squared correlation coefficient R^2 must be greater than 0.99 for the linear regression. The velocity thresholds (U_T) for the trees with and without leaves and flowers are presented in Table 1.

Table 1. Velocity thresholds U_T. *(F-With leaves and flowers, NF-No leaves or flowers)*

Salix	1	2	4	8	10	11	12
F U_T (m/s)	0.62	0.33	0.47	0.34	0.36	0.91	0.50
NF U_T (m/s)	0.49	0.42	0.49	0.38	0.38	0.30	0.51

We note that this method was difficult to apply to *Salix* 3 which was not tested at high enough velocities to obtain a value for the velocity threshold and *Salix* 9, where the non-linear rate of increase of force with velocity appears to continue to rise until over 3.5 m/s (Figure 3a).

It was mentioned above that the drag-area parameter C_dA_p based on the rigid body model can be used to characterize the drag-velocity behaviour of a flexible body. Here we define a modified version referred to as the 'linear drag-area coefficient' for a flexible body when the drag-force relationship is linear. The linear drag-area coefficient is based on the gradient of the force-velocity curve in the flexing zone and is defined as:

$$C_d A_p U_0 = \frac{2\Delta F_x}{\rho \Delta U} \tag{2}$$

where ΔF_x and ΔU_0 refer to the change in longitudinal drag force and the change in the longitudinal velocity respectively. U_0 is a velocity parameter to maintain dimensionality validity. The terms on the L.H.S. of equation (2) together form the composite linear drag-area coefficient term. While the individual value and magnitude of U_0 is not explored here, it will be the subject of future research. According to the identified linear relationship, the linear drag-area coefficient $C_dA_pU_0$ is constant for all velocities in the flexing zone and therefore each tree can be characterized by a single value within this zone. The $C_dA_pU_0$ parameter has an advantage over the previously defined drag-area parameter as it encompasses all the drag and flexing effects of a tree specimen over a range of velocities instead of considering one single velocity.

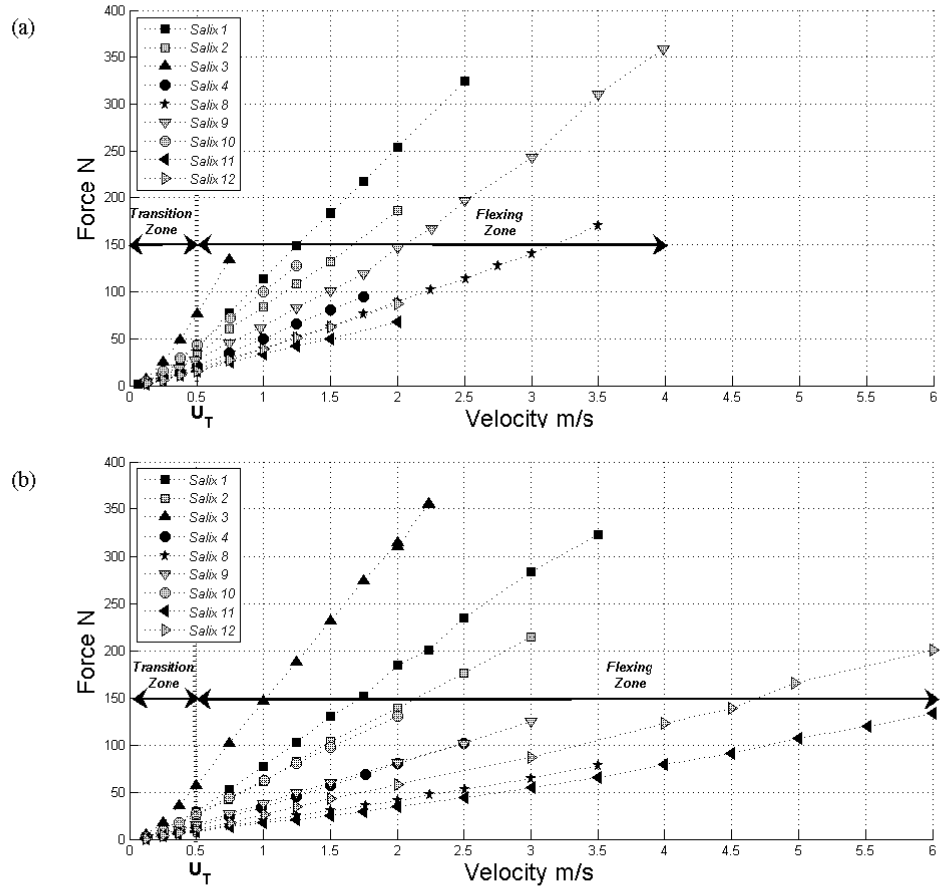

Figure 3: Variation of drag force with velocity for *Salix* trees, (a) with leaves and flowers and (b) without leaves and flowers.

$C_dA_pU_0$ is shown in Figure 4 as a function of various physical tree characteristics. Figures 4 (a) and (b) present $C_dA_pU_0$ as a function of the tree diameter at the first quartile height (as measured from the base of the tree) and the mid-length diameter and Figures 4 (c) and 4 (d) present $C_dA_pU_0$ as a function of the tree dry mass and volume. The data point in the top right corner of all the Figure 4 plots corresponds to *Salix* 3, a specimen which was considerably greater in mass and height than the other specimens.

The linear fit equation was used to parameterise the force-velocity relationship in the flexing zone. The comparison of the results with leaves and flowers against those without enabled the determination of the mean contribution to drag from the presence of the leaves and flowers for each tree. The dry mass fraction of the leaves and flowers and the equivalent percentage contribution to drag for the *Salix* trees are presented in Table 2. We note that tree *Salix* 3 was not tested at sufficient velocities above 0.5 m/s with leaves and flowers and that the leaf and flower mass for tree *Salix* 9 was not recorded. Therefore these data could not be included in Table 2.

Table 2. Leaf and flower dry mass fraction and drag contribution due to the presence of leaves and flowers

Salix	1	2	4	8	10	11	12
Mass fraction (%)	3.1	2.5	8.5	21.0	7.0	12.8	8.6
Drag (%)	28.8	24.7	24.4	54.8	37.8	33.7	27.3

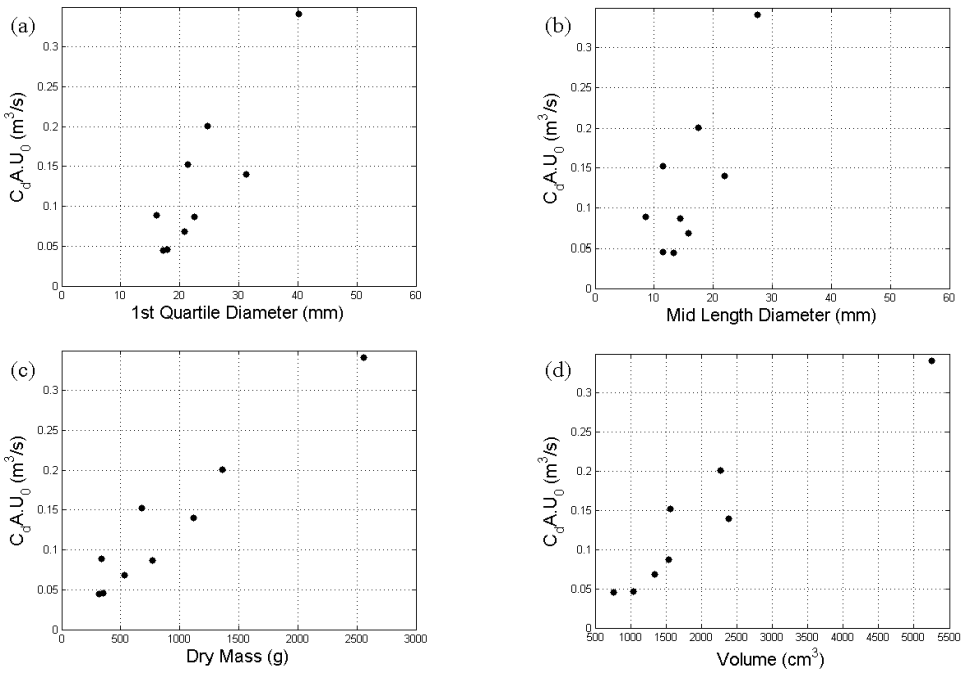

Figure 4: Relationship of linear drag-area coefficient against (a) first quartile diameter (b) mid length diameter c) dry mass and (d) volume.

4 DISCUSSION

The drag force variation with velocity results shown in Figure 3 confirm the experience of previous studies investigating flexing trees, but show an increased accuracy and data resolution. The relatively large number of measurements taken at velocities below 1 m/s, compared to previous studies, demonstrates that there are two zones of drag-velocity behaviour. By determining the value of U_T beyond which the tree displays a linear variation of force with velocity, the data for any given tree can be divided into two zones. The *transition zone* is bounded by the very lowest velocities tested, when the deflection of the tree is negligible and the tree can be assumed to act as a rigid body, until the threshold velocity U_T is reached. In this zone, there is a gradual transition from the tree acting as a rigid body to one acting as a fully responsive flexing body. A similar behaviour for flexible vegetation elements was described in the study of Schoneboom & Aberle (2009) for flexible artificial vegetation elements.

In the *flexing zone*, which is bounded by U_T and the maximum velocities tested the tree streamlines, regardless of whether or not the tree has leaves and flowers. Streamlining causes the projected tree area to decrease with increasing velocity. It appears that the linear drag-velocity relationship is reached at approximately 0.5 m/s (Figure 3, Table 1). The velocity at which U_T is reached for each tree is different depending on whether or not the tree has leaves and flowers. However, the U_T values provided in Table 1 indicate that a consistent variation in the magnitude of U_T between the tests is not existent. This issue will be investigated further in our future analyses taking into account the other 13 tested trees. Nonetheless, by determining the gradient of the assumed linear force variation with velocity in the flexing zone it was possible, with the exception of Salix 3 and Salix 9, to adequately characterise the drag force-velocity relationship of the trees at velocities above 0.5 m/s.

The contribution to drag force from the presence of leaves and flowers varied from 24.4 % to 54.8 % while the equivalent mass fraction of leaves and flowers varied from 2.5 % to 21 % (Table 2) showing that leaves and flowers contribute significantly to the drag (see also Vogel 1994). However, a larger sample of trees may be needed in order for the drag contribution of the

leaves and flowers to be related to the mass fraction.

In general, there is a positive correlation between the linear drag area coefficient and the diameter at the first quartile height and mid-height, dry mass and volume. There appears to be better correlation with dry mass and volume (Figures 4 (c) and (d)), compared to the first quartile and mid-height diameters. Hence, Figure 4 suggests that measurements of mass and volume are more indicative of the drag and flexing behaviour of the tree than a measurement of the main stem diameter.

The observed scatter in Figure 4 may be due to a number of factors. For example, several different species and sub-species were identified among the tested trees, with some more rigid than others. The trees all exhibited varying degrees of existing natural curvature and number and size of side branches, which may have additionally contributed to the wide spread of data points. This issue will also be further investigated analysing the total data set.

5 CONCLUSION AND FUTURE WORK

The drag force variation with velocity has been presented for *Salix* trees exhibiting spring leaves and flowers and for bare stem trees stripped of all leaves and flowers. It has been shown that the presence of leaves and flowers can significantly contribute towards the overall drag of a tree. The results obtained show a velocity-dependent variation in the response of the trees under flow action, with two zones identifiable, a transition zone and a flexing zone. The linear drag-velocity relationship was reached at approximately 0.5 m/s.

The relationship between linear drag-area coefficient $C_d A_p U_0$ and tree physical parameters of stem diameter, height and mass indicates that it is possible to obtain functional relationships to determine the resistance of flexible floodplain woodland vegetation through non-destructive measurement methods. It was found that the measurement of mass and/or volume was more indicative of the overall drag and flexing behaviour of a specimen than a measurement of the main stem diameter. Further analysis, taking into account the available additional data, is currently underway to analyse the video footage from the experiments in order to understand the contribution of tree form and structure to the drag-velocity relationship.

ACKNOWLEDGEMENTS

This work has been supported by European Community's Sixth Framework Programme through the grant to the budget of the Integrated Infrastructure Initiative HYDRALAB III within the Transnational Access Activities, Contract no. 022441. This work has also been supported by Forest Research UK and Deutsche Forschungsgemeinschaft (Grant AB 137/3-1).

REFERENCES

Armanini, A., Righetti, M. & Grisenti, P. 2005. Direct measurement of vegetation resistance in prototype scale, *J. Hydraul. Res.*, 43(5), 481-487

Chow, V.T. 1959. *Open Channel Hydraulics*, McGraw-Hill.

Fathi-Maghadam, M. & Kouwen, N. 1997. Nonrigid, nonsubmered, vegetative roughness on floodplains, *J. Hydraul. Eng.*, 123(1), 51-57.

Freeman, G.E., Rahmeyer, W.J. & Copeland, R.R. 2000. Determination of resistance due to shrubs and woody vegetation, *Technical report, US Army Corps of Engineers.*

Hoerner, S. (1965). *Fluid-Dynamic Drag,* Hoerner, S., Brick Town.

IPCC 2007. Climate change 2007 synthesis report, *Technical report, IPCC.*

Järvelä, J. 2006. Vegetative flow resistance: characterization of woody plants for modeling applications. In: R. Graham (ed), Proc. of the World Water and Environmental Resources Congress 2006. 21-25 May 2006, Omaha, USA, papers on CD-Rom.

James, C.S., Goldbeck, U.K., Patini, A., & Jordanova, A.A. 2008. Influence of foliage on flow resistance of emergent vegetation. *J. Hydraul. Res.*, 46(4), 536-542.

Kane, B. & Smiley, T. 2006. Drag coefficients and crown area estimation of red maple, *Can. J. For. Res.*, 38(6), 1275-1289.

Li, R.-M. & Shen, H.W. 1973. Effect of tall vegetations on flow and sediment, *J. Hydraul. Div.*, 99(HY5), 793- 814.

Mayhead, G.J. 1973. Some drag coefficients for British forest trees derived from wind tunnel studies. *Agricultural Meteorology*, 12, 123-130.

Oplatka, M. 1998. Stabilität von Weidenverbauungen an Flussufern, *PhD thesis*, ETH Zürich.

Pender, G. 2006. Briefing: Introducing the Flood Risk Management Research Consortium." *Water Management*, 159(WM1), 3-8.

Petryk, S. & Bosmajian, G.I. 1975. Analysis of flow through vegetation, *J. Hydraul. Div.*, 101(HY7), 871-884.

Ree, W.O. 1958. Retardation coefficients for row crops in division terraces, *Trans. Am. Soc. Agric. Eng.*, 1, 78- 80.

Rudnicki M., Mitchell S.J. & Novak M.D. 2004. Wind tunnel measurements of crown streamlining and drag relationships for three conifer species. *Can. J. For. Res.*, 34(3), 666-676.

Schoneboom, T. & Aberle, J. 2009. Influence of foliage on drag force of flexible vegetation. 33rd IAHR Congress, Vancouver, Canada, Papers on CD-Rom.

UN 2009. State of the world's forests 2009, Technical report, Food and Agriculture Organization of the United Nations.

Vogel, S. 1994. *Life in moving fluids: the physical biology of flow*. 2nd edition, Princeton, Princeton University Press.
Vollsinger S., Mitchell S.J., Byrne, K.E., Novak, M.D. & Rudnicki, M. 2005. Wind tunnel measurements of crown streamlining and drag relationships for several hardwood species. *Can. J. For. Res.*, 35(5), 1238-1249.
Wilson, C., Hoyt, J. & Schnauder, I. 2008. Impact of foliage on the drag force of vegetation in aquatic flows. *J. Hydraul. Eng.*, 134(7), 885-891.

7.3 **Publikation 3**

Ecological Engineering 43 (2012) 85–90

Contents lists available at SciVerse ScienceDirect

Ecological Engineering

journal homepage: www.elsevier.com/locate/ecoleng

Short communication

Flexural behaviour of selected riparian plants under static load☆

F.J. Sutili[a,*], L. Denardi[a], M.A. Durlo[b], H.P. Rauch[c,1], C. Weissteiner[c,1]

[a] Universidade Federal de Santa Maria (Federal University of Santa Maria), Rio Grande do Sul, Centro de Educação Superior Norte, Departamento de Engenharia Florestal, BR386 km40 Linha 7 de Setembro s/n, CEP: 98400-000 Frederico Westphalen, RS, Brazil
[b] Universidade Federal de Santa Maria (Federal University of Santa Maria), Rio Grande do Sul, Centro de Ciências Rurais (Agricultural Center), Post-Graduation Program in Forest Engineering, Prédio 44, 2° Piso, CEP: 97105-900 Santa Maria, RS, Brazil
[c] Institute of Soil Bioengineering and Landscape Construction, University of Natural Resources and Applied Life Sciences, Vienna, Peter Jordan-Strasse 82, A-1190 Vienna, Austria

ARTICLE INFO

Article history:
Received 24 May 2011
Received in revised form 26 January 2012
Accepted 8 February 2012
Available online 27 March 2012

Keywords:
Soil bioengineering
Phyllanthus sellowianus
Sebastiania schottiana
Salix humboldtiana
Salix × *rubens*
Riparian vegetation
Bending test
Deformation behaviour
Biomechanics

ABSTRACT

Soil bioengineering techniques use plants as construction material for civil and hydraulic engineering purposes such as reinforcement of slopes and erosion control of embankments. The interactions of plants and stress from natural processes have to be quantified to assess such soil bioengineering systems from an engineering point of view.

The objective of this study is to investigate the flexural behaviour of stems and branches of four riparian species of the Southern Brazilian region, suitable for soil bioengineering purposes (*Phyllanthus sellowianus* Müll. Arg., *Sebastiania schottiana* (Müll. Arg.) Müll. Arg., *Salix humboldtiana* Willd. and *Salix* × *rubens* Schrank). 50 green stems of each species were collected in the surroundings of Santa Maria city (29°35′S, 53°32′W), state of Rio Grande do Sul, Brazil, and subjected to static bending tests. Specimens were tested with their bark, immediately after harvesting. The setup of the bending tests was based on the DIN standard (DIN 52186) for 3-point bending tests. Measurements were carried out to obtain characteristic stress × strain diagrams for each stems. The following data analyse resulted in characteristic parameters to describe the overall deformation behaviour (elastic – MOE and plastic – MOR). An additional parameter according to Denardi (2007) was introduced: the "angle of inflection". This parameter describes the elastic and plastic deformation behaviour of a plant under load from an engineering point of view.

Results showed that *P. sellowianus* and *S. schottiana* are very appropriate for the protection of river banks according to the criteria of stem flexural behaviour, rupture strength, angle of inflection, growth rate and plant size. *P. sellowianus* is the most flexible species, followed by *S. schottiana*, *S. humboldtiana* and *Salix* × *rubens*. Therefore riparian forest stands of *S. humboldtiana* and *Salix* × *rubens* need more frequent maintenance in order to keep flexibility.

1. Introduction

Natural disasters worldwide cause major damage to mankind and infrastructure. Nowadays conventional technical solutions have been complemented by ecological alternatives such as soil bioengineering approach. Different soil bioengineering methods have recently regained worldwide recognition for their use in river and civil engineering projects (Howell, 1999; Florineth et al., 2002; Florineth, 2004; Li and Eddleman, 2002; Acharya and Florineth, 2005; Durlo and Sutili, 2005; Lammeranner et al., 2005; Cornelini and Sauli, 2005; Li et al., 2005; Petrone and Preti, 2008, 2010; Bischetti et al., 2010).

The assessment of technical and biological properties of plants from an engineering point of view provides a basement for a successful application and dissemination of soil bioengineering techniques. According to the discussion performed by Burylo et al. (2007), it is well known that vegetation efficiently mitigates erosion in two ways: by active or passive protection. Additional, Wu and Feng (2006) describe the four functions of ecological engineering: (1) improve the revival ability of ecosystem; (2) improve the protective ability of ecosystem; (3) improve the recoverability of ecosystem; (4) improve the functions of streams. Such properties include the capability of vegetative propagation, root penetration, resistance against coarse sediment deposition, tolerance of

☆ Work funded by the Commission for Development Studies at the OeAD Gmbh, Vienna, Austria.
* Corresponding author.
E-mail addresses: fjsutili@gmail.com (F.J. Sutili), lucianodenardi@Yahoo.Com.Br (L. Denardi), migueldurlo@Smail.Ufsm.Br (M.A. Durlo), hp.Rauch@Boku.Ac.At (H.P. Rauch), clemens.Weissteiner@Boku.Ac.At (C. Weissteiner).
[1] Fax: +43 1 47654 7349.

0925-8574/$ – see front matter © 2012 Elsevier B.V. All rights reserved.
doi:10.1016/j.ecoleng.2012.02.012

submersion, elasticity, bending strength, pull out resistance and compound strength.

This paper focuses on the flexural behaviour of selected riparian plants from South Brazil to provide a basis for soil bioengineering implementation work.

Wooden plants have a variable hydraulic impact dependent on the stage of succession. The morphological and material changes over time of plants have to be taken into account from engineers. Riparian plants have different impacts on hydro-morphological processes. On the one hand, they provide bank protection and are responsible for increasing of the hydraulic roughness if they have a high level of flexibility. On the other hand, they cause bank erosion when plants act as rigid elements and after breaking they are the source of hydraulic blockage.

Several studies focused on the hydraulic interaction of flow and plants such as Fathi-Moghadam and Kouwen (1997), Oplatka (1998), Gerstgraser (2000), Righetti and Armanini (2002), Meixner (2004), Rauch (2005), Musleh and Cruise (2006), McBride et al. (2007). The impact depends not only on geometrical properties (e.g. stem and branch diameter, length and leaf density), but also on the dynamic response of plants under flood conditions (stem/branch/leaf bending and reduction of plant height).

Based on the results from a previous study, which focused on the vegetative reproduction potential of suitable plants for soil bioengineering (Sutili et al., 2007), the next step involved quantifying the biomechanical behaviour of plants under specific load.

Mechanical properties such as flexural stiffness, modulus of elasticity and plastic deformation are indicators to assess the impact of plants under load.

Considering the hypothesis that younger plants (smaller diameter of the stems) are more flexible, the objective of this study is comparatively to investigate the behaviour of stems and branches of different riparian species suitable for soil bioengineering (*Phyllanthus sellowianus* Müll. Arg., *Sebastiania schottiana* Müll. Arg., *Salix humboldtiana* Willd. and *Salix* × *rubens* Schrank).

2. Material and methods

2.1. Over view of study area

The specimens were collected along rivers in the surroundings of Santa Maria city (29°35′S, 53°32′W; Brazil). *P. sellowianus* Müll. Arg. is part of the Phyllanthaceae family and grows up to a height of 2–3 m. It is a widely ramified bush with slender and bendable branches. *S. schottiana* (Müll. Arg.) Müll. Arg. (Euphorbiaceae) is also a shrub with a maximum height of 3–4 m. Strong branches, which are highly bendable; are typical. *Salix* × *rubens* Schrank originates from Europe and is a hybrid between *Salix alba* L. and *Salix fragilis* L. (Salicaceae). The plant grows very fast and reaches heights up to 16 m. *S. humboldtiana* Willd. (Salicaceae) is a tree that reaches a height up to 20 m and a stem diameter of about 90 cm. The botanical material was deposited in the Forest Herbarium of the Federal University of Santa Maria, with their numbers: 5588, 5592, 5594, 5590. All of the tested species are known to be well adapted to the environmental conditions along rivers (Denardi, 2007; Sutili et al., 2007).

The minimum diameter was defined at 10 mm and the bending test device limited the maximum diameter. For *P. sellowianus* and *S. schottiana*, no samples that exceeded a diameter of 50 mm for the former and 60 mm for the latter were found in the area under study. Specimens were tested with their bark, immediately after harvesting.

Although riparian vegetation is exposed to dynamic stress during high flood events, static bending tests are useful to identify the bending behaviour of different plant species. 50 static bending tests of each species were carried out, using specimens of different diameters, in green condition. The results have to be considered as a relative comparison between different species.

The setup of the bending tests was based on the DIN standard (DIN 52186) for 3-point bending tests.

The testing equipment automatically recorded the parameters load F [N], center deflection f [mm] and time t [s]. Based on the collected data sets (F [N], f [mm] and t [s]) as well as on the measured diameters d [mm] of the specimens at the loading point and on the span ℓ [mm], it was possible to determine the following parameters: proportional limit load, F_{elast} [N]; ultimate (maximum) load F_u [N]; modulus of elasticity (*MOE*), [N/mm^2]; proportional limit stress, σ_{elast} [N/mm^2]; modulus of rupture (*MOR*) [N/mm^2]; elastic strain, ε_{elast}; plastic strain, ε_{plast}; maximum strain, ε_u; moment of inertia, I [mm^4]; ultimate moment *Mu* [Nmm]; section modulus W [mm^3].

After each bending test, a 100 mm long specimen was taken to access the following properties: moisture content, u [%]; basic apparent density, ρ [g/cm^3]; thickness of bark, tc [mm]; percentage of bark, $\%c$ [%]; age of specimen, Y [years].

2.2. Calculated parameters

The ultimate load (F_u) and proportional limit load (F_{elast}) were directly taken from the load × deflection curve. The modulus of elasticity in bending (*MOE*) [N/mm^2] is used to characterize the tendency to be deformed elastically of the stems and branches. This mechanical parameter expresses the ratio between the stress and strain under load, i.e., how much force is required for a given unit of reversible deformation. The modulus of elasticity for specimens with a circular cross-section, simply supported at ends and under action of a concentrated load at mid-span, is calculated as:

$$MOE = \frac{F_{elast}\ell^3}{48 f_{elast} I} \quad (1)$$

where F_{elast} is the proportional limit load [N], ℓ is the span [mm], f_{elast} is the deflection at proportional limit [mm], I is the moment of inertia [mm^4].

The moment of inertia (I) [mm^4] for a circular section:

$$I = \frac{\pi d^4}{64} \quad (2)$$

where d [mm] is the cross section diameter of the specimen measured at the point of load application.

Replacing I in Eq. (1), the equation changes to:

$$MOE = \frac{F_{elast}\ell^3}{3 f_{elast}(\pi d^4/4)} \quad (3)$$

The strain ε is a dimensionless variable:

$$\varepsilon = f\frac{6d}{\ell^2} \quad (4)$$

where f is the center deflection [mm], d is the diameter of specimen at the point of load application [mm], ℓ is the span [mm].

Eqs. (3) and (4) used for the analysis of *MOE* and ε are based on the assumption that the segment of the specimen has a constant diameter and shear stress is neglected. Tree stems are generally tapered, but in our case, the diameters of the specimens were approximately constant, therefore the tapering effect is negligible. Usually bending resistance of wood is determined with a 4-point bending test. The results of the used 3-point bending test are influenced by shear stress, but for wood, it is conventionally neglected if $\ell/d > 14$.

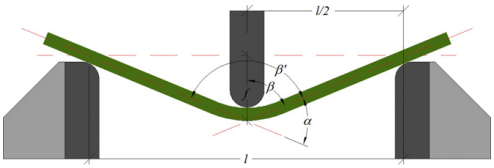

Fig. 1. Bending diagram, indicating the variables used in calculating the angle of inflection (α).

However, the applied equations are considered as approximations and results are highly appropriate to compare the species with each other.

The modulus of rupture *MOR* [N/mm^2] for the specimens with a circular cross-section was obtained from:

$$MOR = \frac{M_{max}}{W_{max}} = \frac{F_u(\ell/4)}{\pi d^3/32} = \frac{8F_u\ell}{\pi d^3} \quad (5)$$

where M_{max} is the maximum bending moment [Nmm], W_{max} is the section modulus [mm^3], F_u is the ultimate load [N], ℓ is the span [mm], d is the diameter of specimen at the point of load application [mm].

The stress up to the proportional limit σ_{elast} [N/mm^2] can be obtained by the formula (5), replacing the ultimate load F_u [N] by the load up to the proportional limit F_{elast} [N] or by "Hooke's Law," which determines:

$$\sigma_{elast} = MOE \cdot \varepsilon_{elast} \quad (6)$$

where *MOE* modulus of elasticity [N/mm^2], ε_{elast} deformation in the elastic region.

Additionally, for each samples branches mechanical test, was calculated the moisture content (%), percentage of the bark (%) and the basic apparent density of the wood (g/cm^3).

After preparation and staining of histological sections, a microscope was used to determine the age of the samples.

An additional parameter according to Denardi (2007) has been used. It describes the whole deformation process of plants under load: angle of inflection at proportional limit, α_{elast} [°] and angle of inflection at ultimate load, α_u [°].

At the original non-inflected position (dashed horizontal line in Fig. 1), the bending point divides the specimen into two equal parts with an angle of zero to the horizontal and 180° between the two. The levels of proportional limit and ultimate load are characterized by the parameters of ℓ (span) and f (deflection) for each individual specimen and used to calculate the angle of inflection (α), respectively α_{elast} and α_u (Fig. 1).

$$\tan\beta = \frac{\ell/2}{f}; \qquad \tan\beta' = 2\tan\beta \quad (7)$$

$$\text{Internal angle}(\beta') = \arctan\beta' \quad (8)$$

$$\text{Inflection angle}(\alpha) = 180 - \arctan\beta' \quad (9)$$

3. Results and discussion

3.1. Basic apparent density, moisture content and dimension of bark

The basic apparent density and the moisture content affect the material properties on the bending conditions. In general, *P. sellowianus* showed, independently of the moisture content (figure not showed), higher values of the basic apparent density (0.51 g/cm^3) when compared with all other species (<0.4 g/cm^3). The slower growth and the higher average age of the specimens of *P. sellowianus* are possible causes.

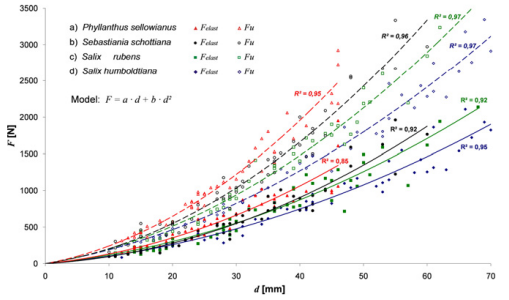

Fig. 2. Relationship between diameter (d) and load (F). Solid line: at the proportional limit, F_{elast}; dashed line: at the ultimate load, F_u.

As expected, the thickness of the bark strongly correlates with the diameters and maintains a relatively constant percentage up to the highest diameters used in this study. The two species with a lower average bark thickness – *P. sellowianus* and *S. schottiana* – consequently show a more discrete increase in bark thickness with increasing diameter. *S. humboldtiana* represents the thickest bark from 5 mm up to 7 mm for stem diameters between 60 and 70 mm. Brüchert et al. (2003) found that the higher initial bark/wood ratio and its decline with the development of the branch may to be a cause of the initial variations regarding the modulus of elasticity (*MOE*). All specimens have been tested in bending, with bark.

4. Modulus of elasticity

Fig. 2 indicates the force (F) for different diameters, which is required to reach the proportional limit – F_{elast} (solid line) and the ultimate load – F_u (dashed line).

P. sellowianus is the most stiff species in bending, whereas *S. humboldtiana* is the most flexible one. This means that for *P. sellowianus* a higher amount of load is necessary to reach the proportional limit and the ultimate load respectively.

Table 1 shows the moduli of elasticity for the different species classified into diameter classes. The standard deviation and the coefficient of variation [%] are shown in brackets. The last column contains the coefficient of determination between the modulus of elasticity and the stem and branch diameter. It can be concluded from the low coefficients of determination that there is in fact no correlation.

The calculated moduli of elasticity are visually lower than those determined by Vollsinger et al. (2000) for green stems and branches of five European species (*Alnus glutinosa* (L.) Gaertn. *Fraxinus excelsior* L., *S. alba* L., *Salix caprea* L. and *Acer pseudoplatanus* L.). The authors obtained values between 6900 and 10,200 N/mm^2 for the different species (with diameters of 40–100 mm). Based on parameter *MOE*, the tested southern Brazilian species are visibly less rigid.

The moduli of elasticity (Table 1) appeared to decline with increasing diameter. However, this suggestion of an inverse correlation between the modulus of elasticity and the stem diameter must be considered with caution due to the small number of tested specimens, the high coefficients of variation and the low coefficients of determination (R^2). Perhaps the distribution of stems and branches diameters could be useful to understand this behaviour. Vollsinger et al. (2000) found similar results. Brüchert et al. (2003) conducted tests on *A. glutinosa* (L.) Gaertn and *Alnus viridis* (Chaix) DC. at an age of 1–24 years and found a slight increase in the

Table 1
Average values of the modulus of elasticity at green state [N/mm²] for the different diameter classes of each species. Standard deviation and coefficient of variation [%] are shown in parentheses.

Species	Modulus of elasticity [N/mm²] per diameter class						R^2
	10–20 mm	20–30 mm	30–40 mm	40–50 mm	50–60 mm	60–70 mm	
Phyllanthus sellowianus	4.513 (889;20)	3.793 (1173;31)	3.329 (835;25)	3.028 (825;27)	–	–	0.27
Sebastiania schottiana	4.615 (1188;26)	3.930 (1126;29)	4.104 (1273;31)	3.485 (432;12)	3.114 (575;18)	–	0.14
Salix × rubens	4.940 (1726;35)	4.562 (1312;29)	4.296 (1054;25)	3.555 (1208;34)	3.625 (766;21)	3.031 (331;11)	0.19
Salix humboldtiana	4.084 (1590;40)	3.347 (630;19)	3.254 (388;12)	2.822 (925;33)	2.419 (285;12)	2.155 (446;24)	0.35

modulus of elasticity up to the fifth year. In older samples, the modulus of elasticity remained relatively constant. Niklas (1992) noted that young cell walls are ductile, while older cells walls tend to be much more elastic and resilient.

4.1. Proportional limit and ultimate load

Fig. 3 shows the stress × strain curve up to the proportional limit (solid line) and then to the ultimate load (dashed line). The first part of the diagram showing a linear behaviour, where the modulus of elasticity and the proportional limit can be determine from. From this point, the deformation becomes plastic and continues up to the ultimate load in a non-linear behaviour.

The variation of the deformation behaviour between the species is much higher at the plastic range compared to the elastic one. Apparently, *S. schottiana* and especially *P. sellowianus*, resist large deformation and stresses up to the ultimate load, while *S. humboldtiana* withstands slightly less stress than *Salix × rubens*. However, *S. humboldtiana* exhibited bigger flexural deformations in comparison to *Salix × rubens*.

4.2. Angle of inflection

The strain ε can be understood as an expression of how the material behaves under load. The angle of inflection up to the proportional limit (α_{elast}) and specifically up to the ultimate load (α_u) is another possibility to express its behaviour.

The angle of inflection at the proportional limit did not correlate with diameter. The α_{elast} area in Fig. 4 represents the range of the inflection angle at the proportional limit for any species and diameter. The angle of inflection at the ultimate load represents the maximum angle to which a stem or branch of a particular species and diameter can be bent before it fails. The results have to be considered as a base to compare the bending behaviour of the tested species.

The diagram shows that *P. sellowianus* exhibited a larger angle of inflection at the ultimate load than the other species. For example, while a branch (d = 20 mm) of *P. sellowianus* exhibited a maximum angle of 45° inflection before failure, a branch of *Salix × rubens* of the same diameter reached a maximum angle of 25° at ultimate load.

The relationship between the angle of inflection at rupture (α_u) and the ultimate load (F_u) for the four species and seven selected diameters (Fig. 5). The nomogram shown in Fig. 5 cannot be used to derive the values at the proportional limit due to the lack of a relationship between the inflection angle and the diameter at this limit (Fig. 4).

The load required to reach the failure increased with larger diameters, whereas the angle of inflection at the ultimate load decreased. For example, a branch of *P. sellowianus* with a

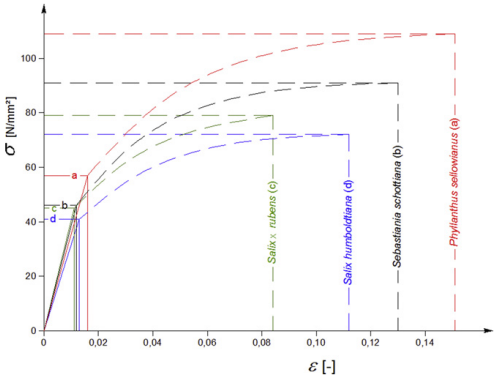

Fig. 3. Average trend stress/strain curves up to proportional limit (solid line) and further to ultimate load (dashed line) for the four species.

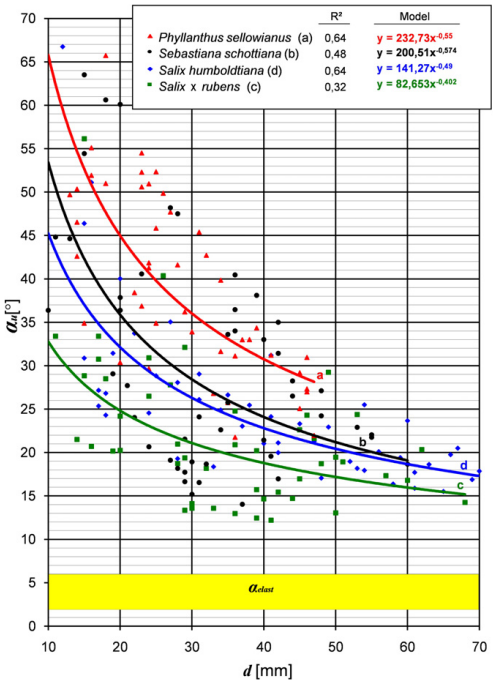

Fig. 4. Relationship between the diameter (d) and the angle of inflection at failure(α_u). The band at the bottom of the graph shows the area of distribution of the angles of inflection at the proportional limit (α_{elast}).

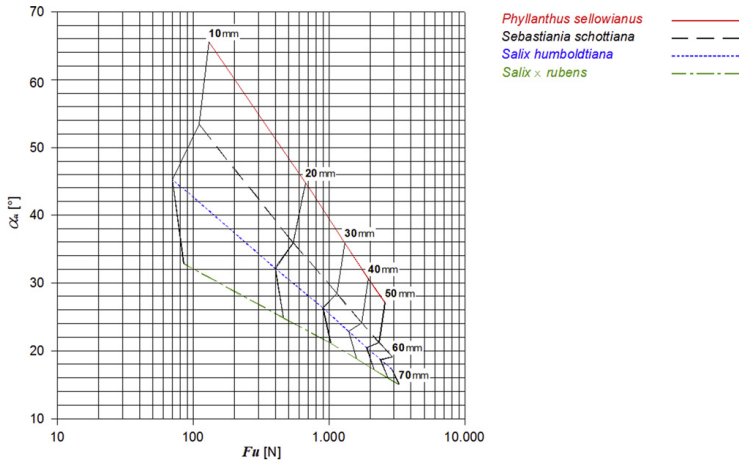

Fig. 5. Relationship between angle of inflection α_u at rupture and log F_u (ultimate load) dependent from the diameter for the four species.

diameter of 20 mm had to be stressed up to a load of 670 N to reach the angle of rupture and formed a 45° angle of inflection. A branch of *S. schottiana* of the same diameter, with a load of 550 N, broke at 36°. *S. humboldtiana* formed a smaller inflection angle (32°) and required a load of 400 N to reach the failure. For the same diameter, *Salix* × *rubens* – despite having an angle of inflection at failure that is even lower than the previous species – needed a higher load (460 N) than *S. humboldtiana* to reach a maximum 25° angle of inflection.

As shown in Fig. 5, the inflection angle gradually declined with the increasing in diameter. *P. sellowianus* is the species that apparently supports the greatest stress and can be bent to higher angles of inflection up to the ultimate load. Moreover, its growth rate is the lowest of all species investigated.

The relationship between age of the stems or branches and their diameter was conducted. This relationship exposed the different local environmental growing conditions and can be taken as reference values for the growth rate of the species according to temporal period of consideration of the specimens.

In a following step, the growth rate (diameter and age) is related to the angle of inflection at ultimate load (α_u) and shown in Fig. 6.

The relationship between age and stem diameter can be seen directly on the *x*- and *y*-axes respectively. The angle of inflection is characterised by means of the marked areas. For example, in order to know the diameter of an specific stem at an age of 4 years, a straight line parallel to the *y*-axis at the 4 years age is traced. At the point where this line crosses the straight line that defines the relations for *P. sellowianus*, one will get a diameter of 16 mm and an inflection angle at failure of 50°. At the same age, *S. schottiana* has a diameter of 23 mm and a 33° inflection angle (interpolated between the lines of 30° and 35°). *Salix* × *rubens* at 4 years shows a diameter of 32 mm and can be bent till it reaches angles of inflection of 21°, while *S. humboldtiana*, reaching a larger diameter (39 mm),

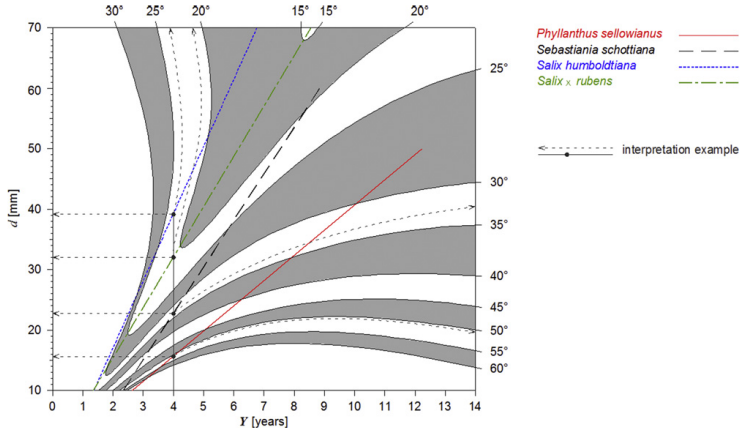

Fig. 6. Relationship with the diameter (d) and angle of inflection at ultimate load (α_u), for different ages (Y).

show approximately 24° angle of inflection at rupture. The same procedure can be applied starting from any diameter (d), age (Y) or angle of inflection (α_u), for each species. Even the relationship between the different parameters is variable due to specific local growing conditions. Fig. 6 provides a useful tool for planning and managing local soil bioengineering work.

5. Conclusions and final remarks

The modulus of elasticity (*MOE*), as a single parameter, does not satisfactorily explain the flexural behaviour of live stems or branches for the assessment of soil bioengineering structures, on river banks.

The angle of inflection is a useful criterion to identify a plant's capacity to stabilise river banks under hydraulic stress. High flexibility means that stressed plants are able to bend down reducing turbulence effects and acting as a protection layer against bank erosion. Additionally, this property improves the free stream flow along the river cross-section.

Based on the parameters inflection angle α_u, ultimate load F_u and age Y, it can be affirmed that plants of a smaller diameter (younger shoots) are more flexible, and better suitable for river banks stabilization, regardless of species. The results showed that the flexibility of the stems and branches decrease over the time, but not equally or proportionally for each of the species studied.

It was found that *P. sellowianus* and *S. schottiana* are very appropriate for the protection of river banks according to the criteria of inflection angle, rupture strength (stem breakage), growth rate and plant size. Riparian forest stands of *S. humboldtiana* and *Salix* × *rubens* need more frequent maintenance (systematic stem cutting procedure) in order to preserve its "flexibility function". According to the literature, any of the four species studied can excellently withstand and respond well to the branch pruning and trunk or stem coppicing.

Furthermore, more studies about the influence of the bark and the anatomical characteristics of the wood can be helpful to clarify additional biomechanical characteristics of the riparian vegetation.

References

Acharya, M.S., Florineth, F., 2005. Bamboo crib wall—a sustainable bioengineering method to stabilise slopes in Nepal. In: International Symposium "Landslide Hazard in Orogenic Zone from the Himalaya to Island Arc in Asia, 25–26 September 2005, Kathmandu, Nepal, pp. 235–244.

Bischetti, G.B., Chiaradia, E.A., D'Agostino, V., Simonato, T., 2010. Quantifying the effect of brush layering on slope stability. Ecol. Eng., 258–264.

Burylo, M., Rey, F., Delcros, P., 2007. Abiotic and biotic factors influencing the early stages of vegetation colonization in restored marly gullies (Southern Alps, France). Ecol. Eng. 30, 231–239.

Brüchert, F., Gallenmüller, F., Bogenrieder, A., Speck, T., 2003. Stem Mechanics, Functional Anatomy and Ecology of *Alnus viridis* and *Alnus glutinosa*, vol. 114. Feddes Repertorium, Berlin, pp. 181–197.

Cornelini, P., Sauli, G., 2005. Manuali di indirizzo delle scelte progettuali per interventi di ingegneria naturalistica. Ministero dell'Ambiente e della Tutela del Territorio/Ministero dell'Economia e delle Finanze. Progetto Operativo Difesa Suolo.

Denardi, L., 2007. Anatomia e flexibilidade do caule de quatro espécies lenhosas, para o manejo biotécnico de cursos de água. Tese (Doutorado em Manejo Florestal) – Universidade Federal de Santa Maria (UFSM), Santa Maria, 113 pp.

DIN 52186, 1978. Prüfung von Holz – Biegeversuch. Deutsches Institut für Normung, Berlin.

Durlo, M.A., Sutili, F.J., 2005. Bioengenharia – Manejo biotécnico de cursos de água. Editora EST, Porto Alegre, 189 pp.

Fathi-Moghadam, M., Kouwen, N., 1997. Nonrigid, nonsubmerged, vegetative roughness on floodplains. J. Hydrogen Eng. 123 (1), 51–57.

Florineth, F., Rauch, H.P., Staffler, H.P., 2002. Stabilization of landslides with bioengineering measures in South Tyrol/Italy and Thankot/Nepal. In: Interpraevent 2002 in the Pacific Rim (Ed.), Interpraevent 2002 in the Pacific Rim, vol. 2. Congress publication, Matsumoto/Japan, pp. 827–837.

Florineth, F., 2004. Pflanzen statt Beton. Handbuch zur Ingenieurbiologie und Vegetationstechnik. Patzer Verlag Berlin, Hannover, 282 pp.

Gerstgraser, C., 2000. Ingenieurbiologische Bauweisen an Fliessgewässern. Grundlagen zu Bau, Belastbarkeiten und Wirkungsweisen. Band 52, Dissertation, Universität für Bodenkultur, Wien.

Howell, J., 1999. Roadside Bio-engineering. Dept. of Roads. His Majesty's Government of Nepal, Kathmandu.

Lammeranner, W., Rauch, H.P., Laaha, G., 2005. Implementation and monitoring of soil bioengineering measures at a landslide in the Middle Mountains of Nepal. Plant Soil 278, 159–170.

Li, M.-H., Eddleman, K.E., 2002. Biotechnical engineering as an alternative to traditional engineering methods. A biotechnical streambank stabilization design approach. Landscape Urban Plan. 60, 225–242.

Li, M.-H., Landphair, H.C., Arnold, M.A., Mullin, K., Eddleman, K.E., 2005. A dormancy extension technique for biotechnical streambank stabilization in warm regions. Landscape Urban Plan. 71, 223–231.

Meixner, H., 2004. Grundsätze zum Management von Ufervegetation. Ingenieurbiologie. Mitteilungsblatt für die Mitglieder des Vereins für Ingenieurbiologie, Nr. 2, pp. 14–18.

Musleh, F.A., Cruise, J.F., 2006. Functional relationships of resistance in wide flood plains with rigid unsubmerged vegetation. J. Hydraulic Eng. 132 (February (2)), 163–171.

McBride, M., Hession, W.C., Rizzo, D.M., Thompson, D.M., 2007. The influence of riparian vegetation on near-bank turbulence: a flume experiment. Earth Surf. Process. Landforms 32 (13), 2019–2037.

Niklas, K.J., 1992. Plant Biomechanics—an Engineering Approach to Plant Form and Function. University of Chicago, Press Chicago & London, 607 pp.

Oplatka, M., 1998. Stabilität von Weidenverbauungen an Flussufern. Mitteilung 156, Versuchsanstalt für Wasserbau, Hydrologie und Glaziologie, ETH-Zürich.

Petrone, A., Preti, F., 2010. Soil bioengineering for risk mitigation and environmental restoration in a humid tropical area. Hydrol. Earth Syst. Sci. 14, 239–250.

Petrone, A., Preti, F., 2008. Suitability of soil bioengineering techniques in Central America: a case study in Nicaragua. Hydrol. Earth Syst. Sci. 12, 1241–1248.

Rauch, H.P., 2005. Hydraulischer Einfluss von Gehölzstrukturen am Beispiel der ingenieurbiologischen Versuchsstrecke am Wienfluss. Dissertation an der Universität für Bodenkultur Wien, 222 pp.

Righetti, M., Armanini, A., 2002. Flow resistance in open channel flows with sparsely distributed bushes. J. Hydrol. 269, 55–64.

Sutili, F.J., Rauch, H.P., Durlo, M.A., Florineth, F., 2007. Investigations on the Selection of Plants for Soil Bioengineering Measures in South Brazil (Poster). European Geoscience Union Assembly, Vienna.

Vollsinger, S., Doppler, F., Florineth, F., 2000. Ermittlung des Stabilitätsverhaltes von Ufergehölzen in Zusammenhang mit Erosionsprozessen an Wildbächen. Universität für Bokenkultur, Wien. Studie in Auftrag des Bundesministeriums für Land- und Forstwirtschaft, 107 pp.

Wu, H.L., Feng, Z., 2006. Ecological engineering methods for soil and water conservation in Taiwan. Ecol. Eng. 30, 333–344.

7.4 Publikation 4

Universität für Bodenkultur Wien
University of Natural Resources and Life Sicences, Vienna

Department für Bautechnik und Naturgefahren

Clemens Weissteiner

Characterizing riparian vegetation by means of physically based plant parameters

Die Ingenieurbiologie als bautechnische Disziplin verwendet lebende Pflanzen und lokal verfügbare Hilfsstoffe wie Holz und Steine als Baustoffe, um die Böschungsstabilität zu erhöhen und erosive Prozesse zu verhindern. Die für die Ingenieurbiologie in Frage kommenden Pflanzen müssen für die extremen standörtlichen Bedingungen bestimmte Voraussetzungen erfüllen können. Für die Entwicklung dieser „grünen" Technologie müssen die hydro- und aerodynamischen Belastungen und die biomechanischen Eigenschaften der Pflanzen erfasst werden. Die Reaktionen auf diese Belastungen sind von der zeitlichen Entwicklung und von den damit verbundenen Änderungen der integralen strukturellen und biomechanischen Eigenschaften der Pflanzen abhängig. Mit dem gegenständigen Dissertationsprojekt wird das systematische Verformungsverhalten von verschiedenen Pioniergehölzen untersucht. Schwingungs- und Dämpfungseffekte sowie die Kontraktion der Gehöze werden untersucht, um das systematische Verformungsverhalten zu charakterisieren.

Keywords Ingenieurbiologie; Ufervegetation; Biomechanik; Kontraktion; Dynamisches Verhalten;

Soil bioengineering is a construction technique, which combines living plants and local natural auxiliary materials such as wooden logs and stones to improve slope stability and prevent erosion. Plants eligible for soil bioengineering purposes have to meet all requirements to resist the unfavourable conditions at the local construction site. As a precondition to develop an efficient biological engineering system, hydro- and aerodynamic forces acting on the system and the biomechanical properties of the plants have to be determined. Furthermore, the response to these forces also depends on the changes of the trees due to the stage of development of the integrating structural and bio-mechanic properties of the plants. The doctoral project aims at investigating the systematic behaviour of various woody riparian plant species under applied loads. The reconfiguration of plants as well as their natural frequency and damping effects will be investigated to characterize the interaction of applied forces and riparian trees

Keywords Soil Bio Engineering; Riparian Vegetation; Biomechanics; Reconfiguration; Dynamics;

1 Background

Soil bioengineering is a technique for civil engineering purposes. It combines living plants and local natural auxiliary materials such as wooden logs and stones to improve slope stability and prevent erosion. Plants eligible for soil bioengineering purposes have to meet all requirements to resist the unfavourable conditions at the local construction site. Characteristic requirements are pull-out resistance, sprouting and rooting capacity, adaptability to prolonged flooding periods, resistance against shear strength etc.. In nature, woody pioneer plant species, which have these properties, are generally found along rivers or in harsh alpine areas e.g. willows, poplars, alders and tamarisks and grow in shape of trees or shrubs. To develop an efficient biological engineering system, forces acting on the system and the technical properties of the plants have to be characterized. Especially in the case of near-nature river engineering it is of crucial importance to identify the plants' response to hydrodynamic processes. Vegetation-flow interactions are central to many problems of hydrologists and hydraulic engineers including flood risk assessment, sediment transport studies and eco-hydraulic studies.

2 State of the art

Vegetation-flow interaction has been investigated for decades. Based on the balance of forces in which gravity forces are opposed to boundary shear stress and vegetation drag, first attempts were made to quantify these processes [1;2]. However, ongoing research in hydrodynamics focused mainly on the impact of plants on hydraulic aspects rather than on the plants behaviour under loading. Whereas investigations in atmospheric flows have focused on the plants' response to dynamic loads [3;4;5;6]. From a systematic point of view the interaction between plants and aerodynamic as well as hydrodynamic loads are subjected to the same physical processes. However, according to the law of resistance the main difference consists in the density of air respectively water.

The following literature review summarizes the main works related to the topic, and is divided into two sections (1) response to hydrodynamic loads and (2) response to aerodynamic loads.

Response to hydrodynamic loads

The hydraulic interaction of flow and plants not only depends on geometrical properties (e.g. stem and branch diameter, length, leaf area), but also on the dynamic response of plants under flood conditions (stem/branch/leaf bending and horizontal and vertical contraction processes; e.g. [7;8;9;10]). Several studies investigated the impact of plants on discharge capacity. In most lab studies artificial obstructions [11;12;13;14;15;], plant saplings, plant parts (branches) [16;17;18) or whole plants [8;19;20] were used. However, most studies focused more on hydraulic aspects than on biomechanical and structural parameters of plants. Beside plant architecture, mechanical properties like flexural stiffness, modulus of elasticity and plastic deformation are indicators to assess the impact of plants on hydraulic conditions [21].

Response to aerodynamic loads

Vegetation-flow interaction has also been investigated intensely in several studies in the context of plant exposure to aerodynamic loads [e.g.22;23;24].

In order to describe the plants response to wind loads, biomechanical properties of different plant species have largely been investigated [e.g. 25;26;27]. By analysing a tree's deformation under static loads, failure occurs when the maximal bending moment exceeds the maximal resistive moment. In nature, trees act as dynamic systems, oscillating and streamlining under applied loads. [28] comes to the conclusion that models applying static loads on trees are insufficient to predict mechanical stability. In fact, much lower dynamic loads than those predicted by static tests can lead to failure. Investigations in this field of research included static pulling tests [e.g.29;30], dynamic swaying experiments [3;4;5;24] as well as wind tunnel experiments [31,32].

[29] was the first to propose a theoretical model for a tree submitted to dynamic wind loading. Papesch's model was based on beam theory, drag forces are assumed to apply all around the tree and wind force varied sinusoidal at frequencies similar to trees natural frequencies. [33] as well as [34] introduced models discretizing the geometry of trees. Those studies have all focused on the stem of the plant while simplifying the rest of the aerial system. [35] stated in their work that branches need to be considered as individual damped harmonic oscillators coupled to the main stem and not simply as lumped masses. [36] report in their experiments on young Pinus saplings foliage as the major source of damping in the structure. [17] summarizes that each branch is a mass that sways in the wind and interacts dynamically with other branches and the trunk in a complex way.

However, most of the studies regarding wind on trees, or forest stands investigate tree species, which are interesting from a silviculture point of view. Plants used in soil bioengineering haven't been subject of these types of studies yet. Within soil bioengineering particularly pioneer plants are used to reinforce slopes and riverbanks. These plants are capable to grow on poor stands under adverse circumstances. Riparian vegetation shows biomechanical properties to withstand strong dynamic loads, young plants are able to streamline and adapt gradually after floods even if the elastic range was by far exceeded. Therefore, biomechanical tests, in combination with static and dynamic loading tests of typical plants used in soil bioengineering are absolutely essential for a better understanding and quantification of the systems impact.

3 Problem identification and aims

Although international research activities have been carried out on hydraulics of vegetated flow over the past decades, many aspects are still poorly understood. The situation arises from knowledge gaps and hence a lack of suitable models integrating structural properties of flexible riparian vegetation cover, biomechanical properties of individual plants and hydrodynamic characteristics of flow.

While in civil engineering calculation of stability against collapse represents the state of the art, engineers using plants as stabilizing elements are faced with problems to dimension the mechanical effects of this complex multilevel system in a temporal and spatial context. Generally speaking, dimensioning complex plants as engineering elements is a key issue and a precondition to develop standards in the field of soil bioengineering respectively near nature river engineering. The geometric representation of plants, the interaction of plants with loads (static as well as dynamic) and the resulting forces are of crucial importance to dimension biomechanical systems. However, the plant – load interaction in soil bioengineering systems rises in complexity because typical young, woody riparian vegetation has specific capability to bend.

In order to model a force on a plant, first of all the plant has to be represented geometrically in a high detailed 3D computer model. The architecture of a plant is, at any given time, the expression of equilibrium between endogenous growth processes and exogenous constraints exerted by the environment [37].

Until now research focused mainly on forest plants under wind load at single plant scale and forest stand scale as well as on decurrent solitary trees and the drag exerted on plants. However, these results of wind studies can hardly be applied to soil bioengineering systems because plant material properties and their architecture are rather different. The drag force exerted on plants is of crucial importance, but without the missing link of the plants' deformation, (horizontal and vertical contraction) results are limited. Furthermore, plants behave differently in water or air if considering the effect of viscosity of both media in relation to their dynamic response.

Therefore this study aims to fill these gaps by:

- Modelling the architecture of riparian shrubs
- Determining material properties of different plant structural components typically used in soil bioengineering (e.g. willows)
- Investigating the bending behaviour and the dynamic response of whole plants under applied loads in water and air
- Developing an integrated approach including plant architecture and material properties to model the dynamic response of riparian shrubs on loads

Literature

[1] LI, R.-M.; SHEN, H.W.: EFFECT OF TALL VEGETATIONS ON FLOW AND SEDIMENT. J HYDRAULICS DIVISION, 99 (1973), PP. 793–814.

[2] PETRYK, S.; BOSMAJIAN, G.B.: ANALYSIS OF FLOW THROUGH VEGETATION. J HYDRAULICS DIVISION, 101 (1975), 871–884.

[3] MILNE , R.: DYNAMICS OF SWAYING PICEA SITCHENSIS . TREE PHYSIOL. 9 (1991), 383 – 399.

[4] GARDINER, B.A.: WIND – TREE INTERACTIONS. IN WIND AND TREES. M. COUTTS AND J. GRACE (EDS). CAMBRIDGE UNIVERSITY PRESS, CAMBRIDGE (1995), 41 –59.

[5] MOORE, J.R.; MAGUIRE, D.A.: SIMULATING THE DYNAMIC BEHAVIOR OF DOUGLAS-FIR TREES UNDER APPLIED LOADS BY THE FINITE ELEMENT METHOD. TREE PHYSIOLOGY 28(2007), 75-83

[6] SELLIER, D.; FOURCAUD, T.: CROWN STRUCTURE AND WOOD PROPERTIES: INFLUENCE ON TREE SWAY AND RESPONSE TO HIGH WINDS. AMERICAN JOURNAL OF BOTANY 96(5)(2009): 885-896.

[7] FATHI-MOGHADAM, M.; KOUWEN, N.: NONRIGID, NONSUBMERGED, VEGETATIVE ROUGHNESS ON FLOODPLAINS. JOURNAL OF HYDRAULIC ENGINEERING 123(1)(1997): 51-57.

[8] OPLATKA, M.: STABILITÄT VON WEIDENVERBAUUNGEN AN FLUSSUFERN.. MITTEILUNGEN 156. VERSUCHSANSTALT FÜR WASSERBAU, HYDROLOGIE UND GLAZIOLOGIE. ETH ZÜRICH (1998).

[9] GERSTGRASER, C.; RAUCH, H.P.: EFFECT OF VEGETATION ON RIVERBANK STABILITY. EUROPEAN GEOPHYSICAL SOCIETY (ED.): GEOPHYSICAL RESEARCH ABSTRACTS, VOL.2, 25TH GENERAL ASSEMBLY (2000).

[10] RAUCH, H.P.: EFFECTS OF A VEGETATED RIVER BANK ON THE FLOW FIELD. EUROPEAN GEOSCIENCES UNION: EUROPEAN GEOSCIENCES UNION GENERAL ASSEMBLY 2005, VIENNA; GEOPHYSICAL RESEARCH ABSTRACTS, VOLUME 7.

[11] SHIMIZU, Y.; TSUJIMOTO, T.: NUMERICAL ANALYSIS OF TURBULENT OPEN-CHANNEL FLOW OVER VEGETATION LAYER USING A KTURBULENCE MODEL. J. OF HYDROSCIENCE AND HYDRAULIC ENGRG., JSCE, 11 (2)(1994): 57-67.

[12] TSUJIMOTO, T., KITAMURA, T., FUJII, Y., NAKAGAWA, H.: HYDRAULIC RESISTANCE OF FLOW WITH FLEXIBLE VEGETATION IN OPEN CHANNEL. JOURNAL OF HYDROSCIENCE AND HYDRAULIC ENGINEERING 14(1)(1996): 47-56

[13] NEPF, H.M.: DRAG, TURBULENCE, AND DIFFUSION IN FLOW THROUGH EMERGENT VEGETATION. WATER RESOURCES RESEARCH 35(2)(1999): 479-489.

[14] LÓPEZ, F. AND GARCÍA, M.H.: MEAN FLOW AND TURBULENCE STRUCTURE OF OPEN-CHANNEL FLOW THROUGH NON-EMERGENT VEGETATION. JOURNAL OF HYDRAULIC ENGINEERING. 127 (5)(2001): 392-402.

[15] POGGI, D.; PORPORATO, A.; RIDOLFI, L.; ALBERTSON, J. D.; KATUL, G. G.: THE EFFECT OF VEGETATION DENSITY ON CANOPY SUBLAYER TURBULENCE. BOUNDARY-LAYER METEOROLOGY (111)(2004): 565–587.

[16] ARMANI, A.; RIGHETTI, M. AND GRISENTI, P.: DIRECT MEASUREMENT OF VEGETATION RESISTANCE IN PROTOTYPE SCALE. JOURNAL OF HYDRAULIC RESEARCH 43(5)(2005): 481-487.

[17] JAMES, K.R.; HARITOS, N.; ADES, P.A.: MECHANICAL STABILITY OF TREES UNDER DYNAMIC LOADS, AMERICAN JOURNAL OF BOTANY 93 (10)(2006): 1522-1530.

[18] WILSON, C.A.M.E.,XAVIER, P.; SCHONEBOOM, T.; ABERLE, J.; RAUCH, H.P.; LAMMERANNER, W.; WEISSTEINER, C.; THOMAS, H.: THE HYDRODYNAMIC DRAG OF FULL SCALE TREES. IN: PROCEEDINGS OF THE INTERNATIONAL CONFERENCE ON FLUVIAL HYDRAULICS; VOLUME 1 (2010); 453-460.

[19] FREEMAN, G. E.; RAYMEYER, W. J. AND COPLAND, R. R.: DETERMINATION OF RESISTANCE DUE TO SHRUBS AND WOODY VEGETATION. US ARMY CORPS OF ENGINEERS. REPORT ERDC/CHLTR-00-25 (2000).

[20] XAVIER, P.; WILSON, C.A.M.E.; ABERLE, J.; RAUCH, H.P.; SCHONEBOOM, T.; LAMMERANNER, W.; THOMAS, H.: "DRAG FORCE OF FLEXIBLE SUBMERGED TREES." PROC. HYDRALAB CLOSING EVENT, HANNOVER (2010).

[21] ISHIKAWA, H.; AMANO S. AND YAKUSHIJI, K.: FLOW AROUND A LIVING TREE, JSME INTERNATIONAL JOURNAL SERIES B, VOL. 49 (2006), NO. 4 SPECIAL ISSUE ON JETS, WAKES AND SEPARATED FLOWS,1064-1069.

[22] PELTOLA, H.; KELLOMÄKI, S.; HASSINEN, A.; LEMETTINEN, M.; AHO, J.: SWAYING OF TREES AS CAUSED BY WIND: ANALYSES OF FIELD MEASUREMENTS. SILVA FENN., 27(2)(1993): 113-127.

[23] GAFFREY, D.; KNIEMAYER, O.: THE ELASTO-MECHANICAL BEHAVIOUR OF DOUGLAS FIR, ITS SENSITIVITY TO TREE-SPECIFIC PROPERTIES, WIND AND SNOW LOADS, AND IMPLICATIONS FOR STABILITY – A SIMULATION STUDY. JOURNAL OF FOREST SCIENCE, 48, (2)(2002): 49-69

[24] SELLIER, D.; BRUNET, Y. AND FORCAUD, T.: A NUMERICAL MODEL OF TREE AERODYNAMIC RESPONSE TO A TURBULENT AIRFLOW. FORESTRY (2008), VOL 81, NO. 3.

[25] SPATZ H.-CH.; KÖHLER, L. AND NIKLAS, K.J.: MECHANICAL BEHAVIOUR OF PLANT TISSUES: COMPOSITE MATERIALS OR STRUCTURES? , JOURNAL OF EXPERIMENTAL BIOLOGY 202(1999), 3269-3272.

[26] BRÜCHERT, F.; GALLENMÜLLER, F.; BOGENRIEDER, A.; SPECK, T.: STEM MECHANICS, FUNCTIONAL ANATOMY AND ECOLOGY OF ALNUS VIRIDIS AND ALNUS GLUTINOSA, FEDDES REPERTORIUM (2003) 114, 3/4: 181 – 197.

[27] SONE, K., NOGUCHI, K., TERASHIMA, I.: MECHANICAL AND ECOPHYSIOLOGICAL SIGNIFICANCE OF THE FORM OF A YOUNG ACER RUFINERVE TREE: VERTICAL GRADIENT IN BRANCH MECHANICAL PROPERTIES. TREE PHYSIOLOGY 26 (2006), 1549-1558

[28] PELTOLA, H.M.: MECHNICAL STABILITY OF TREES UNDER STATIC LOADS. AMERICAN JOURNAL OF BOTANY 93(2006) (10), 1501-1511.

[29] PAPESCH, A. J. G.; MOORE, J.R.; HAWKE, A.E.: MECHANICAL STABILITY OF PINUS RADIATA TREES AT EYREWELL FOREST INVESTIGATED USING STATIC TESTS. NEW ZEALAND JOURNAL OF FORESTRY SCIENCE 27 (1997): 188–204.

[30] PELTOLA, H.; KELLOMÄKI, S.; HASSINEN, A.; GRANANDER, M.: MECHANICAL STABILITY OF SCOTS PINE, NORWAY SPRUCE AND BIRCH: AN ANALYSIS OF TREE-PULLING EXPERIMENTS IN FINLAND. FOREST ECOLOGY AND MANAGEMENT (2000) 135 : 143 – 153.

[31] RUDNICKI, M.; MITCHELL, S.J. AND NOVAK, M.D.: WIND TUNNEL MEASUREMENTS OF CROWN STREAMLINING AND DRAG RELATIONSHIPS FOR THREE CONIFER SPECIES. CANADIAN JOURNAL OF FOREST RESEARCH 34(2004): 666–676.

[32] VOLLSINGER, S.; MITCHELL, S.J.; BYRNE, K.E.; NOVAK, M.D.; RUDNICKI, M.: WIND TUNNEL MEASUREMENTS OF CROWN STREAMLINING AND DRAG RELATIONSHIPS FOR SEVERAL HARDWOOD SPECIES. CANADIAN JOURNAL OF FOREST RESEARCH 35 (2005): 1238–1249.

[33] GUITARD , D. AND CASTÉRA , P.: EXPERIMENTAL ANALYSIS AND MECHANICAL MODELLING OF WIND-INDUCED TREE SWAYS . IN WIND AND TREES. M.P. COUTTS AND J. GRACE (EDS). CAMBRIDGE UNIVERSITY PRESS (1995), 182 – 194.

[34] KERZENMACHER, T. AND GARDINER, B.A.: A MATHEMATICAL MODEL TO DESCRIBE THE DYNAMIC RESPONSE OF A SPRUCE TREE TO THE WIND. TREES. 12(1998) , 385 – 394

[35] MOORE, J.R. AND MAGUIRE, D.A.: NATURAL SWAY FREQUENCIES AND DAMPING RATIOS OF TREES: INFLUENCE OF CROWN STRUCTURE. TREES. 19 (2005), 363 – 373.

[36] SELLIER, D. AND FORCAUD, T.: A MECHANICAL ANALYSIS OF THE RELATIONSHIP BETWEEN FREE OSCILLATIONS OF PINUS PINASTERAIT. SAPLINGS AND THEIR AERIAL ARCHITECTURE. JOURNAL OF EXPERIMENTAL BOTANY, VOL. 56 (2005)NO. 416, 1563-1573.

[37] BARTHELEMY, D. AND CARAGLIO, Y.: PLANT ARCHITECTURE: A DYNAMIC, MULTILEVEL AND COMPREHENSIVE APPROACH TO PLANT FORM, STRUCTURE AND ONTOGENY, ANNALS OF BOTANY 99(2007): 375–407.

Universität für Bodenkultur Wien
University of Natural Resources and Life Sicences, Vienna

Department für Bautechnik und Naturgefahren

Autor:

DI Clemens Weissteiner

clemens.weissteiner@boku.ac.at

Betreuerteam:

Priv.-Doz. Dipl.-Ing. Dr. Johann Peter Rauch

Em.O.Univ.Prof. Dr.phil. Florin Florineth

Prof. Dr. Eva Hacker

Assoc. Prof. Phd. João Paulo Fernandes

7.5 **Publikation 5**

Ecological Engineering 85 (2015) 85–94

Contents lists available at ScienceDirect

Ecological Engineering

journal homepage: www.elsevier.com/locate/ecoleng

Spatial–structural properties of woody riparian vegetation with a view to reconfiguration under hydrodynamic loading

Clemens Weissteiner[a,*], Johanna Jalonen[b], Juha Järvelä[b], Hans Peter Rauch[a]

[a] University of Natural Resources and Life Sciences, Institute of Soil Bioengineering and Landscape Construction, Peter-Jordanstraße 82, 1190 Vienna, Austria
[b] Aalto University, School of Engineering, Otaniementie 17 PL 15500, 00076 Aalto, Helsinki, Finland

ARTICLE INFO

Article history:
Received 11 December 2014
Received in revised form 4 August 2015
Accepted 7 September 2015

Keywords:
Woody riparian vegetation
Tree structure
Tree architecture plant model
Eco-hydraulics
Porosity
Ecological engineering

ABSTRACT

This paper investigates the structural properties of four common riparian tree species and their reconfiguration under hydrodynamic loading in a towing tank in foliated and defoliated conditions. 3D tree models were generated by digitizing twenty 0.8–3.3 m tall specimens at branch level. Branch diameters and lengths were measured in order to calculate the one-sided stem area and stem volume over the plant height. The novelty of the investigations originated from the characterization of the reconfiguration which was achieved by combining the contracted width, the deflected height, and the underwater projected area in order to determine the porosity at different velocities. The results showed that the basal diameter could be used to predict the entire total one-sided stem area, although this method was not capable of reproducing the observed non-linear vertical distributions. The flow-induced width contraction contributed significantly to the reduction of the rectangular cross-sectional area occupied by the plant. The porosity of the foliated trees increased at the lower velocities, and then decreased at the higher velocities. Overall, detailed spatial–structural analyses of woody vegetation provided valuable information about plant behaviour under load, and thus are helpful for improving the determination of the physically based parameters of complex vegetative elements which is highly relevant for environmental modelling in order to fill the gap of knowledge concerning the hydrodynamic and aerodynamic flow around trees.

1. Introduction

Plants growing within riparian areas are responsible for various ecological, hydraulic–hydrological as well as landscape forming effects. They are a vital element of riverine environments and increase the structural and morphological diversity of the biosphere. They are highly relevant for shadowing effects (Holzapfel et al., 2013) and build an essential source of organic material for the livelihood of aquatic organisms. From a technical point of view, riparian vegetation reinforces riverbanks and retains sediments, however at the same time it can cause erosive processes and increase flow resistance. A sound understanding of the processes and parameters governing vegetated flow is therefore needed (Aberle and Järvelä, 2013, 2015) in order to guarantee both flood risk safety and natural river landscapes.

Hydrodynamic and hydro-ecological studies investigating the flow field of woody riparian vegetation are commonly based on high resolution spatial and temporal flow field data sets. The drag induced bending of the plant structure in flow direction and the drag induced compression were addressed by considering the decrease in projected area and the plant height (Fathi-Maghadam and Kouwen, 1997; Jalonen and Järvelä, 2014; Oplatka, 1998). Conversely, vegetation elements and their spatial properties are generally analyzed on the basis of an integral approach. This approach involves simplifying the complex structure of shrubs and trees which are comprised of heterogeneous plant parts (Västilä and Järvelä, 2014). Attempts to characterize plant area or volume were based on cylinder-analogy with an estimation of stem diameter at a certain height above ground (e.g. DVWK, 1991), photographic image analysis (e.g. Järvelä, 2002), measurement of projected area of the trunk and principal branches (e.g. Armanini et al., 2005; Righetti, 2008), decomposition of entire trees in small increments (Wilson et al., 2006) and the product of effective plant height and effective plant width (Freeman et al., 2000), leaf area index (Järvelä, 2004; Jalonen et al., 2013), and foliage-stem reference area ratio (Västilä et al., 2013). Describing the key hydraulic

* Corresponding author.
E-mail addresses: clemens.weissteiner@boku.ac.at (C. Weissteiner), johanna.jalonen@aalto.fi (J. Jalonen), juha.jarvela@aalto.fi (J. Järvelä), hp.rauch@boku.ac.at (H.P. Rauch).

http://dx.doi.org/10.1016/j.ecoleng.2015.09.053
0925-8574/

Notation

A_P	frontal projected area of plant [cm^2]
A_{P_tot}	total frontal projected area of plant [cm^2]
A_{PW}	underwater frontal projected area of foliated plant [cm^2]
$A_{PW,0}$	underwater frontal projected area of foliated plant in still water [cm^2]
A_{PWS}	underwater frontal projected area of defoliated plant [cm^2]
$A_{PWS,0}$	underwater frontal projected area of defoliated plant in still water [cm^2]
$A_{PW}/A_{PW,0}$	relative projected area of foliated plant under water [–]
$A_{PWS}/A_{PWS,0}$	relative projected area of defoliated plant under water [–]
A_{RP}	rectangular cross-sectional area occupied by the plant [cm^2]
$A_{RP}/A_{RP,0}$	relative rectangular cross-sectional area occupied by the plant [–]
A_S	one-sided stem area [cm^2]
A_{S_tot}	total one-sided stem area [cm^2]
D_S	diameter of segment [cm]
D_B	basal diameter of plant [cm]
D_m	mean diameter of segment [cm]
$H(z)$	plant height in function of the z-axis [cm]
$H_{\_tot}$	total plant height in still air [cm]
H_d	deflected height of foliated specimen [cm]
$H_{d,0}$	deflected height of foliated specimen in still water [cm]
$H_{d,S}$	deflected height of defoliated specimen [cm]
$H_{dS,0}$	deflected height of defoliated specimen in still water [cm]
$H_d/H_{d,0}$	relative deflected plant height at foliated condition [–]
$H_{dS}/H_{dS,0}$	relative deflected plant height at defoliated condition [–]
L_S	length of stem segment [cm]
u	towing velocity [m/s]
V_S	stem volume [cm^3]
V_{S_tot}	total stem volume [cm^3]
W_c	contracted width of the foliated specimen [cm]
W_{cS}	contracted width of the foliated specimen [cm]
$W_c/W_{c,0}$	relative contracted width of the foliated specimen [–]
$W_{cS}/W_{cS,0}$	relative contracted width of the defoliated specimen [–]
ε_{PW}	porosity of the foliated plant [–]
ε_{PWS}	porosity of the defoliated plant [–]

properties of plants, geometry and flexibility, with species-specific parameters is more sophisticated than the rigid cylinder analogy commonly used in hydraulic engineering practice (Aberle and Järvelä, 2013). Furthermore Aberle and Järvelä (2013) underline the need to elaborate on objective and accurate methods for the characterization of natural vegetation.

Natural riparian plants are increasingly being used instead of artificial plants in laboratory experiments to investigate the resistance and turbulence characteristics of vegetated flows (e.g. Armanini et al., 2005; Jalonen and Järvelä, 2014; Järvelä, 2004; Righetti, 2008; Sukhodolova and Sukhodolov, 2012; Västilä et al., 2013; Whittaker et al., 2013; Wilson et al., 2006). To achieve a better understanding of the influence of natural woody riparian vegetation on flow, it is essential to record and analyze plant data at the same level of detail as hydraulic measurements. An accurate 3D geometrical model of plants enables an extraction of spatial–structural and topological plant parameters, which characterize the plant specimens at different levels of detail (Barthelemy and Caraglio, 2007). As a result, the generated plant model and hydraulic model can be interrelated and form the basis for a holistic approach for considering plant flow interactions. Therefore, a better description and determination of the plant architecture is required for hydro-environmental modelling applications. Furthermore, analyses of species-specific tree growth relationships are essential in order to generalize individual results on species and growth basis.

From a fluid mechanics point of view, trees and bushes are highly complex porous media which consists of stems, branches, stalks and leafs or needles, each of them forming a boundary layer in wind flow, consequently the application of principles of classical bluff body aerodynamics is limited (Gromke and Ruck, 2008). Up until now little attention has been paid to the lateral contraction (Oplatka, 1998) or to the porosity (Gosselin and de Langre, 2011; Righetti, 2008; Schnauder et al., 2007; Zinke, 2010) of riparian plants at full scale under hydrodynamic loading.

The purpose of this study is to explore physically based parameters for an improved characterization of riparian trees in hydro-environmental modelling applications. The specific objectives of this paper are (1) to analyze the woody plant structure of four different riparian species, (2) to correlate the structural plant parameters with the streamlining of the plant specimens in terms of contracted width, deflected height and projected area and (3) to quantify the change in plant porosity at different stages of hydrodynamic loading in foliated and defoliated conditions. The investigations comprise of measurements of 20 selected specimens of four common riparian species. The experiments were conducted parallel to a towing tank study, focusing on the drag of the trees (Jalonen and Järvelä, 2014).

2. Methods

2.1. Plant specimens and description of their structure

Investigations were performed at the hydraulic laboratory of the Department of Civil and Environmental Engineering, Aalto University, Finland. 20 plant specimens were harvested in a nearby wetland area. The species investigated were Black Alder (*Alnus glutinosa* (L.) Gaertn.), Silver Birch (*Betula pendula* Roth), White Birch (*Betula pubescens* Ehrh.) and Goat Willow (*Salix caprea* L.). The specimens were selected in such a way that they strongly differed in terms of morphology and height (80–330 cm), for a wide range of natural variability to be covered.

In the present paper, the description of the plant architecture (topology and geometry) follows the rules of the Multi-scale Tree Graph (MTG) formalism (Godin and Caraglio, 1998). The plant is described in terms of axes and segments. The stem is defined as the 1st order axis. Each branch directly connected to the 1st order axis is defined as a 2nd order axes, each branch directly connected to the 2nd order axes is defined as 3rd order axes, and so on (see Fig. 1). A segment is defined as a portion of a woody part without branching between two measurement points (Sinoquet and Rivet, 1997). As a comparison, the Strahler ordering scheme used by e.g. Antonarakis et al. (2009), Järvelä (2004) and Wilson et al. (2006) for the purpose of characterizing trees in relation to hydraulic drag assign the lowest order number to the outmost branches, increasing the number order towards the main stem. The order numbers are summed up at the joins of the branches with equal order. The Strahler ordering scheme contains information on topology but not on the geometry of the tree segments.

Table 1
Geometric characteristics of the investigated specimens for structural analyses: mean values with minimum and maximum values in parentheses.

Plant species	Symbol	No. of specimens	Mean total height of plant (min.–max.) [cm]	Mean total one-sided stem area (min–max.) [cm^2]	Mean total volume of plant (min.–max.) [cm^3]
Alnus glutinosa	AG	6	216 (110–328)	833 (225–1893)	547 (106–1415)
Betula pendula	BPe	3	185 (87–259)	759 (177–1490)	376 (73–750)
Betula pubescens	BPu	3	200 (143–233)	465 (248–594)	218 (104–296)
Salix caprea	SC	8	228 (123–312)	820 (228–1455)	524 (91–1149)

In our experiments, the measurement points were recorded with the Polhemus FASTRAK electromagnetic digitizing device (FASTRAK System), along the axes at a maximum distance of 1–20 cm, depending on the change in diameter or direction of the axis. Geometrical parameters were determined on a segment basis. Overlaps or gaps between consecutive segments were neglected, due to small changes in direction between the segments of the same axis order. The one-sided stem area of a segment was defined as the cross sectional area ($A_S = L_S D$) of a segment, whereby A_S represents the one-sided stem area of a segment, L_S the length of the segment and D the mean diameter of the segment. Hence A_S includes all branches, in contrast to the photographic image analysis, in which branches can shade each other. The volume of tree segments (V_S) was determined as $V_S = \pi(D/2)^2 L_S$. Table 1 shows the main geometrical properties (mean values with minimum and maximum values in parentheses).

2.2. Digitization of the plant structure

The 3D plant models were generated by measuring the position coordinates along all of the branches of the specimens with the Polhemus FASTRAK electromagnetic digitizing device (FASTRAK System). The device was equipped with a Long Ranger transmitter and a digitizing stylus (Polhemus Inc., Colchester, Vermont). The FASTRAK system uses low frequency electromagnetic field (EMF) sensing in order to determine the position and orientation of a remote object (Polhemus, 2005). The Long Ranger (transmitting unit) and the digitizing stylus (receiving unit) are connected through a system electronics unit (SEU). The measurement sphere must be free of electro-magnetic emitting sources. According to the manufacturer of the device the spatial coordinates can be measured within a 4.6 m radius around the transmitter, with a resolution of 0.05% and a standard error of 0.8 cm for each receiver position (Polhemus, 2005). However, Moulia and Sinoquet (1993) state that the main source of error, when digitizing a tree does not generally arise from the nominal accuracy of the device but from the manual operating process. Plant digitizing was performed in the centre of a large hall with the long ranger suspended from the ceiling. Before digitizing the plants, the accuracy of the system was checked by measurements on a 1-m ruler. Measurements were recorded with the piafDigit plant digitizing software (Danjon and Reubens, 2008; Donès et al., 2006). Two persons were needed to digitize the trees; one person operated the digitiser and measured the diameters and coordinates manually, stepwise along all of the branches, and the second person checked the measurements on the PC and also entered the measured diameters and topological information manually. Trees were digitized at branch level from the bottom to the top of the plant following all axes (branches). The diameter was measured at the measurement points using a plastic calliper, and the coordinate of the axes segment was recorded by the EMF device.

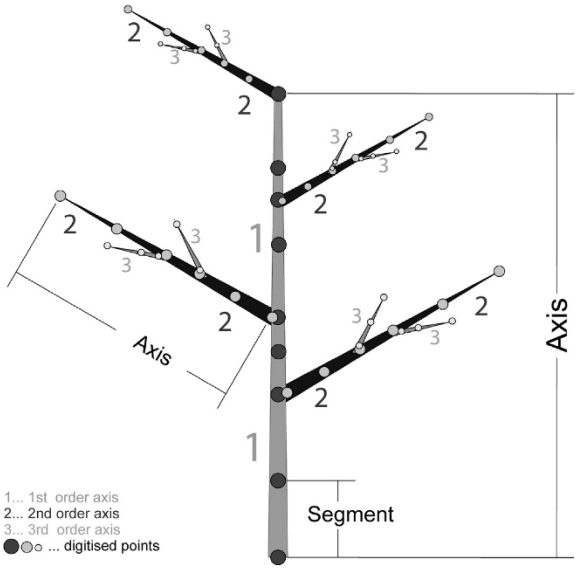

Fig. 1. Definition sketch of the MTG formalism applied in the structural analyses of the presently investigated specimens.

2.3. Towing tank experiments and video footage analysis

After recording the plant structure, the tree specimens were exposed to hydrodynamic loading in the Aalto University towing tank. Drag forces were directly measured with load cells. The trees were towed in foliated and defoliated conditions, at a velocity range of 0.1–1.5 m/s (in velocity steps of 0.1, 0.2, 0.3, 0.4, 0.5, 0.6, 0.8, 1, 1.25 and 1.5 m/s) and 0.1–2.5 m/s respectively (in velocity steps same as in foliated conditions adding 1.75, 2.0, 2.25 and 2.5 m/s). For a detailed description of the towing tank experiments the reader is referred to Jalonen and Järvelä (2014).

Video footage was recorded by two cameras mounted underwater on the side and the rear of the towing direction, at a distance from the plant of 3 m and 5.5 m, respectively. Side view camera recordings were used to determine the deflected heights of the specimens, H_d and H_{dS} (the distance between the tree base and the highest part of the tree during streamlining), for foliated and defoliated conditions respectively, by means of the datinf software. The scale for the heights was obtained by using both a ruler placed to the side of the plant and the known submerged height measured before the towing of the specimens. Contracted width, W_c and W_{cS} in foliated and defoliated conditions respectively, was measured using rear view camera images by AutoCAD. Due to the bending of the plant towards the rear view camera, side view camera images were used to adjust the scaling of the outmost parts of the plant, in order to measure the contracted width. Deflected heights and contracted width were determined in foliated and defoliated conditions for 7 *S. caprea* specimens and for 7 *A. glutinosa* specimens.

To determine the porosity (ε_{PW}) of the trees under hydrodynamic loading, a rectangular cross-sectional reference area occupied by the plant (A_{RP}, A_{RPS}) was defined, which was delimitated by the deflected height (H_d, H_{dS}) and the actual (contracted) width (W_c, W_{cS}) of the plant. The porosity of the plants under water ε_{PW} was then calculated by the rectangular cross sectional

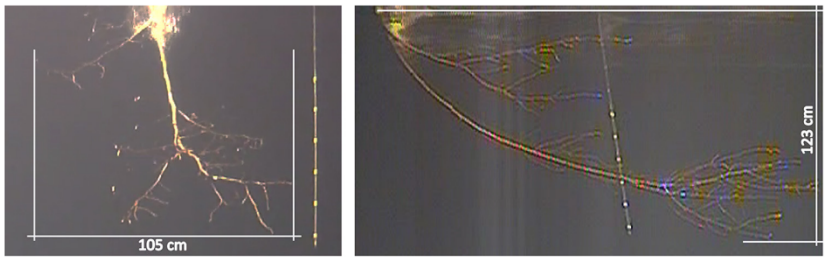

Fig. 2. Rear and side view of the *A. glutinosa* specimen AG 5 at a velocity of 1.5 m/s.

area occupied by the plant (A_{RP}, A_{RPS}) and the underwater frontal projected area (A_{PW}, A_{PWS}). Eq. (1) shows the formula used to calculate the porosity of the plants under water ε_{PW} in foliated condition.

$$\varepsilon_{PW} = \frac{(A_{RP} - A_{PW})}{A_{RP}} \quad (1)$$

The underwater frontal projected area (A_{PW}, A_{PWS}) was derived from images of the video footage in Matlab by determining the pixels covered by the plant (Jalonen and Järvelä, 2014), whereby the scale was obtained from a ruler placed in the centre of the plant (Fig. 2).

3. Results and discussion

3.1. Structural properties of the trees

The basal diameter and total one-sided stem area of the specimens showed a linear correlation (Fig. 3A). *S. caprea* specimens revealed, in comparison to *A. glutinosa* specimens, a higher total one-sided stem area in relation to the basal diameter. Fit lines were only added for *A. glutinosa* and *S. caprea*, since for *B. pendula* and *B. pubescens* we only investigated three specimens each (Fig. 3A and B). Studying eight Crack Willow (*Salix fragilis* L.) specimens Wilson et al. (2006) found that the total plant volume increases with basal diameter. Similar results could be found for the specimens investigated: total plant volume increased linearly with basal diameter for all species (R^2 = 0.808). Correlation of total one-sided stem area and total height of the trees showed a logarithmic relationship (Fig. 3B). This can be explained by the pioneer character of the plants. During the first period of growth, trees mainly grow in a vertical direction due to their competition for light. This growth stage involves a small development of side axes, whereas later trees start growing in width (Yang et al., 2014). Fig. 3C shows the total one-sided stem areas of the main axes (stem, axis of 1st order) and the total one-sided stem area of the higher order axes (2nd order and higher), normalized with the A_{tot} of the specimen. The mean values of the total one-sided stem area of higher order axes are clearly higher for all species, in comparison to the one-sided stem area of the axes of 1st order. For instance, the main axes of *A. glutinosa* showed an average contribution of 40% and higher order axes made up 60% of the total one-sided stem area. In the case of *S. caprea* the main axes contributed on average 38% and higher order axes 62% to the average total one-sided stem area. *B. pendula* showed the highest differences between the average total one-sided stem area of the main axes (34%) and the higher order axes (66%), whereas for *B. pubescens* the 1st order axes and the higher order axes made up on average 42% and 58% of the average total one-sided stem area, respectively. The larger differences in the amount of the first order and higher order axes for *B. pendula* and *B. pubescens* can be partly ascribed to the lower number of specimens investigated, and consequently a lower variability in plant geometrical structure. Wilson et al. (2006) found that the contribution of the first and second order branches (Strahler ordering scheme; see Section 2.2) to the overall plant volume of eight 3 year old *S. fragilis* specimens (h = 1.5–2 m) had less impact on total volume relative to the single trunk volume. Similar results could not be found for the specimens presently investigated, although in the Strahler ordering scheme the main axis is defined as a fraction (lower part) of the main axis in comparison to the definition of the MTG formalism. The high share of the one-sided stem area of higher order axes means that they represent a significant contributory role in terms of drag force. However, it can be assumed that branches of higher order axes have a lower flexural rigidity due to the smaller basal diameter of the axes.

3.2. Vertical variability and species-specific properties

The specimens investigated showed a wide range of distributions in the cumulative one-sided stem area and volume over height (Fig. 4). Smaller specimens (up to ~2 m) showed an almost linear correlation of the cumulative one-sided stem area over height. In contrast, taller specimens showed a more pronounced increase of

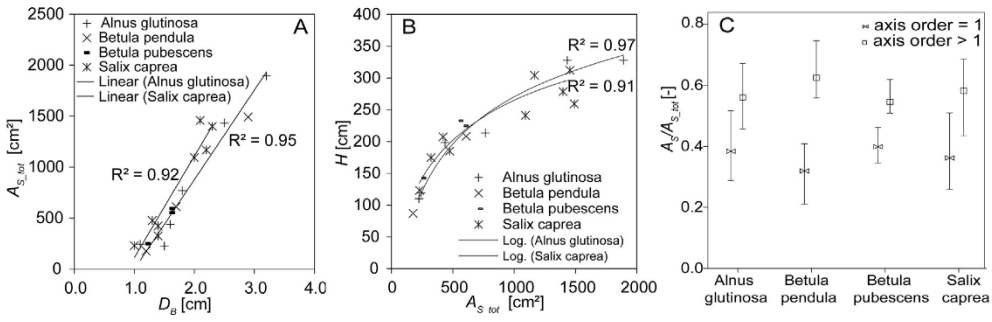

Fig. 3. Structural characteristics of the investigated specimens: (A) basal diameter against total one-sided stem area, (B) total one-sided stem area against total plant height and (C) mean one-sided stem areas of main stems (axis order = 1) and branches (axis order > 1) for each species (bars show full data range).

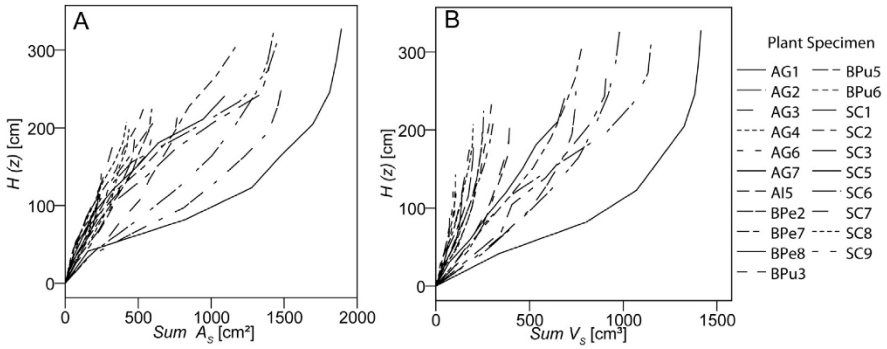

Fig. 4. Cumulative one-sided stem area (A) and cumulative volume (B) over height of all specimens investigated.

cumulative one-sided stem area over height. In comparison, Nobile (2007) and Righetti (2008) found the relationship between cumulative frontal projected area and plant height to be similar for 0.7 m tall bushes as for 1.5–3.5 m tall willows. Järvelä (2004) assumed a linear increase of the one-sided stem area over height suitable for estimating the flow resistance caused by woody vegetation. In the present study, this assumption can only be confirmed in terms of the smaller specimens, whereas the taller specimens deviate from the linear correlation. Similar findings can be stated for the distribution of the cumulative volume over height. The total one-sided stem area varied significantly for taller specimens within species, even when the plant height was similar (Fig. 4). For example AG1 and AG2 both had a total height of 327 cm, but they differed in total one-sided stem area by about 24%. Wilson et al. (2006) state similar findings for the increase in plant volume and projected area over height.

Fig. 5 depicts the mean cumulative one-sided stem areas over height for each axis order of the species investigated. Both first and second order axes were the main relative contributors to the one-sided stem area of the trees (30–50%). *A. glutinosa* and *B. pendula* presented a higher contribution of the mean total sum of the one-sided stem areas for the 2nd order axes, in comparison to the 1st order axes, whereas *B. pubescens* and *S. caprea* showed a higher relative contribution of the 1st order axes to the total one-sided stem area. The impact of 3rd order axes on the total one-sided stem area reached mean values of 10–30%, whereas higher order axes (>3rd order) contributed around 10% only to the total one-sided stem area. This can be ascribed to the relatively small to medium size of the specimens investigated. Regarding the larger trees, the contribution of higher order axes to the total one-sided stem area reached higher relative values.

Due to the low number of specimens of *B. pendula* and *B. pubescens*, *A. glutinosa* and *S. caprea* were selected in order to highlight the natural variability of the structural characteristics of the plant. The one-sided stem area over height of *A. glutinosa* is considerably higher in the lower part of the trees, whereas *S. caprea* specimens show their largest increase in the lower part (Fig. 6A–C).

Specimens with a high amount of total one-sided stem area revealed, for both *A. glutinosa* and *S. caprea*, that the species differed in terms of the increase of the cumulative one-sided stem area over height (Fig. 7). In comparison, specimens with a lower total amount of one-sided stem area, divided by their total height showed an almost linear relation of cumulative one-sided stem area over height. Specimens of *A. glutinosa* showed their largest increase in one-sided stem area at a relative height between 0.125 and 0.625 (Fig. 6). *S. caprea* specimens exhibited the largest increase in one-sided stem area, starting from 0.375 up to 0.875 of the total height. If one assumes similar material properties for both species, hydraulic resistance in the lower part of the plants for *A. glutinosa* is higher in comparison to *S. caprea*, due to the higher share of total one-sided stem area. Similarly, a different bending behaviour between the species can be assumed during natural floods when water level is rising from the tree base towards the top of the trees. From an ecological point of view, the differences in the distribution of the one-sided stem area over height can be explained by the natural habitat of the species. *S. caprea* grows close to the riverbank and *A. glutinosa* grows mostly on the top of riverbanks. *S. caprea* has adapted its architecture, due to frequent flooding events, by reducing the one-sided stem area at the tree base, and therefore its bending properties.

3.3. Reconfiguration and porosity of the foliated and defoliated trees

Fig. 8 shows the deflected heights and the contracted widths against the velocity of the foliated specimens of *A. glutinosa* and *S. caprea*. Both species reduced their heights in foliated conditions by 77% and 76% respectively, at a velocity of 1.5 m/s. The deflected height of *S. caprea* specimens reduced much more than that of *A. glutinosa* specimens, at the lowest velocity measured. The deflection behaviour changed at higher velocities (0.2–1.5 m/s), when the plant heights of *A. glutinosa* were deflected slightly more in comparison to *S. caprea* (Fig. 8A). Fig. 8B depicts the contracted width of foliated specimens at different velocities. Specimens reduced their lateral extension 20% less (almost 60% of total contracted width at $u = 1.5$ m/s) in comparison to the relative deflection in height. *S. caprea* specimens underwent a stronger lateral contraction up to a velocity of 0.6 m/s. At the velocity range of 1.0–1.5 m/s *A. glutinosa* specimens reduced their width more extremely.

At the highest measured velocity of 2.5 m/s, the height of the defoliated *A. glutinosa* and *S. caprea* specimens had reduced by 77% and 79%, respectively (Fig. 9A), and at a velocity of 1.5 m/s the reduction in height was 63% for both species (Fig. 9A). On the other hand, the foliated specimens reached a height reduction of 77% (*A. glutinosa*) and 76% (*S. caprea*) at $u = 1.5$ m/s (Fig. 8A), indicating that the foliage drag accounted for 13–14% of mean height reduction at this velocity. Interspecific differences in the height reduction of leafless trees were observed up to a velocity of 0.6 m/s. Little interspecific differences in height reduction were notable for velocities from 0.8 m/s to 2.5 m/s. Interspecific differences for contracted width increased with velocity in defoliated conditions (Fig. 9B). *S. caprea* specimens showed a maximum contracted width of 72% in comparison to 56% of *A. glutinosa* specimens, at a velocity of 2.5 m/s. The differences in contracted width between the foliated and defoliated *S. caprea* specimens increased with velocity. Defoliated *S. caprea* specimens contracted on average 14% less than the foliated ones at

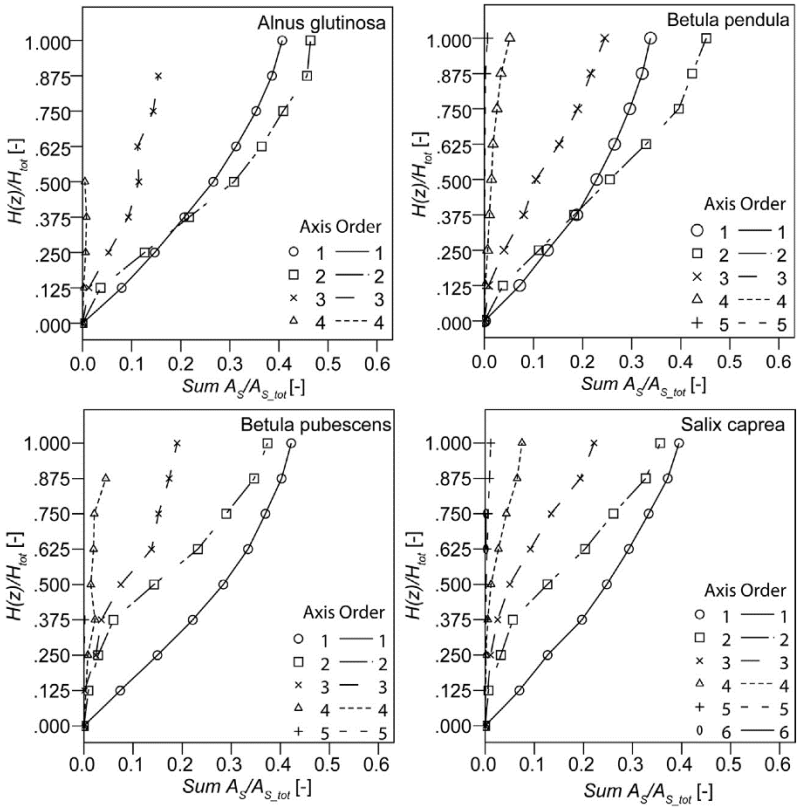

Fig. 5. Mean cumulative one-sided stem area over height of different axis orders.

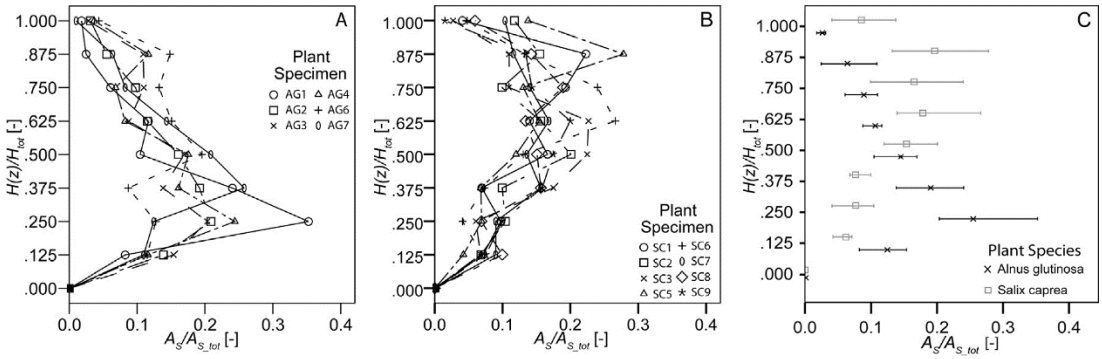

Fig. 6. One-sided stem area over height of (A) *A. glutinosa*, (B) *S. caprea* and (C) mean values of both species with full data ranges as bars.

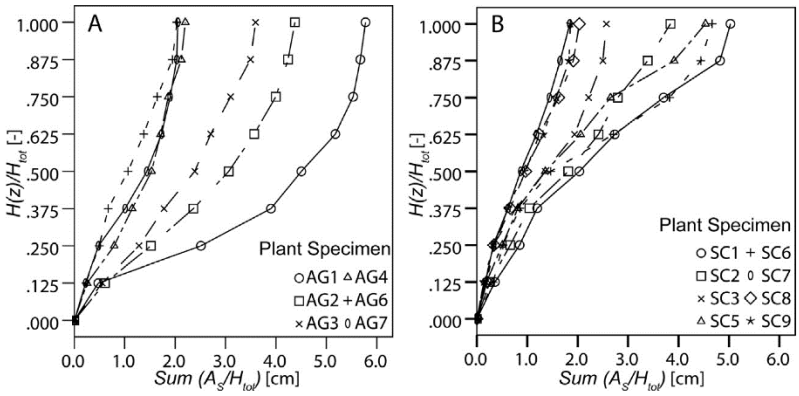

Fig. 7. Cumulative one-sided stem area over height of the investigated specimens of (A) *A. glutinosa* and (B) *S. caprea*.

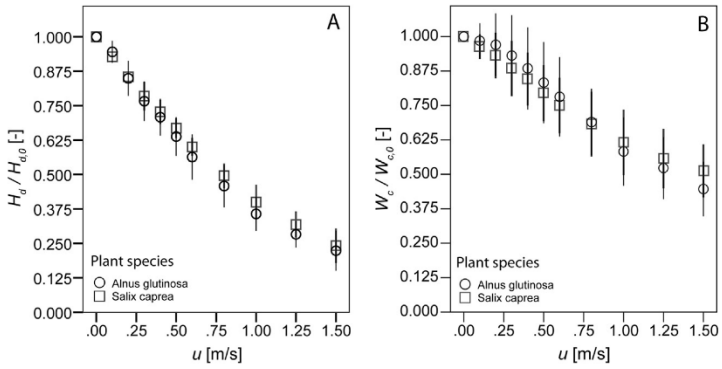

Fig. 8. Species-averaged deflected height $H_d/H_{d,0}$ (A) and contracted width $W_c/W_{c,0}$ (B) for *A. glutinosa* and *S. caprea* in foliated conditions. Measured velocities were 0.1–1.5 m/s. Error bars show ±1 standard error.

a velocity of 1.5 m/s (Figs. 8B and 9B). For *A. glutinosa*, the difference between the contracted widths of the foliated and defoliated specimens was less than 7%.

The higher reduction in the contracted width of *S. caprea* in comparison to *A. glutinosa* in defoliated conditions could be explained by the different structural properties of the species. *S. caprea* specimens showed a larger one-sided stem area (Fig. 6A) in the upper part of the trees, whereas *A. glutinosa* specimens had their main share of one-sided stem area in the lower part of the plant (Fig. 6B). The quantity of thinner branches was higher in the upper part of the specimens in comparison to the lower part of the plant, and these branches likely bent easier due to lower flexural rigidity. The 3 m tall foliated willows in the Oplatka towing tank experiments (1998) showed a contracted width of 70–85% at a velocity of 4 m/s. At comparable velocities (1.5 m/s) Oplatka (1998) reported a contracted width of 42–70%, corresponding with the present results for the *A. glutinosa* and *S. caprea* specimens, which showed a contracted width of 44–67% and of 39–66%, respectively.

The species averaged rectangular cross-sectional area occupied by the plant (A_{RP}) in relation to the A_{RP} at zero velocity ($A_{RP,0}$) showed a strong linear decrease up to a velocity of 0.6 m/s for both species (Fig. 10A). At 0.6 m/s $A_{RP}/A_{RP,0}$ diminished by about 60%, and for the velocity range between 0.8 m/s and 1.5 m/s $A_{RP}/A_{RP,0}$ tended towards 10% of its original area. At velocities larger than 0.6 m/s, *A. glutinosa* specimens reduced their $A_{RP}/A_{RP,0}$ slightly more than in comparison to *S. caprea* specimens.

The decrease of the underwater frontal projected area (Fig. 10B) was pronounced for velocities up to 0.5 m/s, after which the relative decrease reduced and arrived at a minimum of 19%, at a velocity of 1.5 m/s. The strong decrease for the lower velocities was due to the impact of the leaves on the reconfiguration. *S. caprea* reduced its underwater frontal projected area slightly more than *A. glutinosa* specimens.

The porosity of the plants (Fig. 10C) for foliated specimens increased linearly for velocities up to 0.4 m/s and then diminished almost linearly. The initial increase in porosity was due to the stronger decrease of the underwater frontal projected area (A_{PW}) in comparison to the rectangular cross-sectional area occupied by the plant (A_{RP}). This stronger decrease in underwater frontal projected area may have been caused by the contraction and streamlining of the leaves and the thin branches, whereas the main structure did not contract as strongly. The foliated *A. glutinosa* specimens generally showed a smaller porosity at all velocities than the foliated *S. caprea* specimens. At higher velocities (0.6–1.5 m/s), the porosity of *A. glutinosa* specimens reduced stronger than that of *S. caprea*, which led to an average porosity value for *A. glutinosa* of 74% and 82% for *S. caprea*, at a maximum velocity of 1.5 m/s. The lower porosity values of *A. glutinosa* might have been affected by the differences in leaf shape and leaf size between the two species. The larger and more serrated leaves of *A. glutinosa* likely streamline differently than the smaller and smoother *S. caprea* leaves, as leaf shape is an important factor in determining flow–leaf interaction (Albayrak et al., 2012).

The determination of the underwater frontal projected area in leafless conditions could only be analyzed up to a velocity of 1.5 m/s, due to the induced turbulences and difficulties in distinguishing

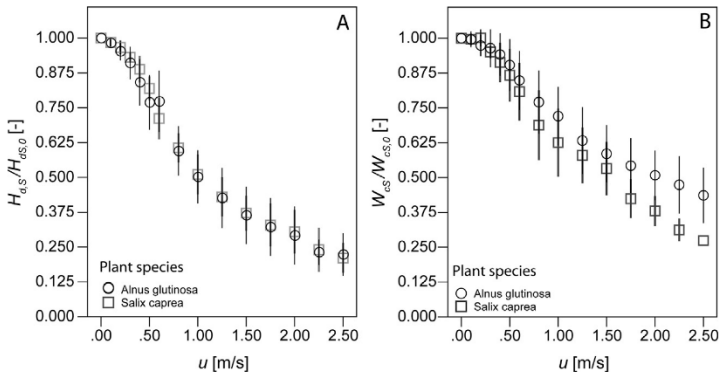

Fig. 9. Species-averaged deflected height $H_{dS}/H_{dS,0}$ (A) and contracted width $W_{cS}/W_{cS,0}$ (B) for *A. glutinosa* and *S. caprea* in defoliated conditions. Error bars show ±1 standard error.

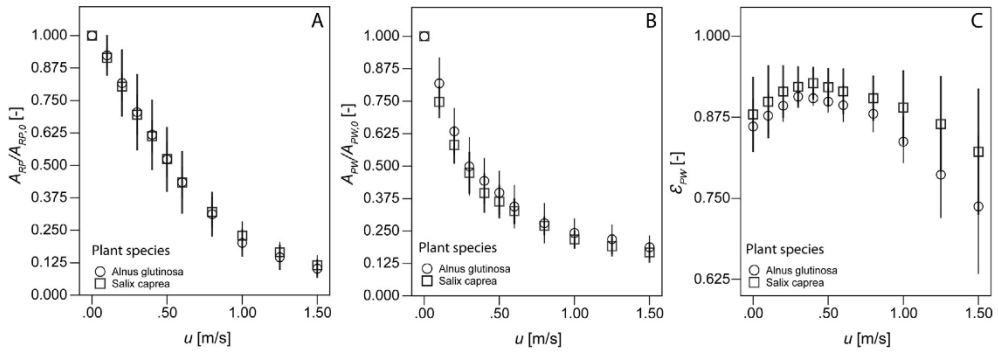

Fig. 10. The species averaged rectangular cross-sectional area occupied by the plant $A_{RP}/A_{RP,0}$ (A), underwater frontal projected area $A_{PW}/A_{PW,0}$ (B) and the underwater porosity of the plants ε_{PW} (C) as a function of the velocity in foliated conditions. Note the different scaling for *Y*-axis in (C). Error bars show ±1 standard error.

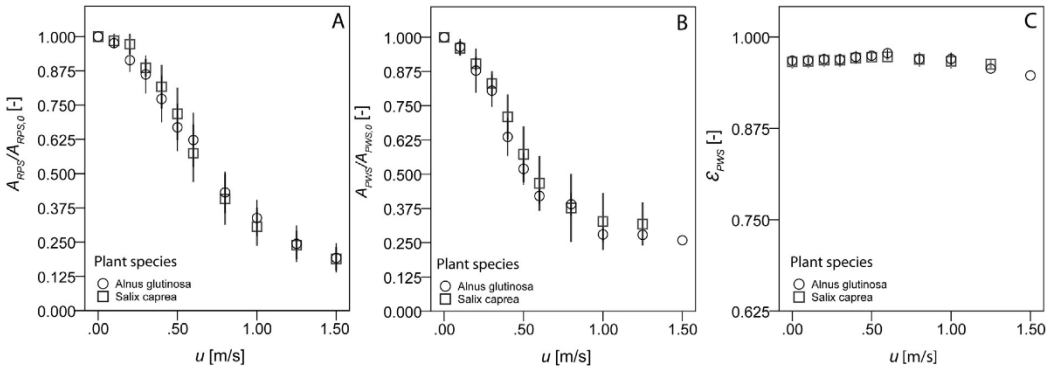

Fig. 11. Species-averaged rectangular cross-sectional area occupied by the plant $A_{RPS}/A_{RPS,0}$ (A), underwater frontal projected area ($A_{PWS}/A_{PWS,0}$) (B) and the porosity of the plants under water ε_{PWS} (C) as a function of the velocity in defoliated conditions. Note the different scaling for *Y*-axis in (C). Error bars show ±1 standard error.

tree and non-tree pixels. The rectangular cross-sectional area occupied by the plant (Fig. 11A) and the frontal projected plant area (Fig. 11B) showed different behaviour in leafless conditions than in leafy conditions. The rectangular cross-sectional area occupied by the plant appeared to decrease almost linearly at the velocity range between 0.3 and 0.6 m/s, reaching a value of 60% (at $u = 0.6$ m/s). At higher velocities, the rectangular cross-sectional area occupied by the plant decreased asymptotically to 10% of its state in still water. The underwater frontal projected area of the plant (Fig. 11B) decreased similarly to the rectangular cross-sectional area occupied by the plant in defoliated conditions. Therefore, the porosity of the defoliated specimens (Fig. 11C) remained almost the same at all velocities. A comparison of the frontal projected area in foliated and defoliated conditions showed different behaviour for velocities of up to 0.3 m/s. Whilst foliated plant specimens already greatly reduced their frontal projected area already at low velocities, defoliated specimens only showed a greater reduction at higher velocities (>0.4 m/s).

Nobile (2007) in Righetti (2008) analyzed the porosity along the plant height of riparian vegetation growing along the banks of naturalized torrents, taking into consideration the trunk and the main branches for the frontal area definition. He found the porosity to be rather uniform from the base to the trunk and suggested that it can be assumed almost constant (Righetti, 2008). The results of the present study showed that the porosity of leafless trees remains almost constant at different velocities. In contrast, the porosity of foliated riparian trees changed substantially at different velocities, and porosity at higher velocities differed for different species. Investigating the application of different porosity definitions at patch scale, Montakhab et al. (2012) found that the volumetric method for porosity measurements is more practical and accurate than other methods (frontal area method using digital image analysis, frontal area method (Nepf and Ghisalberti, 2008)) and vegetation porosity formula (Zhang and Su, 2008). In a porous media model for natural emergent vegetation, Zinke (2010) applied a porosity definition based on the plant volume and a defined control volume. Schnauder et al. (2007) showed in their study on the effect of permeability on flow velocities and turbulence, a fundamental difference in the flow structure between a rigid immersed body and natural emergent vegetation. The porosity of the investigated treetop of a cypress plant was not determined (Schnauder et al., 2007). Artificial poroelastic systems were used by Gosselin and de Langre (2011) to study the impact of porosity on reconfiguration: the drag of the synthetic poroelastic systems studied showed particularities similar to those of real trees, as the drag increased in a more pronounced way than squared velocity, due to realignment of upstream filaments.

4. Conclusions

Experimental investigations were conducted in order to relate the complex structure (geometry and topology) of riparian trees to their reconfiguration (bending and streamlining) under hydrodynamic loading. 3D plant models were constructed with a view to describing the spatial–structural properties of four common

riparian tree species at a height range of 0.8–3.3 m. The following findings can be summarized:

A detailed spatial–structural analysis of the trees at branch level revealed a broad variability in the parameters used to describe the geometry and topology at different plant scales. For all four species, the total one-sided stem area could be estimated using the basal diameter, although this approach cannot reproduce vertical variability. The specimens of *A. glutinosa* and *S. caprea* both showed a species-specific, non-linear vertical distribution of the one-sided stem area and the stem volume, which explained the observed differences in streamlining. The species-specific non-linear distribution of the one-sided stem area corresponded with the natural habitat of both species: *S. caprea* which typically grows close to the riverbank has adapted its architecture to frequent flooding. From an ecological and hydraulic perspective it is therefore important to take into account the natural habitats of different riparian woody species, considering river morphological and hydrological boundary conditions in the frame of river restoration projects.

The new approach characterizing the reconfiguration of the trees by combining the deflected height, contracted width and frontal projected area allowed a determination of the porosity at different velocities. Conventionally, only the height reduction or the projected area is taken into account. The porosity of foliated specimens increased at lower velocities (<0.5 m/s), whereas it decreased for the higher velocities. This was attributed to the more efficient streamlining of the leaves in comparison to the stem at the lower velocities.

The implementation of a vegetative Cauchy number for full scale vegetation as proposed by Whittaker et al. (2013, 2015) highlighted the need for further physically based data to be able to accurately characterize riparian vegetation, in order to fully understand all processes involved in the interaction between hydrodynamic loads and the reconfiguration of riparian woody vegetation. The present study has proved the importance of considering the vertical distribution of these characteristics, in order to model the impact of vegetation on different water levels in relation to plant heights.

Moreover, the lessons we have drawn from the results cover a wide range of areas related to flow around trees. The quantification of structural parameters and differences in the morphology of trees are also key topics in tree sway dynamics and responses to high winds (Sellier and Fourcaud, 2009). The link between tree architecture and its damping behaviour affects the stability of trees in winds (e.g. Kane et al., 2014). Furthermore, a quantifying of the drag and windthrow risk is needed for urban tree management, such as structural pruning (e.g., Cullen, 2005, Gilman et al., 2015) as well as for forest stands (e.g. Ancelin et al., 2004). For all of these applications the structural parameters of trees are an important factor, which has to be addressed quantitatively in order to close the knowledge gap about the hydrodynamic and aerodynamic flow around trees.

For future investigations of riparian flow–plant interactions, it will be essential that the combination of the bio-mechanical material properties and the architectural structure is profoundly considered. The use of other techniques such as laser scanning (e.g. Jalonen et al., 2015) to derive characteristic plant properties is encouraged as the present EMF technique is highly time-consuming.

Acknowledgements

This study was supported by the Maa-ja vesitekniikan tuki ry and the Academy of Finland (Flow–vegetation–sediment interaction project, grant no. 133113). We acknowledge the trainees Anja Zogan and Ferran Garcia for their help with the experiments.

References

Aberle, J., Järvelä, J., 2013. Flow resistance of emergent rigid and flexible floodplain vegetation. J. Hydraul. Res. 51 (1), 33–45, http://dx.doi.org/10.1080/00221686.2012.754795.

Aberle, J., Järvelä, J., 2015. Hydrodynamics of vegetated channels. In: Rowinski, P., Radecki-Pawlik, A. (Eds.), Rivers – Physical, Fluvial and Environmental Processes. GeoPlanet: Earth and Planetary Sciences. Springer, Berlin, pp. 519–541, http://dx.doi.org/10.1007/978-3-319-17719-9_21.

Albayrak, I., Nikora, V., Miler, O., O'Hare, M., 2012. Flow–plant interactions at a leaf scale: effects of leaf shape, serration, roughness and flexural rigidity. Aquat. Sci. 74 (2), 267–286, http://dx.doi.org/10.1007/s00027-011-0220-9.

Ancelin, P., Courbaud, B., Fourcaud, T., 2004. Development of an individual tree-based mechanical model to predict wind damage within forest stands. For. Ecol. Manag. 203 (1–3), 101–121, http://dx.doi.org/10.1016/j.foreco.2004.07.067.

Antonarakis, A.S., Richards, K.S., Brasington, J., Bithell, M., 2009. Leafless roughness of complex tree morphology using terrestrial lidar. Water Resour. Res. 45 (10), http://dx.doi.org/10.1029/2008WR007666.

Armanini, A., Righetti, M., Grisenti, P., 2005. Direct measurement of vegetation resistance in prototype scale. J. Hydraul. Res. 43 (5), 481–487.

Barthelemy, D., Caraglio, Y., 2007. Plant architecture: a dynamic, multilevel and comprehensive approach to plant form, structure and ontogeny. Ann. Bot. Lond. 99 (3), 375–407, http://dx.doi.org/10.1093/aob/mcl260.

Cullen, S., 2005. Trees and wind: a practical consideration of the drag equation velocity exponent for urban tree risk management. J. Arboric. 31, 101–113.

Danjon, F., Reubens, B., 2008. Assessing and analyzing 3D architecture of woody root systems, a review of methods and applications in tree and soil stability, resource acquisition and allocation. Plant Soil 303 (1–2), 1–34, http://dx.doi.org/10.1007/s11104-007-9470-7.

Donès, N., Adam, B., Sinoquet, H., 2006. PiafDigit – Software to Drive a Polhemus Fastrak 3 SPACE 3D Digitiser and for the Acquisition of Plant Architecture. Version 1.0. UMR PIAF INRA-UBP, Clermont-Ferrand, pp. 15.

DVWK, 1991. Hydraulische Berechnung von Fließgewässern. Merkblätter zur Wasserwirtschaft, vol. 220. Verlag Paul Parey, Hamburg/Berlin (in German).

Fathi-Maghadam, M., Kouwen, N., 1997. Nonrigid, nonsubmerged, vegetative roughness on floodplains. J. Hydraul. Eng. ASCE 123 (January (1)), 51–57, http://dx.doi.org/10.1061/(ASCE)0733-9429(1997)123:1(51).

Freeman, G., Rahmeyer, W., Copeland, R.R., 2000. Determination of Resistance due to Shrubs and Woody Vegetation. Report No. ERDC/CHL TR-00-25. US Army Corps of Engineers Engineer Research and Development Centre.

Gilman, E.F., Miesbauer, J.W., Masters, F.J., 2015. Structural pruning effects on stem and trunk strain in wind. Arboric. Urban For. 41 (1), 3–10.

Godin, C., Caraglio, Y., 1998. A multiscale model of plant topological structures. J. Theor. Biol. 191 (1), 1–46, http://dx.doi.org/10.1006/jtbi.1997.0561.

Gosselin, F.P., de Langre, E., 2011. Drag reduction by reconfiguration of a poroelastic system. J. Fluid Struct. 27 (7), 1111–1123, http://dx.doi.org/10.1016/j.jfluidstructs.2011.05.007.

Gromke, C., Ruck, B., 2008. Aerodynamic modelling of trees for small-scale wind tunnel studies. Forestry 81 (3), 243–258, http://dx.doi.org/10.1093/forestry/cpn027.

Holzapfel, G., Weihs, P., Rauch, H.P., 2013. Use of the shade-a-lator 6.2 model to assess the shading potential of riparian purple willow (*Salix purpurea*) coppices on small to medium sized rivers. Ecol. Eng. 61, 697–705, http://dx.doi.org/10.1016/j.ecoleng.2013.07.036.

Jalonen, J., Järvelä, J., 2014. Estimation of drag forces caused by natural woody vegetation of different scales. J. Hydrodyn. 26 (4), 608–623, http://dx.doi.org/10.1016/S1001-6058(14)60068-8.

Jalonen, J., Järvelä, J., Virtanen, J.-P., Vaaja, M., Kurkela, M., Hyyppä, H., 2015. Determining characteristic vegetation areas by terrestrial laser scanning for floodplain flow modeling. Water 7 (2), 420–437, http://dx.doi.org/10.3390/w7020420.

Jalonen, J., Järvelä, J., Aberle, J., 2013. Leaf area index as vegetation density measure for hydraulic analyses. J. Hydraul. Eng. 139 (5), 461–469, http://dx.doi.org/10.1061/(ASCE)HY.1943-7900.0000700.

Järvelä, J., 2002. Determination of flow resistance of vegetated channel banks and flood plains. In: Bousmar, D., Zech, Y. (Eds.), Proc. Int. Conf. River Flow 2002, Louvain-La-Neuve. A.A. Balkema, Rotterdam, NL, pp. 311–318, ISBN 9058095096.

Järvelä, J., 2004. Determination of flow resistance caused by non-submerged woody vegetation. JRBM 2 (1), 61–70, http://dx.doi.org/10.1080/15715124.2004.9635222.

Kane, B., Modarres-Sadeghi, Y., James, K.R., Reiland, M., 2014. Effects of crown structure on the sway characteristics of large decurrent trees. Trees – Struct. Funct. 28 (1), 151–159, http://dx.doi.org/10.1007/s00468-013-0938-1.

Montakhab, A.B.T., Yusuf, B., Ghazali, B.H., Mohamed, T.A., 2012. Estimation of vegetation porosity in vegetated waterways. Proc. Inst. Civil Eng.: Water Manag. 166 (6), 333–340, http://dx.doi.org/10.1680/wama.11.00058.

Moulia, B., Sinoquet, H., 1993. Three-dimensional digitizing systems for plant canopy geometrical structure: a review. In: Varlet-Granchet, C., Bonhomme, R.,

Sinoquet, H. (Eds.), Crop Structure and Light Microclimate. Characterization and Applications. INRA Editions, Paris, France, pp. 183–193.
Nepf, H., Ghisalberti, M., 2008. Flow and transport in channels with submerged vegetation. Acta Geophys. 56 (3), 753–777, http://dx.doi.org/10.2478/s11600-008-0017-y.
Nobile, I., (Ph.D. thesis) 2007. Dendrometric Analysis of Riparian Vegetation in Mountain Streams. University of Trento, Italy (in Italian).
Oplatka, M., 1998. Stabilität von Weidenverbauungen an Flussufern, Diss. Techn. Wiss. ETH Zürich Nr. 12575., http://dx.doi.org/10.3929/ethz-a-001920916.
Polhemus, 2005. 3SPACE™ FASTRAK® User's Manual. Colchester, Vermont, USA., pp. 1–124.
Righetti, M., 2008. Flow analysis in a channel with flexible vegetation using double-averaging method. Acta Geophys. 56 (3), 801–823, http://dx.doi.org/10.2478/s11600-008-0032-z.
Schnauder, I., Yagci, O., Kabdasli, S., 2007. The effect of permeability of natural emergent vegetation on flow velocities and turbulence. In: Proceedings of the 32nd IAHR Congress, 1–6 July, Venice, Italy.
Sellier, D., Fourcaud, T., 2009. Crown structure and wood properties: influence on tree sway and response to high winds. Am. J. Bot. 96 (5), 885–896, http://dx.doi.org/10.3732/ajb.0800226.
Sinoquet, H., Rivet, P., 1997. Measurement and visualization of the architecture of an adult tree based on a three-dimensional digitising device. Trees – Struct. Funct., Springer 11 (5), 265–270.
Sukhodolova, T.A., Sukhodolov, A.N., 2012. Dynamics of turbulent flow along and behind vegetation patches: field experiments. In: Murillo (Ed.), River Flow 2012, vol. 1. Taylor & Francis Group, London, pp. 279–286.
Västilä, K., Järvelä, J., 2014. Modelling the flow resistance of woody vegetation using physically based properties of the foliage and stem. Water Resour. Res. 50 (1), 229–245, http://dx.doi.org/10.1002/2013WR013819.
Västilä, K., Järvelä, J., Aberle, J., 2013. Characteristic reference areas for estimating flow resistance of natural foliated vegetation. J. Hydrol. 492, 49–60, http://dx.doi.org/10.1016/j.jhydrol.2013.04.015.
Whittaker, P., Wilson, C., Aberle, J., Rauch, H.P., Xavier, P., 2013. A drag force model to incorporate the reconfiguration of full-scale riparian trees under hydrodynamic loading. J. Hydraul. Res. 51 (5), 569–580, http://dx.doi.org/10.1080/00221686.2013.822936.
Whittaker, P., Wilson, C., Aberle, J., 2015. An improved Cauchy number approach for predicting the drag and reconfiguration of flexible vegetation. Adv. Water Resour. 83 (2015), 28–35, http://dx.doi.org/10.1016/j.advwatres.2015.05.005.
Wilson, C.A.M.E., Yagci, O., Rauch, H.P., Stoesser, T., 2006. Application of the drag force approach to model the flow-interaction of natural vegetation. JRBM 4 (2), 137–146, http://dx.doi.org/10.1080/15715124.2006.9635283.
Yang, X.-D., Yan, E.-R., Chang, S.X., Da, L.-J., Wang, X.-H., 2014. Tree architecture varies with forest succession in evergreen broad-leaved forests in Eastern China. Trees – Struct. Funct., 1–15, http://dx.doi.org/10.1007/s00468-014-1054-6.
Zhang, J.T., Su, X.H., 2008. Numerical model for flow motion with vegetation. J. Hydrodyn. 20 (2), 172–178, http://dx.doi.org/10.1016/S1001-6058(08)60043-8.
Zinke, P., 2010. Flow resistance parameters for natural emergent vegetation derived from a porous media model. In: Dittrich, A., Koll, K., Aberle, J., Geisenhainer, P. (Eds.), Proc. Riverflow 2010. Braunschweig.

7.6 Publikation 6

Ecological Engineering 123 (2018) 161–167

Contents lists available at ScienceDirect

Ecological Engineering

journal homepage: www.elsevier.com/locate/ecoleng

The architecture and dynamic properties of young *Salix purpurea* trees in the context of riparian engineering systems

Clemens Weissteiner*, Hans Peter Rauch

University of Natural Resources and Life Sciences, Institute of Soil Bioengineering and Landscape Construction, Peter-Jordanstraße 82, 1190 Vienna, Austria

ARTICLE INFO

Keywords:
Eco-engineering
Dynamic tree properties
Tree architecture
Woody riparian vegetation
Salix purpurea

ABSTRACT

Soil and Water Bioengineers using plants for civil engineering purposes are faced with challenges to determine the interrelation of dynamic and architectural properties of riparian trees. This study aims to improve the characterization of young riparian trees (*Salix purpurea* L.) in the framework of such an eco-engineering approach. Dimensioning the mechanical effects of a complex multilevel system in a temporal and spatial context is a key issue understanding the plant-fluid interaction. We investigated the natural frequency (f_n), the damping ratio (ζ) and the architectural properties of three 4 year old purple willow specimens. From a tree architectural point of view, we found a clear distinction of the specimens in terms of the distribution of the projected area along the tree height, and for the slenderness ratio over the axes orders. The foliage of the specimens had a significant impact on the damping ratio depending on the tree architecture. A high slenderness ratio across the tree axes increased the flexibility of the branching system, and reduced the share of the foliage impact on the damping ratio. In comparison, a low slenderness ratio led to a stiffer tree structure, and therefore the damping ratio, due to the aerodynamic drag of the leaves, had received a higher share of the total damping ratio. Linking tree architectural analysis with its dynamic properties proved to be helpful in advancing the physical characterization of complex riparian trees.

1. Introduction

Soil and water bioengineering interventions are based on the application of living plants in combination with local natural auxiliary materials such as wooden logs and stones, in order to initiate a natural environment (Hacker, 2015). These interventions are implemented by means of specific bioengineering techniques to obtain: (i) natural hazard control (e.g. soil erosion, torrential floods, landslides) and (ii) ecological restoration or nature-based re-introduction of species on degraded lands, river embankments and disturbed environments (Rey et al., 2018). Plants eligible for these purposes have to meet specific requirements: on the one hand, growing under unfavourable conditions at the local construction site (Evette et al., 2012), and on the other hand resisting the mechanical stresses which act on this kind of engineering system (Fernandes and Guiomar, 2016). First a specific selection of plants is required and second the applied techniques have to be dimensioned. This approach requires a parametrization of plants as "living" construction material. The eco-engineering governing processes between trees and hydro- and aerodynamic loads are therefore highly relevant for interventions based on soil and water bioengineering techniques.

Along with wind and plant interaction, which has been the subject of many studies on different temporal and spatial scales and with different thematic backgrounds (Moore and Maguire, 2004; de Langre, 2008, Spatz and Theckes, 2013; James et al., 2014), the impact of plants is also of particular interest in hydrodynamic research (e.g. Aberle and Järvelä, 2013; Jalonen and Järvelä, 2014). Ongoing research in hydrodynamics has focused mainly on the impact of plants on hydraulic conditions, and not on the plants' behaviour under loading. The hydraulic interaction of flow and plants not only depends on geometrical properties (e.g. stem and branch diameter, length, leaf area), but also on the dynamic response of plants under turbulent hydrodynamic loads (stem/branch/leaf bending and horizontal and vertical reconfiguration); e.g. (Whittaker et al., 2013; Weissteiner et al., 2015; Järvelä and Aberle, 2016).

Most studies have focused more on hydraulic aspects than on biomechanical and architectural plant parameters. The architecture of a plant (including geometrical and topological information) depends on the nature and on the relative arrangement of each of its parts; it is, at any given time, the expression of an equilibrium between endogenous growth processes and exogenous constraints exerted by the environment (Barthelemy and Caraglio, 2007). Investigating plant

* Corresponding author.
E-mail addresses: clemens.weissteiner@boku.ac.at (C. Weissteiner), hp.rauch@boku.ac.at (H.P. Rauch).

https://doi.org/10.1016/j.ecoleng.2018.09.014
Received 21 February 2018; Received in revised form 14 August 2018; Accepted 9 September 2018

architectural properties with the same level of detail as the investigation of hydraulic loads offers therefore a new perspective on the interaction of both elements (Whittaker et al., 2013; Weissteiner et al., 2015).

In contrast to plant hydrodynamic studies, research concerning atmospheric flows has focused on the plants' response to dynamic loads (e.g. Milne, 1991; Gardiner, 1995; Moore and Maguire, 2008; Sellier and Fourcaud, 2009). In this context, the plants response to wind together with biomechanical and dynamical properties of different plant species have been investigated (e.g. Spatz et al., 1999; Sellier and Fourcaud, 2005, 2009; Kane and James, 2011). The quantification of maximum static bearable loads delivers valuable information on the biomechanical properties of trees, but does not reflect the degree of interaction in the case of dynamic loads. In fact, much lower dynamic loads than those predicted by static tests can lead to failure (Peltola, 2006). Therefore, to characterize the response of plants to turbulent fluid loading (air and water), the dynamic properties of the plants (natural frequency (f_n) and damping ratio (ζ)) have to be determined (Moore and Maguire, 2005).

In the case of soil and water bioengineering systems, trees interact with fluid-dynamic loads during different growth stages. Plant growth can trigger changes in the system status and its dynamic properties. However, the juvenile growth stage is especially important, in order to guarantee a rapid protective effect of the vegetation (Rauch et al., 2014). For a full understanding of the interaction processes between loads and plants it is crucial to close the gap of knowledge of the dynamic behaviour of soil and water bioengineering plants.

The purpose of this study is to determine the dynamic and architectural properties of young riparian trees (*Salix purpurea* L.) in order to improve the characterization of trees for soil and water bioengineering interventions. The specific objectives of this paper are: (1) to determine the natural frequency (f_n) and the damping ratio (ζ) of Salix purpurea saplings, (2) to investigate the differences in the aerial architecture (geometrical and topological parameters) of the specimens and (3) to quantify the impact of different axes orders resp. the differences in architecture on the dynamic properties of the investigated specimens.

2. Materials and methods

Our experiments were carried out at the laboratory of the Institute of Soil Bioengineering and Landscape Construction, University of Natural Resources and Life Sciences, Vienna. We harvested the plant specimens from a willow plantation at the Institute's testing garden. All of the specimens (Gamma 1–3) were taken from purple willow (*Salix purpurea* L.) cuttings, which were nearly 4 years old. We selected three specimens in order to ensure a broad spectrum of architectural variability (for morphology and height, see Fig. 1 and Table 1). The experiments we undertook for Gamma 1 and 3 (G1, G3) were performed in July 2012 and August 2013, and the Gamma 2 (G2) experiment was carried out in April 2013. Due to the growing season, the experiments for the G2 specimens where carried out without leaves.

Following harvesting, we transported the specimens to the laboratory and fixed the base of the stems with polyurethane foam in a 30 cm long plastic tube. The plastic tube with the tree inside was installed in an aluminium tube emerging from a concrete block (65 × 65 × 20 cm, approx. 210 kg) and fixed with plastic screws. The concrete block acted as a base for the pull and release experiments. Due to the experimental setup, damping through contact with neighbouring trees, and damping as a result of the root-soil-complex was avoided. An influence of the concrete block basis on the dynamic properties of the specimens was neglected. Before carrying out pull and release tests, we recorded the aerial architecture of the trees using the Polhemus FASTRAK 3D-digitizing device (Polhemus Inc, Colchester, VT). The measurement included the spatial coordinates, the diameter along the axes, the insertion angle of the axes and the topological information on the axes. For a detailed description of the digitizing method, the reader is referred to Weissteiner et al. (2015).

Free oscillation of saplings was obtained by attaching a string to the trees main axis at one-fourth of the total tree height. The string was pulled slightly downwards with a cable winch until a horizontal displacement of 15 cm to its rest position at one-fourth of the trees total height (h_{tot}) was reached. The force we applied to bring the trees into this position, was measured by a load cell attached between the string and the cable winch. We released the trees by cutting the string. The tests were repeated two times in the same directions and with the same initial displacement. Specimens were submitted to pull and release tests at different architectural states. We carried out a first cycle with intact trees (all axes + leaves). In the cases of Gamma 1 and Gamma 3, we performed additional pull and release tests after removing the foliage (all axes). After completion of the first two cycles we removed all of the axes with an order number greater than four (A1-4). Each axis order was removed successively, reaching up to the final cycle, with only the main stem intact (A1-3, A1-2 and A1). The motion of the stem and one 2nd order axis was recorded by the Polhemus FASTRAK device. Two teardrop receiver sensors were fastened to the stem at approximately one-fourth and one-half of h_{tot}. The third teardrop receiver was fixed at a dominant second order axis at one-half of h_{tot}. The sensors weighed 2.83 g each, with a diameter of 1 cm and a sampling rate of 40 Hz. The FASTRAK system delivers 3D-coordinates and orientation angles with a position resolution of 0.14 cm and an angular resolution of 0.1266° at a range (distance emitter-receiver) of 120 cm. Since the system is sensitive to electro-magnetic emitting sources, the tests were performed outside, sheltered from the wind. The data was recorded with a personal computer connected to the electronic control unit of the FASTRAK system. Fast Fourier Transformation was used to determine the specimens' damped natural frequency (f_n), and Power Spectral Density was plotted for each cycle and used for the purpose of deriving the natural frequency in Matlab (Mathworks, Natick, MA). The amplitude(y) peaks i = 1 and (i + n) = 4 were used in order to derive the logarithmic decrement (δ) and, successively, the damping ratio (ζ):

$$\zeta = \frac{\delta}{\sqrt{(2\pi)^2 + \delta^2}} \quad [1]$$

where

$$\delta = \frac{1}{n} \ln \frac{y_i}{y_{i+n}} \quad [2]$$

and y_i and y_{i+n} are the first and fourth peaks in a plot of displacement versus time for tree sway.

3. Results and discussion

3.1. Architectural properties of the specimens

Table 2 gives an overview of the geometrical and biomass data for the specimens, as a function of their axes. The total tree heights ranged from 217.3 cm (G2) up to 266.7 cm (G1), and the basal diameters of the main axes from 2.2 to 2.7 cm. Specimen G3 had the highest number of axes (540), followed by G1 with 468 and G2 with 217 axes. Regarding the specimens G1 and G3, the majority of the axes were within the 4th and 5th axes order. In comparison, the specimen G2 showed the highest amount of axes at the 3rd and 4th axes order. G3 had a total axes length of 11.1 m, G1 and G2 6.8 m and 3.95 m respectively. For all specimens, approximately two thirds of the total axis length were distributed at axes of 3rd and 4th axes order.

For all of the axes, fresh biomass ($m_f/m_{f,tot}$) showed similar shares of the total fresh biomass. Leaf biomass of G1 and G3 represented a share of 10% and 20% resp. (Fig. 2), G2 was harvested in springtime without any leaves, and therefore 100% of the relative fresh biomass is related to the wooden biomass. The relative amount of biomass decreased for all of the specimens concave over the axes orders, with a biomass

Fig. 1. Architectural system of Gamma 1–3 projected on the y-plane.

Table 1
Characteristic architectural plant parameters of the three plant specimens (G1–G3).

		G1	G2	G3
H_{tot}	[cm]	247.5	217.3	266.73
D_{B_Stem}	[cm]	2.3	2.2	2.7
mean $D_{B\_allAxes}$	[cm]	0.2 (0.1–2.3)	0.2 (0.1–2.2)	0.2(0.1–2.7)
mean L_A	[cm]	14.6 (0.2–266.9)	18.2 (1.3–154.3)	20.5 (1.9–299.0)
mean L_A/D_B	[cm]	62.4 (1.4–157.1)	69.2 (1.6–170)	102.5 (19.2–269.5)
L_{A_tot}	[cm]	6836	3950	11,101
A_{P_tot}	[cm^2]	2052.39	1340.97	2979.23
$m_{f,A}$	[g]	779	449	1158
$m_{f,L}$	[g]	89	0	260

proportion of 50% for the first order axis for G1 and G2, and 40% for G3. The biomass of the first two axes orders reached from 60 up to almost 80% of the total biomass (Fig. 2).

The vertical distribution of the projected area emphasised the differences in the architectural system of the three specimens (Fig. 3). G3 showed the highest total amount in projected area (A_p) (2979 cm^2), followed by G1 (2052 cm^2) and G2 (1340 cm^2).

This shows that G2 represented almost only one third of the A_p of G3, and G1 represented two thirds of the A_p of G3. With increasing A_{p_tot}, the centre of the area decreased in height. Gamma 3 showed the highest increase in A_p in the upper half of the tree, whereas the specimen G1 showed a strong increase of A_p in the upper fourth of the specimen. G2 had his centre of A_p as well in the upper fourth of its tree height, but in general terms it displayed a rather poor developed projected area in comparison to the other two specimens. The first two axes orders of all the specimens dominated the lower half of the projected area, whereas axes orders higher than 2 dominated the upper half, due to a strong increase in the projected area of the axes. The Salix caprea specimens, analysed by Weissteiner et al. (2015), showed a similar vertical distribution in A_p, whereas *Alnus glutinosa* specimens showed their centre of the area in the lower part of the tree.

All three specimens had a mean basal diameter (D_B) of 0.2 cm for all axes, with minimum and maximum basal diameters of 0.1 and 2.7 cm per axis. Mean D_B values decreased with increasing axes order and advancing pruning phase (Fig. 4a). We found the highest D_{B_tot} values at the 3rd and 4th axes order, with mean values of 16.3 cm for G2 and 25.5 cm and 35.6 cm for G1 and G3 respectively (Table 2). As a result of the progressing pruning steps mean axes length increased. We noted slightly higher values for mean D_B and mean L_A for specimen G2 for the axes of the 2nd axes order, and slightly lower values for the main stem. This was due to the premature death of the main axes, which resulted in a stronger growth strategy of the axes of the 2nd axes order. The mean L_A/D_B ratio of the specimens G1 and G2 were 62.4 and 69.2, whereas G3 had a ratio of 102.5. The mean L_A/D_B ratios for the specimens G1 and G2 decreased with increasing axes order, with the exception of the first order axis of G2, due to the premature death of the main stem (Table 2). In comparison, the L_A/D_B ratio (also called slenderness ratio) for G3 remained more or less the same for all of the axes orders (100–110 for the first five axes orders). The specimen G3 also had, during all pruning phases, a similar mean slenderness ratio. In comparison, the mean slenderness ratio for the axes of G1 and G2 increased during the progressive pruning phase, which indicates that in terms of all the axes, the trees were less slender than at their final pruning phase, with just the main axis left (Fig. 4c). The more slender axes, at all of the pruning phases of the specimen G3 implied a less rigid structure, due to a smaller second moment of area (I) in comparison to the axis length.

3.2. Dynamical properties of the specimens

The tree specimens oscillated visually up to 7–8 s after release. However, particularly in fully leaved conditions, a rapid return to the resting position, which included only a few notable cycles, was observed (Fig. 5). Natural frequency (f_n) didn't vary substantially between cycles or at different positions on the main stem. Our findings showed, that with regards to the second order axis branch, f_n was rather similar to the f_n of the main stem. This was also demonstrated by Spatz et al. (2007) for a small Douglas fir and by Kane et al. (2014) for large open grown trees.

Table 2
Mean and total architectural parameters in function of the specimens' axes order. Values marked with (*) represent the total fresh biomass of axis orders higher than four.

Specimen	Axes order	No of Axes	L_{A_tot} [cm]	Mean L_A [cm]	D_{B_tot} [cm]	Mean D_B [cm]	Mean L_A/D_B	$m_{f,A}$ [g]
Gamma 1	1	1	266.9	266.9	2.3	2.3	116.1	427.0
	2	19	1048.2	55.2	9.6	0.5	103.7	176.0
	3	90	2067.0	23.0	22.6	0.3	78.7	100.0
	4	165	2025.8	12.3	28.3	0.2	62.8	51.0
	5	139	1064.9	7.7	19.7	0.1	50.5	25.0 (*)
	6	44	304.2	6.9	5.6	0.1	49.3	–
	7	10	59.1	5.9	1.2	0.1	51.2	–
Gamma 2	1	1	154.7	154.7	2.2	2.2	70.3	212.0
	2	10	916.9	91.7	7.0	0.7	127.1	135.7
	3	59	1349.4	22.9	16.1	0.3	78.2	66.0
	4	95	1114.9	11.7	16.6	0.2	65.1	29.0
	5	48	404.4	8.4	7.0	0.1	58.2	6.0 (*)
	6	4	9.8	2.5	0.4	0.1	24.6	–
Gamma 3	1	1	299.0	299.0	2.7	2.7	110.8	549.0
	2	27	1536.4	56.9	15.0	0.6	101.6	302.0
	3	125	3309.1	26.5	33.0	0.3	106.0	172.0
	4	220	3823.3	17.4	38.3	0.2	104.4	98.0
	5	133	1807.8	13.6	18.5	0.1	100.5	37.0 (*)
	6	34	325.1	9.6	3.8	0.1	86.0	–

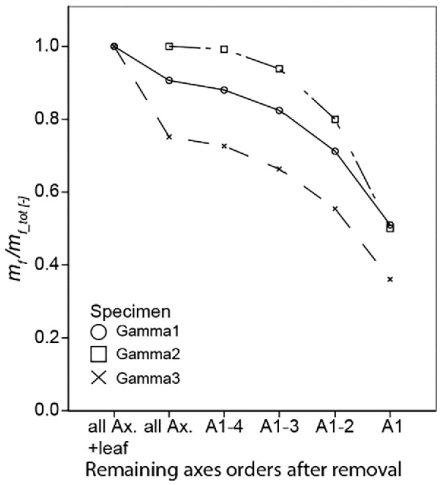

Fig. 2. Relative fresh biomass distribution for the different pruning phases of the trees (G1 and G3, leaves included, G2 harvested without leaves).

Mean f_n increased for all pruning phases (Fig. 6a and b). For the first pruning steps (up to pruning phase A1-2) f_n increased slightly. For the last pruning step instead, reducing the tree structure to the main stem, we noticed a strong increase in f_n (Fig. 6 and Table 3). At the last pruning step, G2 showed an increase of almost 200% in f_n, which was due to the relatively short main stem of the specimen.

In comparison to the 4 year old pine saplings (h = 1.76–2.57 m), tested by Sellier and Fourcaud (2005), the mean f_n values of the *Salix purpurea* specimens where a little higher in fully leaved conditions (10%), and 40% and 50% higher during the pruning phase after the removal of the 3rd and 2nd order axes respectively. However, pine saplings had substantially higher D_B-values for all axes orders. Excluding the main stem, G1–G3 showed, at all pruning phases, a linear decrease of f_n with increasing fresh biomass (Fig. 6). The normalised natural frequency (f_n/f_{n_tot}) showed, during all of the pruning phases, a linear correlation with increasing fresh biomass (Fig. 6b). Moore and Maguire (2005) found that, 80% of the biomass had to be removed from a 15 to 20 m high Douglas-fir before a difference in natural frequencies could be observed. This was not the case for the *Salix pupurea* specimens tested in our experiment.

G1 and G3 presented, in fully leaved conditions, a mean damping ratio of 0.270 and 0.253 respectively (Table 3). The impact of the leaves on the damping ratio was quite different. Concerning specimen G1, the mean damping ratio decreased to 0.146, an almost 46% difference from fully leaved to un-leaved conditions, with a share of fresh leave biomass of 11% of the wooden tree mass. In comparison, specimen G3 showed a 22.4% share of leaf biomass in relation to the wooden biomass, and a minor decrease of 8.3% in the damping ratio between leaved and un-leaved conditions (Fig. 7a and c Table 1). The strong decrease in the damping ratio for G1 can be explained by a different ratio in slenderness for all of the axes. In unpruned conditions G1 presented an L_A/D_B ratio of 62 and G3 of 102, which means that the axes of G3 were more flexible. Trees with flexible axes can better dissipate energy, due to their reconfiguration and a reduction of the projected area, and therefore reduction in drag. This means that slenderer axes are able to counteract a high sailing area, which is a result of the trees' foliage. G3 had only one third of the leaf biomass of G1, in absolute terms, and half of the leaf biomass relative to the mass of the axes. However, it reduced its damping ratio after defoliation by just one fifth in comparison to the reduction in the damping ratio of G1. Kane and James (2011), as well as Sellier and Fourcaud (2005) found that leaves have significant impact on the damping ratio of trees, which could not be proven in the case of G3. The characterization of young flexible plants, from a technical point of view, based only on the leaf-area-index or other indices related to the leaf area, could therefore be misleading. It is highly relevant how the axes, their vertical distributions as well as the slenderness ratio, are contributing to the system behaviour.

Prediction of ζ by morphometric key parameters was complex. Generally, G3 demonstrated a somewhat different behaviour in terms of damping ratio for the different pruning steps. Variations in ζ among trees are quite common (Jonsson et al., 2007). The mean damping ratio of G3 decreased constantly during each pruning step (Fig. 7a), and increased linearly with an increasing projected area (Fig. 7b) and fresh biomass (Fig. 7c). At the same time, the L_A/D_B ratio of specimen G3 remained almost constant during the different pruning steps (see Fig. 4c). Concerning the pruning steps without leaves, G1 and G2 demonstrated a slight increase (G2 up to A1-3 and G1 up to A1- 2) and, in

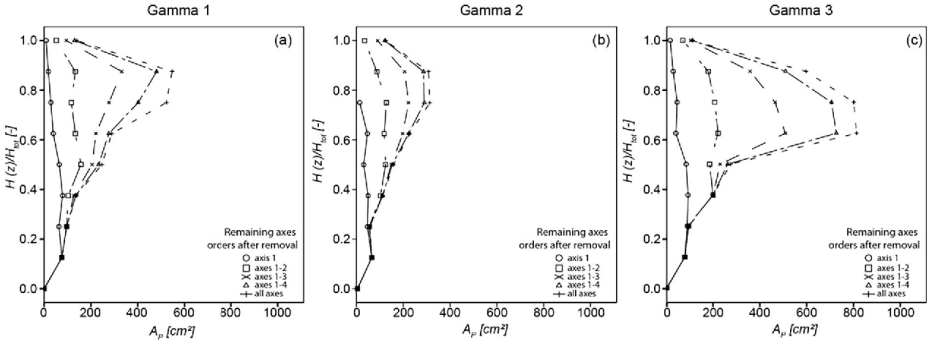

Fig. 3. Projected area over height of different axes orders fort the specimens G1–G3 (a–c).

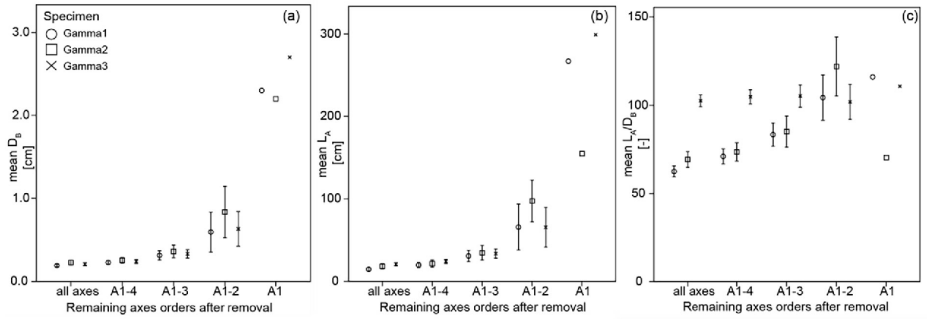

Fig. 4. Mean D_B (a) L_A (b) and L_A/D_B ratio (c) for the different pruning phases (all axes, axes 1–4 (A1-4), axes 1–3 (A1-3), axes 1–2 (A1-2), axis 1 (A1)). Error bars show ± 2standard error.

the last pruning phase(s), a strong decrease in damping ratio (Fig. 7a). In relation to the projected Area (A_P), the damping ratio of G1 changed substantially only during the last pruning step (Fig. 7b). In relation to the biomass, we found two significant changes in damping ratio for G1, after the removal of the leaves and after the removal of the 2nd axes order. This is not reflected in Fig. 7b, because leaf area was not recorded and could therefore not be accounted for. The damping ratio for G2 presented a strong increase up to A1-3, and afterwards a strong decrease in relation to the biomass and A_P. This reveals that, in comparison to G3, the removal of branches up to the 3rd or 2nd axes order for G2 and G1 respectively had a positive effect on the damping ratio of the specimens. The findings of Sellier and Fourcaud (2005), which showed that the damping ratio increased after the removal of the third axes order could not be confirmed. For G2 and G3 the damping ratios decreased by 25% and 17% respectively. On the other hand, G1 presented a slight increase of 4% in the damping ratio after removal of the third axes order, even though the architectural properties for G2 and G3 were quite similar (mean L_A/D_B ratio and mean L_A). However,

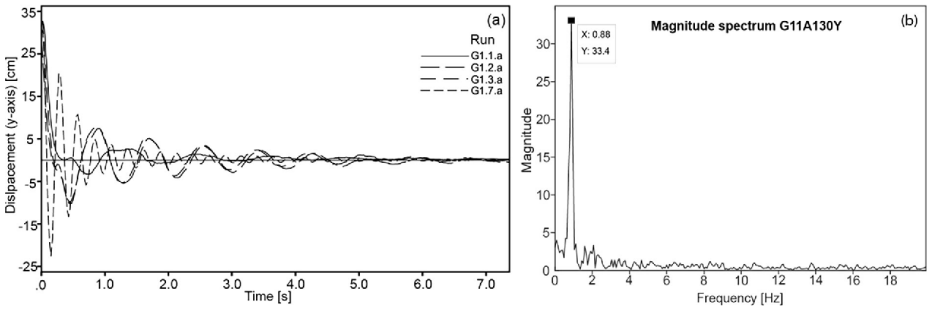

Fig. 5. Time history of the displacement of the main stem on the y-axis for Gamma 1 for different pruning stages, at a height of 130 cm (G1.1a: all axes with leaves, G1.2a: all axes without leaves, G1.3: axes 1–4 and G1.7 only main stem), during pull and release tests (a). For reasons of readability, intermediate steps have been omitted. Spectral analyses for G1 in fully leaved condition (b).

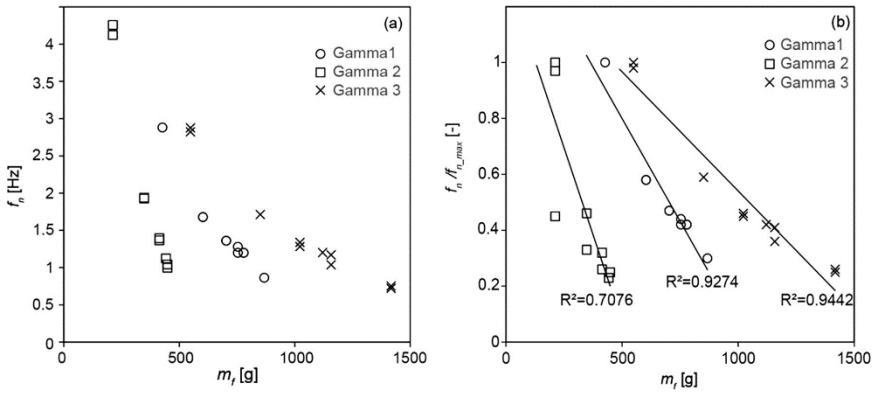

Fig. 6. Scatterplot of the relationship between the natural frequency f_n (a) and the normalised natural frequency $f_n/f_{n,wt}$ (b) with the fresh biomass m_f of the three specimens at different pruning phases (all axes with leaves-main stem).

Table 3
Change of the dynamic characteristics of the specimens for different pruning phases.

		All axes + leaves	All axes	A1-4	A1-3	A1-2	A1
G1	Mean f_n [Hz]	0.86 (0.019)	1.17 (0.041)	1.20 (0.051)	1.37 (0.06)	1.68 (0.00)	2.88 (0.00)
	Mean ζ [–]	0.270 (0.021)	0.146 (0.018)	0.156 (0.017)	0.158 (0.018)	0.165 (0.016)	0.133 (0.02)
G2	Mean f_n [Hz]		1.02 (0.025)	1.13 (0.00)	1.54 (0.257)	1.93 (0.005)	4.19 (0.077)
	Mean ζ [–]		0.179 (0.031)	0.202 (0.021)	0.208 (0.024)	0.156 (0.029)	0.088 (0.01)
G3	Mean f_n [Hz]	0.74 (0.017)	1.10 (0.074)	1.20 (0.00)	1.31 (0.031)	1.71 (0.00)	2.85 (0.031)
	Mean ζ [–]	0.253 (0.016)	0.232 (0.020)	0.200 (0.015)	0.190 (0.12)	0.157 (0.008)	0.116 (0.013)

the architecture of pine trees is rather different in comparison to that of *Salix pupurea* trees, due to the almost perpendicular inclination of the axes of the higher axes order in comparison to their "mother axes". Salix purpurea branches tend to grow along their higher order axes with smaller insertion angles.

4. Conclusions

Our experiments were conducted in order to relate the architectural properties of young *Salix purpurea* trees to their dynamic properties (natural frequencies and damping ratio). The three specimens selected reflected the broad variability in the growth of this pioneer species. All axes orders had an influence on the natural frequency of the trees. Biomass reduction resulted in an increase of natural frequency, from the first removal of the highest axes order, and increased more during further pruning steps. From a tree architectural point of view, we found a sharp distinction of the specimens in terms of the distribution of the projected area along the tree heights, and for the slenderness ratio over the axes orders. The foliage of the tree has a significant impact on the damping ratio, however, it strongly depends on the slenderness ratio of the underlying axes. A high slenderness ratio across the tree axes increased the flexibility of the branching system, and reduced the share of the foliage impact on the damping ratio. In comparison, a low slenderness ratio led to a stiffer tree structure, and therefore the damping ratio, due to the aerodynamic drag of the leaves, had received a higher share of the total damping ratio. From an eco-engineering perspective,

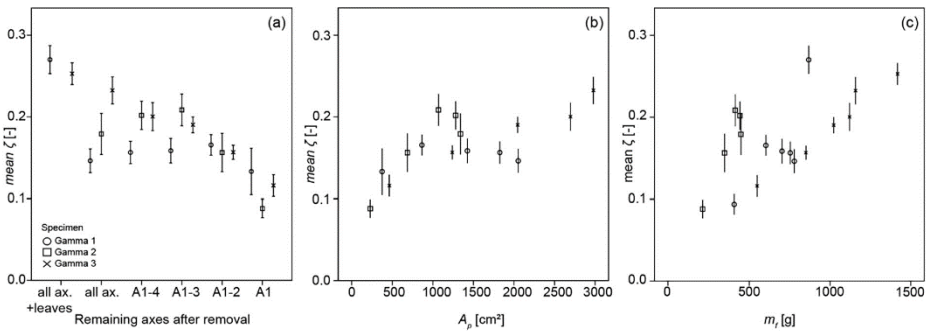

Fig. 7. Mean damping ratio (ζ) at different pruning steps (a). Interrelation between mean ζ and the projected axes area (A_P) (b) and between mean ζ and fresh biomass (m_f) of the specimens (c). Values in (b) and (c) represent damping ratios at the different pruning steps. Error bars show ± 2standard error.

it is therefore important to take into account the projected area, the slenderness ratio and the foliage. These results should also be extended to encompass a broader approach, covering different pioneer tree species which are often used for ecological restoration work.

References

Aberle, J., Järvelä, J., 2013. Flow resistance of emergent rigid and flexible vegetation. J. Hydraul. Res. 51 (1), 33–45. https://doi.org/10.1080/00221686.2012.754795.

Barthelemy, D., Caraglio, Y., 2007. Plant architecture: a dynamic, multilevel and comprehensive approach to plant form, structure and ontogeny. Ann. Bot. Lond. 99 (3), 375–407. https://doi.org/10.1093/aob/mcl260.

de Langre, E., 2008. Effects of wind on plants. Annu. Rev. Fluid Mech. 40, 141–168. https://doi.org/10.1146/annurev.fluid.40.111406.102135.

Evette, A., Balique, C., Lavaine, C., Rey, F., Prunier, P., 2012. Using ecological and biogeographical features to produce a typology of the plant species used in bioengineering for riverbank protection in Europe. River Res. Appl. 28 (10), 1830–1842. https://doi.org/10.1002/rra.1560.

Fernandes, J.P., Guiomar, N., 2016. Simulating the stabilization effect of soil bioengineering interventions in mediterranean environments using limit equilibrium stability models and combinations of plant species. Ecol. Eng. 88, 122–142. https://doi.org/10.1016/j.ecoleng.2015.12.035.

Gardiner, B.A., 1995. The interactions of wind and tree movement in forest canopies. Wind Trees 41–59.

Hacker, E. (Ed.), 2015. European Guidelines for Soil and Water Bioengineering. European Federation of Soil Bioengineering, Aachen.

James, K.R., Dahle, G.A., Grabosky, J., Kane, B., Detter, A., 2014. Tree biomechanics literature review: dynamics. Arboric. Urban For. 40 (1), 1–15.

Järvelä, J., Aberle, J., Jalonen, J., 2016. Dynamic reconfiguration of riparian trees in towing tank experiments. In: Garcia, Hanes, (Eds.). River Flow 2016 – Constantinescu. ISBN 978-1-138-02913-2.

Jalonen, J., Järvelä, J., 2014. Estimation of drag forces caused by natural woody vegetation of different scales. J. Hydrodyn. 26 (4), 608–623. https://doi.org/10.1016/S1001-6058(14)60068-8.

Jonsson, M.J., Foetzki, A., Kalberer, M., Lundström, T., Ammann, W., Stöckli, W., 2007. Natural Frequencies and damping ratios of Norway spruce [*Picea abies* (L.) Karst] growing on subalpine forested sploes. Trees (Berl.) 21 (5), 541–548. https://doi.org/10.1007/s00468-007-0147-x.

Kane, B., James, K.R., 2011. Dynamic properties of open-grown deciduous trees. Can. J. For. Res. 41 (2), 321–330. https://doi.org/10.1139/X10-211.

Kane, B., Modarres-Sadeghi, Y., James, K.R., Reiland, M., 2014. Effects of crown structure on the sway characteristics of large decurrent trees. Trees – Struct. Funct. 28 (1), 151–159. https://doi.org/10.1007/s00468-013-0938-1.

Milne, R., 1991. Dynamics of swaying of *Picea sitchensis*. Tree Physiol. 9 (3), 383–399.

Moore, J.R., Maguire, D.A., 2004. Natural sway frequencies and damping ratios of trees: concepts, review, and synthesis of previous studies. Trees (Berl.) 18, 195–203. https://doi.org/10.1007/s00468-003-0295-6.

Moore, J.R., Maguire, D.A., 2005. Natural sway frequencies and damping ratios of trees: influence of crown structure. Trees (Berl.) 19 (4), 363–373. https://doi.org/10.1007/s00468-004-0387-y.

Moore, J.R., Maguire, D.A., 2008. Simulating the dynamic behavior of Douglas-fir trees under applied loads by the finite element method. Tree Physiol. 28 (1), 75–83.

Peltola, H., 2006. Mechanical stability of trees under static loads. Am. J. Bot. 93 (10), 1501–1511. https://doi.org/10.3732/ajb.93.10.1501.

Rauch, H.P., Sutili, F.J., Hörbinger, S., 2014. Installation of a riparian forest by means of soil bio engineering techniques – monitoring results from a river restoration work in Southern Brazil. Open J. For. 4 (2), 161–169 ISSN 2163-0429.

Rey, F., Bifulco, C., Bischetti, G.B., Bourrier, F., De Cesare, G., Florineth, F., Graf, F., Marden, M., Mickovski, S.B., Philips, C., Peklo, K., Poesen, J., Polster, D., Preti, F., Rauch, H.P., Raymond, P., Sangalli, P., Tardio, G., Stokes, A., 2018. Soil and water bioengineering: practice and research needs for reconciling natural hazard control and ecological restoration. Sci. Total Environ (in press).

Sellier, D., Fourcaud, T., 2005. A mechanical analysis of the relationship between free oscillations of Pinus pinaster Ait. Saplings and their aerial architecture. J. Exp. Bot. 56 (416), 1563–1573. https://doi.org/10.1093/jxb/eri151.

Sellier, D., Fourcaud, T., 2009. Crown structure and wood properties: influence on tree sway and response to high winds. Am. J. Bot. 96 (5), 885–896. https://doi.org/10.3732/ajb.0800226.

Spatz, H.C., Köhler, L., Niklas, K.J., 1999. Mechanical behaviour of plant tissues: composite materials or structures? J. Exp. Biol. 202, 3269–3272.

Spatz, H.C., Brüchert, F., Pfisterer, J., 2007. Multiple resonance damping or how do trees escape dangerously large oscillations? Am. J. Bot. 94 (10), 1603–1611. https://doi.org/10.3732/ajb.94.10.1603.

Spatz, H.C., Theckes, B., 2013. Oscillation damping in trees. Plant Sci. 207, 66–71. https://doi.org/10.1016/j.plantsci.2013.02.015.

Weissteiner, C., Jalonen, J., Järvelä, J., Rauch, H.P., 2015. Spatial-structural properties of woody riparian vegetation with a view to reconfiguration under hydrodynamic loading. Ecol. Eng. 85, 85–94. https://doi.org/10.1016/j.ecoleng.2015.09.053.

Whittaker, P., Wilson, C., Aberle, J., Rauch, H.P., Xavier, P., 2013. A drag force model to incorporate the reconfiguration of full-scale riparian trees under hydrodynamic loading. J. Hydraul. Res. 51 (5), 569–580. https://doi.org/10.1080/00221686.2013.822936.

Danksagung

An dieser Stelle möchte ich mich bei all denjenigen bedanken, die mich während der Anfertigung dieser Dissertation unterstützt und motiviert haben.

Mit Hans Peter Rauch habe ich einen motivierenden, unterstützenden, konstruktiven Doktorvater und guten Freund gefunden, der mir im Laufe der Arbeit bei Fachlichem und Privatem immer hilfreich zur Seite gestanden ist.

Florin Florineth hat mich auf das Thema der Ingenieurbiologie aufmerksam gemacht. Mit ihm habe ich meine ersten ingenieurbiologischen Schritte gemacht, viele Projekte unter seiner Leitung ausgeführt und viele Erfahrungen gesammelt, die wie er wohl kein anderer in der Ingenieurbiologie vermitteln kann.

Bei João Paulo Fernandes und Eva Hacker möchte ich mich für eine gute Beratung und konstruktive Begutachtung der Arbeit bedanken.

Meine ZimmerkollegInnen im Laufe meiner Tätigkeit am Institut für Ingenieurbiologie und Landschaftsbau gilt großer Dank für viele Diskussionen und Ratschläge. Besonderer Dank gilt dabei Walter Lammeranner, Gerda Kalny und Stephan Hörbinger mit denen mich viel Berufliches und Privates verbindet und mit denen ich lange Zeit ein Zimmer geteilt habe.

Bei meinen ArbeitskollegInnen möchte ich mich für ein sehr angenehmes und entspanntes Arbeitsklima und eine schöne Zeit am Institut bedanken.

Den IB-VolleyballerInnen, allen voran Präsident Max Hable, mit denen ich während der wärmeren Monate wöchentlich Institutssport betrieben habe und ein toller Teamgeist entstanden ist gilt auch großer Dank, Ich werde mich in Zukunft ab und an als Gastspieler melden!

Großer Dank gilt meiner kleinen und großen Familie für die ständige Unterstützung dem Verbreiten von Lebensfreude und dem Tolerieren meiner Launen and schwierigeren Tagen.